UNIVERSITÀ DI PARMA

UNIVERSITA' DEGLI STUDI DI PARMA

DOTTORATO DI RICERCA IN
SCIENZA E TECNOLOGIA DEI MATERIALI

CICLO XXXII

Novel HDPE-based bio-composites for bones replacement application

Coordinatore:
Chiar.mo Prof. Enrico DALCANALE

Tutore:
Chiar.ma Dr.ssa Maria Giulia FAGA

Dottorando: Mattia DI MARO

Anni 2016/2019

INDEX

CHAPTER 1

Introduction

CHAPTER 2

Alumina toughened Zirconia (ATZ) as filler of HDPE-based composites for biomedical purpose

CHAPTER 3

Chitosan as filler of HDPE-based composites for biomedical purpose

Chapter 1

Introduction

1.1 Materials for biomedical application.

1.1.1 General aspects about the biomaterials

The use of man-made materials or materials already existing in nature but suitably modified by man for the replacement of parts of the human body finds its origins in ancient times. Artificial eyes, ears, teeth, and noses were found in Egyptian mummies, waxes, glues, and tissues in reconstructing missing or defective parts of the body were used by Chinese and Indian ancient people **[1]**.

Nowadays, in the biomedical field, a biomaterial is defined as a material capable of replacing or improving the functionality of any living tissue. Biomaterials in the form of prostheses (bone plates, hip joints, dental implants) and medical devices, such as pacemakers, biosensors and artificial hearts, are widely used to replace and / or restore the functions of degenerated tissues to prepare them for healing, improving their functionality, correcting anomalies and therefore improving the quality of patient life **[2]**.

The concept of biocompatibility was introduced in the 70s to describe the properties that a material used for the construction of these implants should possess. It plays a fundamental role in the choice of the starting materials and provides the basis to the birth of new devices for biomedical application. A definition of biocompatibility, widely mentioned, has been proposed during a conference in the 1986 by D.F. Williams and defines the biocompatibility like *"the ability of a material to perform with an appropriate host response in a specific application"* **[3]**. The biocompatible materials, used to make these new biomedical devices, represent a wide part of what are called biomaterials. In particular, *"a biomaterial is a substance that has been engineered to take a form which, alone or as a part of a complex system, is used to direct, by control of interactions with components of living systems, the course of any therapeutic or diagnostic procedure, in human or veterinary medicine."* **[4]**.

These general definitions highlight the fact that biocompatibility is a property hard to be defined and studied in detail. In fact, biocompatibility means not generating negative interactions with the organism, but non-harmful interactions can be generated either by materials that interact with the organism or by materials that do not interact with the body at all. Both these types of materials are considered biocompatible but the former are also called bioactive, the latter are generally named as bioinert.

Metals, polymers, ceramics and a large amount of their composites are used as biomaterials. Numerous materials belonging to these different categories have found application in the biomedical field, almost without undergoing modifications.

The use of metals in medical application has a long history and research has continued to modify their microstructure **[5]** or change their surface properties **[6,7]** with the aim to increase biocompatibility. As example, gold, titanium alloys, stainless steel and shape memory NiTi alloys are metals widely used as biomaterials. In the same way, a large amount of polymers like polyethylene (PE), polypropylene (PP), silicon rubber (SR), polyetheretherketone (PEEK), polyurethane (PU) and poly(lactic acid) PLA are also considered biomaterials used in different applications **[8]**. Titania,

alumina, zirconia, bioglass, carbon fiber and hydroxyapatite have been also used as ceramic biomaterials in dentistry and orthopedic surgery **[9,10]**. Their biocompatibility depends on their chemical compositions and in particular on the presence of ions commonly found in the physiological environment (such as Ca^{2+}, Na^{+} and K^{+}). Ions such as Al^{3+} and Ti^{2+} do not cause substantial toxic effects to the body tissues.

1.1.2 Biomaterials for prosthetic applications: state of the art

Many efforts have been conducted in the field of tissue engineering with the aim of finding potential alternatives to conventional bone tissue reconstruction and replacement techniques **[11]**. For the replacement of injured tissues or for the recovery of their functionalities, biomedical engineering can now make use of innovative metal, polymer, ceramic materials and their composites. These materials should possess appropriate and preferably tunable mechanical, degradation, biological, and immunological properties as well as they should be cheap and easy to produce. Generally, metals possess high strength, ductility and resistance to wear but many of them have a low biocompatibility, high stiffness compared to tissues and could release metal ions that may cause allergic tissue reactions **[12]**. Ceramic materials have good biocompatibility, high resistance to corrosion and compression but are expensive, difficult to manufacture and inherently brittle **[10]**. Compared to metallic and ceramic materials used in the same field, the polymers have the advantage of a lower cost and a greater ease of forming even in complex geometries. Their main defects are the weak mechanical properties (elastic modulus and tensile strength), lower than those of bone **[12]**.

The use of materials originally developed for general engineering applications rather than the replacement of damaged human tissues has been successful and it is certain that most of them will still be used in the

future for sanitary applications. However, this does not exclude the fact that the use of these materials in the biomedical field can lead to several practical drawbacks. One of the main problems is the mismatch of stiffness between the implants and the bone **[13]**. In the load sharing between bone and implant, the amount of stress carried by each of them is directly related to their stiffness. Thus, when using ceramic or metallic materials as implants, bone is insufficiently loaded compared to them, and this phenomenon is called *stress shielding*. It was been widely shown that the *stress shielding* degree depends on the degree of stiffness mismatch. This effect influences the bone remodeling and healing process leading to increased bone porosity **[13,14]**. Therefore, the use of polymers that have a low modulus would represent an interesting alternative. However, low strength associated with low modulus usually impairs their potential use. In order to overcome these problems, the use of *"analogue biomaterial"* was exploited by Bonfield since the 1981 **[15]**.

The concept of *"analogue biomaterials"* is based on the biomimicry according to which a good material for the replacement of a body tissue must mimic its characteristics. If similar biological and mechanical properties can be achieved, then *stress shielding* at the interfaces between the material and the tissue in which it is implanted will be minimized **[16]**.

Generally, tissues are divided into two categories: *hard tissues* and *soft tissues*. Bones and teeth are examples of hard tissues; skin, blood vessels, cartilage and ligaments are examples of soft tissue. As the names suggest, hard tissues are more stiff (elastic modulus) and more resistant (tensile strength) than soft tissues **[12]**.

In order to obtain *"analogue biomaterials"* suitable for biomedical applications, the use of composite materials is mainly considered.

A composite material is defined as a combination of one or more additives held together by some type of glue or matrix. In particular, a polymer-based composite is a mixture of a polymer matrix and one or more inorganic/organic fillers, with a certain morphology (fibres, flakes, spheres and particulates). The properties of the composite material are the result of the contribution given by the phases that compose it. In general, fillers

improve mechanical performance of the matrix and, depending on the type of filler, give new properties to the resulted material. When the fillers are in nanoscale dimensions, the materials are also known as polymer nanocomposites **[17]**.

Bone itself is a natural composite material, consisting of a hierarchical structure with different levels of organization, from macro- to micro-scale. **[18]** The lowest hierarchical level (at the microscale) consists of collagen and hydroxyapatite (HA) as the main constituents of the nanocomposite-forming mineralized collagen fibrils, which further assemble into fibers arranged in geometrical patterns in lamellae and osteons **[18]**. Human HA has a Ca/P ratio of 1.67 and carbonate (CO_3^{2-}), fluoride (F^-), citrate ($C_6H_5O_7^{4-}$) and hydroxyl (OH^-) ions as substituent **[18]**. (Figure 1.1)

Taking a cue from this structure, a polymer based composite, containing a filler that gives the bioactivity to the material and that improves the mechanical properties of the polymer matrix, would be a natural choice to achieve a biomaterial for replacement of cortical bone.

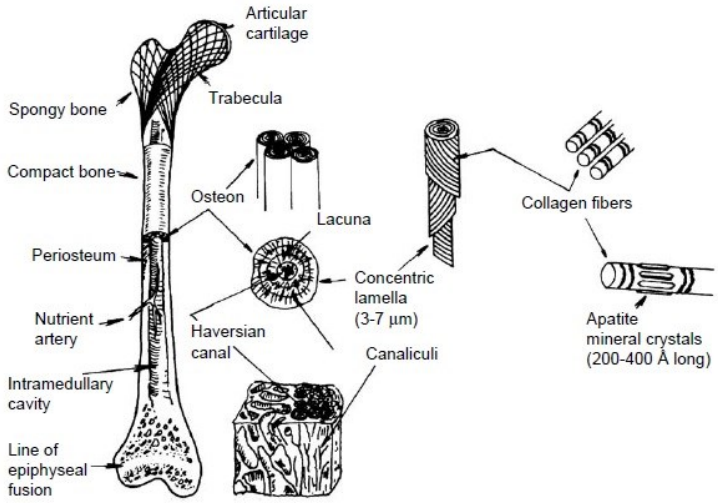

Figure 1.1: Structural organization of human bone. **[2]**

The polymer matrix has to be bioinert, biocompatible and able to give the ductility required for tissue replacement materials. The bioactive component of the material will promote the growth of the biological tissue upon the implant and the following formation of a strong link between this one and the body.

Polymer composites also have the advantage of a radio-transparency adjustable by contrast, while metals and ceramics, being radio-opaque, cause undesirable artifacts in X-ray radiographs **[19]**. Furthermore, polymer composites are compatible with modern diagnostic methods such as computerized tomography and magnetic resonance imaging.

The pioneering work of Bonfield and Grynpas **[15]**, conducted on Hydroxyapatite / High Density Polyethylene (HA/HDPE) system, paved the way for several studies with this strategy, starting from different polymer matrix and a wide number of bioactive fillers. **[20-23]**.

Over the years, numerous studies have focused on the development of polymer matrix composites reinforced with bioactive materials for bones replacement applications. In particular, HDPE, Ultra High Molecular Weight Polyethylene (UHMWPE), Polyetheretherketone (PEEK), Polytetrafluoroethylene (PTFE) and Poly(methyl_methacrylate) (PMMA) were widely used as matrix for composites materials in biomedical field. Based on extensive clinical investigations, these polymers have been defined biocompatible in numerous research **[24]**. Similarly, bioactive glass, tricalcium phosphate (TCP), a large amount of metal oxides (such as alumina and zirconia) and the aforementioned hydroxyapatite (HA) have been considered as bioactive fillers. These kind of ceramic materials are able to react with physiological fluids, forming an active layer of apatite on the surface. When in contact with living tissues, this apatite form a strong link between the tissues and itself. This ability is called bioactivity **[25]**.

1.2 Bioactive composites: Structure, properties and interactions

1.2.1 General aspects about bioactive composites

A bioactive composite is a composite material in which one or more components show bioactivity. For many biomedical applications, it is essential to improve the mechanical performance of the polymer matrix. As previously discussed, materials intended for prosthetic applications must simulate the bone mechanical properties. The bone has the young modulus that varies between 7 and 30 GPa depending on the type of bone considered, 1-3% of elongation at break and 50-150 MPa for the tensile strength **[26]**. In addition, the bones are subjected to a stress of about 4 MPa during daily activities and a hip joint must bear up to three times the weight of the human body, with peaks, which occur for example during a jump, up to 10 times **[26]**. In order to be used for these applications, the polymer matrix have to be therefore reinforced with suitable fillers.

Two types of fillers are used as components for biomedical composites: fibres and particles. Generally, these are harder and stronger than the matrix in order to improve its mechanical properties. The resulting properties of biomedical compounds depend on several factors, some of which are summarized here and will be discussed in detail in the next paragraphs.

- Filler properties, shape, size and size distribution
- Matrix properties and its molecular weight
- Distribution of the filler in the matrix
- Interfaces between matrix and filler

1.2.2 Influence of the filler properties on the mechanical behavior of the bioactive composites

The physical properties of the filler play a fundamental role in determining the final mechanical properties of a bioactive composite.

In the theoretical treatment of the mechanical behavior of a composite material, it is assumed that the fillers have a spherical shape. In practice, they may have irregular, sometimes flat or acicular shapes. For example, HA particles have an irregular shape, formed by several crystallites strongly linked together **[10]**. Particles with irregular shape have a greater reinforcement effect than spherical ones **[27]**. This behavior can be explained considering that, during the processing, the polymer in the molten state can hook itself to the particles going to form mechanical interlocks when the material is brought to the operating temperature **[24,27]**. In the absence of chemical bonds between matrix and particles, the spherical fillers are more easily detached from the matrix by mechanical stress than fillers of irregular shape. On the other hand, fillers of irregular and porous shape can undergo rupture as a result of the stress shear applied during the processing step. TCP particles are an example of this type of fillers **[10]**.

Another important factor to take in consideration is the average particles size. The aggregation tendency of fillers increases with decreasing particles size **[28]**. Very small particles have a high surface energy and a greater tendency to aggregate. The formation of aggregates can lead to an unevenness in particle distribution which results in the formation of crack initiation sites in impact **[28,29]**. The forces that play a fundamental role in adhesion among the particles are schematized in figure 1.2. According to Hornsby **[30]**, they are mechanical interlocking, electrostatic forces, van der Waals forces, liquid bridges, and solid bridging in increasing order of adhesive strength.

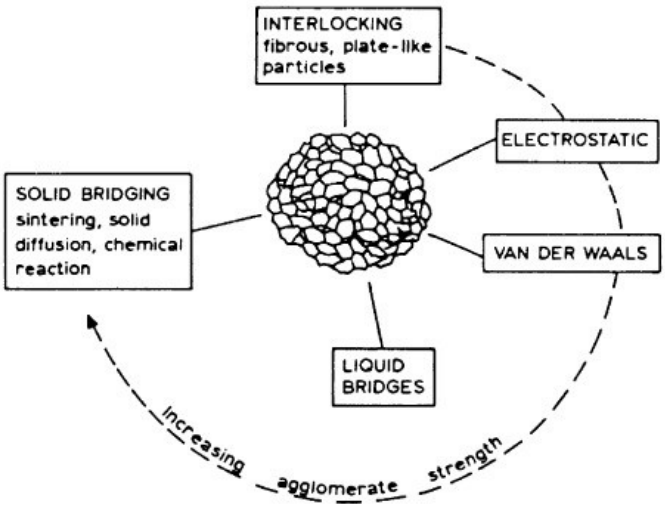

Figure 1.2: Adhesion forces in an agglomerate of particles in increasing order of adhesive strength. **[24]**

For the same reason, particles of very large dimensions dramatically alter the properties of the composite leading to a premature rupture of the material when subjected to a load **[27]**. The dispersion and the distribution of the fillers into the matrix can be evaluated by employing scanning electron microscopy (SEM) and other image analysis technique.

The wear behavior of the composites is also influenced by size, shape and hardness of the particles **[27]**. Filler addition can increase or reduce the friction coefficient of the resulting material with respect to the polymer matrix. The reduction of the friction coefficient seems to depend substantially on the deformability of the fillers and its consequent compaction **[31]**. Another factor that can influence the wear behavior is the particle size. Small and well dispersed particles seem to decrease the friction coefficient.

1.2.3 Influence of polymer matrix crystallinity and molecular weight on the mechanical behavior of the bioactive composites

Semi-crystalline polymers are the most commonly used class of materials as matrix of bioactive composite for prosthetic applications. HDPE, UHMWPE, PEEK, PMMA are typical examples of this kind of polymers. They are biocompatible and do not interact with body fluids, and then they are called bio-inert **[8]**. The mechanical properties of these polymers depend substantially on the respective amount of amorphous and crystalline phases and on the size of the crystallites **[32]**. The presence of the filler can modify the crystalline nature of polymer-matrices.

The most important effect of the filler on the matrices is to be able to behave as a nucleating agent. During the transition from molten to solid state, following the processing of composite material, a nucleating agent promotes the crystallization of polymeric matrices leading to a possible increase in the crystalline phase and to the change in the size of the spherulites. The addition of nucleating agents to semi-crystalline polymers, results in a rapid growth of the spherulites with greater speed which can lead to an improvement of some mechanical properties, such as flexural modulus, strength and stiffness **[33,34]**. The nucleating effect of talc used as filler of PP was extensively studied **[35]**. Similar effects have been found with different layer silicates, like MMT **[34,36]**, and $CaCO_3$ **[33]**. In general, the nucleating effect may depend on a large number of factors, including the particle size, their surface area, and their concentration and distribution into the polymeric matrix **[37]**. Small particles can have more important nucleating effects than larger ones. Nucleating effect could be neglected for composites at high filler concentration **[37]**.

A further factor to consider is the average molecular weight of the polymeric matrix, which in addition to influencing its mechanical properties (hardness, strength and modulus) can also determine its crystallization behavior. In the biomedical field, where the mechanical behavior of the

resulting material is fundamental, it would be advisable to choose polymer with high average molecular weight. However, it should be borne in mind that high molecular weight polymers are even more viscous and therefore difficult to process, which is why it is necessary to find a good compromise **[38]**.

1.2.4 Influence of interfacial interaction between filler and matrix

Interfacial interactions between the components of a composite material play a decisive role in the determination of the mechanical properties of the resulting material. Very strong interactions between the phases lead to the formation of composite materials with high mechanical performance. Polymers used as matrix and their fillers could have the most different physical and chemical structures, thus a wide variety of interactions could be established between them. These interactions between the phases can have very different strength. Ionic, covalent and metallic bonds are called primary forces **[39]**. These forces are very strong but rarely occur spontaneously between the phases of the resulting material and, mainly, they occur following special surface treatments of the filler. Instead, van der Waals forces, dipole-dipole interactions and London dispersion forces are secondary interactions that occur more frequently **[39]**.

Generally, the strongest interaction is achieved between surfaces having opposite polarity and high surface energies. However, evaluating the interfacial tension between the components is not easy. Not being directly measurable, it can be derived from thermodynamic calculations that take into account the surface tensions of the starting components, which allows to obtain a good reliability in predicting the macroscopic properties of the composites, especially for apolar systems **[37,40]**.

1.3 Polyethylene in biomedical field: state of the art

Polyethylene is the most widely produced thermoplastic polymer worldwide and one of the most consumable product in everyone's daily life.

Because of its high mechanical ductility and other important characteristics, polyethylene is considered a unique material, used in various industrial applications such as health and energy. Polyethylene processing is simple and inexpensive and it is widely used in the biomedical field where is recognized as a "gold standard" due to its biocompatibility and chemical inertia. Indeed, a large amount of devices in cardiovascular treatments and reconstructive surgery **[41-43]** have been developed using different types of polyethylene.

Starting from the pioneering work of Bonfield **[15]**, using HA as the bioactive and reinforcing phase in HDPE to produce a bone analogue, polyethylene was also identified as a suitable material for the realization of bioactive composites for prosthetic applications. Hydroxyapatite (HA) reinforced high density polyethylene (HA/HDPE) composite has been the first bioactive ceramic–polymer composite tailored with the aim to mimic the structure and match the bone properties. At high content of HA, the comprehensive performance of the HA/HDPE system, especially the bioactivity, was improved. In particular, the material containing 40 vol% of HA has been patented under the trade name of HAPEX™, which has been used in clinical applications as example for the orbital floor prostheses **[44]**, and middle ear implants **[45]**.

The reason why it is advantageous to use polyethylene as polymer matrix is that it allows the incorporation of a large amount of bioceramic particles, remaining easily processable even at high concentration of filler. In addition, polyethylene is a linear polymer whose molecular chains can be oriented using special processing techniques to improve its final mechanical properties **[46]**. This way, different types of polyethylene were also used for scientific research and for product development like Ultra-high-molecular-weight polyethylene (UHMWPE), introduced clinically for joint replacements

in 1962, widely used for total joint arthroplasty bearings **[47]** and different grades of HDPE have been exploited in various study filled with different particles **[22,48,49]**. Unfortunately, the poor mechanical properties of these materials, such as a low tensile strength (17–23 MPa), have limited their application to none or modest load-bearing bone substitutes.

1.3.1 Synthesis, structure and properties of polyethylene

Polyethylene is a thermoplastic polymer: it melts above a specific temperature and solidifies with cooling in a reversible process that can be repeated cyclically without leading to a significant degradation of the polymer **[50]**. This important property allows the extensive use of polyethylene on an industrial level, as a material for plastic packaging and construction materials. Cristallinity degree of polyethylene can vary greatly and this can affect its density and chemical stability. **[50]**. Most types of polyethylene are highly resistant to many chemicals and can be dissolved only at high temperatures in a short number of solvents, including toluene, xylene and trichlorobenzene.

Numerous methods have been developed for the production of polyethylene, among which the most common was developed by Ziegler and Natta, and consists in the polymerization process of pure ethylene using as catalyst titanium (III) chloride. **[51]**. Metallocene catalysts, metal ions inserted between two carbon-based rings, are also used in order to control the polymerization process and the structure of the produced polyethylene **[50]**. Choosing a catalyst rather than another makes it is possible to obtain polyethylene with different density and with different molecular weights.

Density is directly related to crystalline content and in fact can be used to estimate the crystallinity in polyethylene. It ranges between 0.88 and 0.96 g/cm^3. Polyethylene can be classified according to its molecular weight, its density and its branching (figure 1.3) **[50]**:

Low density PE (LDPE) has a density that varies between of 0.917 – 0.930 g/cm^3. It is produced only by free radical polymerization of ethylene initiated by organic peroxides or other reagents that readily decompose into free radicals. LDPE is highly branched and shows high ductility but low tensile strength with respect other polyethylene varieties. Its high amorphous content results in outstanding clarity in film for food packaging, a major application.

Linear low density PE (LLDPE) has a density that varies between of 0.915 – 0.930 g/cm^3. It is a more linear type of LDPE, with shorter branches and higher tensile strength. LLDPE is produced by copolymerization of ethylene with α-olefins using Ziegler-Natta catalyst, supported chromium or single site catalysts and cannot be produced by free radical polymerization. Its applications include a wide range of products such as toys, containers and pipes **[41]**.

Medium density PE (MDPE) has a density that varies between 0.930 – 0.940 g/cm^3. It has a linear structure similar to LLDPE, but comonomer content is lower. Typical applications involve the production of geomembrane and pipe.

High density PE (HDPE) is the most common type of polyethylene, given its extremely cheap production process. Its density ranges between of 0.940 – 0.970 g/cm^3. It is produced by polymerization of ethylene using Ziegler-Natta or supported chromium ("Phillips") catalysts conducted at low pressure. HDPE has higher modulus, yield and tensile properties with respect to LLDPE and MDPE. However, because it has higher crystallinity, HDPE cannot match the clarity of LDPE or LLDPE film. HDPE is widely used in extruded pipe for potable water and gas distribution and is commonly used in medical implant devices.

Ultra high molecular weight PE (UHMWPE) has extremely long polymer chains, which give the material the properties suitable for high load applications. Indeed, long chains make stronger the structure of the polymer by transferring the load on the polymer backbone more effectively through overlapping bonds **[41]**. It has a high resistance to abrasion and

corrosion of chemical agents. UHMWPE has a surprisingly low density (0.94 g/cm^3), most likely owing to crystalline defects and lamellar effects caused by the enormously long polymer chain. It can be obtained in fibers shape, which exhibit tensile strength many times higher than steel and is often incorporated into high-performance equipment such as bulletproof vests. Other applications involves UHMWPE as a constituent of medical devices such as artificial hips **[41]**.

Cross-linked PE (XLPE) is produced by cross linking of HDPE or MDPE using free radicals generated by peroxides, ultraviolet or electron beam irradiation. Its properties are more like a thermoset than a thermoplastic, with an improving of the chemical resistance as well as dielectric properties compared to its uncrosslinked form. Applications of XLPE include replacing copper as a plumbing and electrical cable material as well as for ducts and automotive housings.

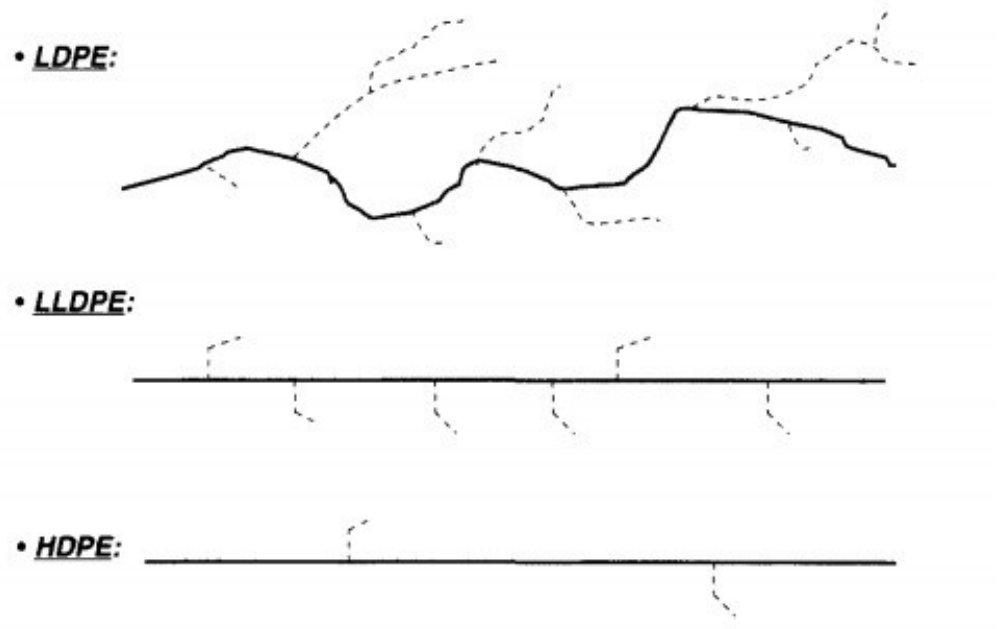

Figure 1.3: Schematic representation of the microstructure of mainly type of polyethylene. **[50]**

1.3.2 Biocompatibility and biodegradation of polyethylene

The fact that PE has proved to be biocompatible has played a key role in the success this material has achieved in the biomedical field. Its biocompatibility has been extensively studied and confirmed in several *in vitro* and *in vivo* studies. Researchers have examined the biological response of a large amount of orthopedic implants, including UHMWPE implants for hip replacements, and observed that, while the bulk properties of the entire implant appear to be biocompatible particles formation as a result of wear processes can induce inflammatory reactions at the surgical site **[52]**.

In times when the waste disposal is a widely felt problem, the high chemical and mechanical PE stability is well known. As example, the degradation of a PE bag can last from 10 to 1000 years, depending on the environment in which it degrades (presence of light, water, chemical and physical agents). If this feature is a big problem for waste disposal, the high chemical stability of polyethylene (bio-inertia) is a huge advantage for the use of this material in the biomedical field, where the production of permanent and highly stable implants is required.

1.3.3 Mechanical properties, oxidative stability, and wear behavior of polyethylene

Among various type of polyethylene, high density polyethylene (HDPE) glass transition occurs at about -100°C and its melting temperature is about 130°C **[50]**. This allows HDPE to be used in a very wide temperature range ranging from -50 to 100 °C.

Mechanical properties strongly depend on the molecular weight of the polymer and on its density as well as its crystallinity degree. Generally,

HDPE has a young modulus of about 800-1000 MPa and a tensile strength of about 15-20 MPa **[50]**.

Polyethylene undergoes photodegradation if exposed to UV rays, which leads to a thermal oxidation and to the consequent loss of color and to a fall of the mechanical performance. For this reason, photodegradation processes can have negative effects also on the lifetime of PE products **[53]**. Photo and thermal oxidation mechanism of polyethylene have been studied extensively. The surface oxidation of polyethylene can also be generated within the human body, caused by the highly aggressive character of body fluids. The oxidative processes of the matrix can lead to the degradation of the polymer, with consequent deterioration of the mechanical properties of the implant **[54]**.

The wear behavior of polyethylene-based implants has been widely studied in order to increase their longevity, in particular for implants used in total knee or hip arthroplasty, usually subjected to higher stress. In this view, a large amount of polyethylene acetabular cup devices, including those consisting of XPE and UHMWPE, was studied using a hip joint simulator for up to 2 million cycles *in vitro*. Significant mass loss was observed in the devices, using micro-Raman spectroscopy to evaluate stress-induced crystallization **[55]**.

A study conducted in vivo on over 120 patients revealed that, after 10 years, XPE acetabular cup linings has significantly lower wear and a higher implant survival rate compared to the UHMWPE ones **[56]**. Further research has involved the use of both computational gait models **[57]** and clinical studies **[58]** to predict and assess the impact of patient gait on implant wear behavior.

1.4 Description of the thesis work

Substantial research efforts have been invested to develop bioactive composites as bone analogue replacement materials by reinforcing polyethylene (PE) with different bioactive molecules. Main advantages of using polyethylene as the matrix materials of bioactive composites include its biocompatibility, that allow the use of polyethylene in a wide range of biomedical applications. In addition, polyethylene is a cheap polymer, easy to process, with a high ductility, which allows the incorporation of a large amount of bioceramic particles in the system, such that even composites with a higher amount of fillers can be processed with the most common and cheaper melt extrusion techniques. However, the use of HDPE as material for bone replacement application is limited by its poor mechanical properties (in particular its low young modulus and low tensile strength) and by the fact that PE is not bioactive.

Over the years, different fillers have been considered to enhance the mechanical properties of PE and to endow it with bioactivity. The system hydroxyapatite (HA)/high density polyethylene (HDPE) was the first bioactive composite used to mimic the structure of a bone, since its employment as material for middle ear implant **[15,21]**, which has paved the way for the development of other bioactive composites using the same strategy. Also bioglasses were considered as filler of HDPE in order to enhance the bioactivity in a shorter period of time **[22]**, since they are more bioactive than HA. The composite containing up to 30% of bioglass has shown mechanical properties comparable to those of soft connective tissues.

With the aim to improve the mechanical properties of these composites, different strategies were adopted. Nath et al. **[59]** have considered the use of alumina coupled with HA to improve the stiffness, the hardness as well as the biocompatibility of the composite, obtaining promising results in terms of enhancement of the young modulus and biological response.

Unfortunately, the low tensile strength (17–23 MPa) of these materials, has limited their application to none or modest load-bearing bone substitutes.

In order to overcome these drawbacks, an interesting approach has been used coupling HA with zirconia particles, reinforced with 4 wt% CaO **[60,61],** with the aim to stabilize tetragonal form of zirconia (TZP), which is a well-known material with high toughness and hardness **[62]**. This approach has led to obtaining materials with good mechanical properties: indeed, the presence of zirconia positively affected the biological behavior of the composites, that was still higher than HDPE/HA system. **[61]**. Among the various types of TZP, Alumina toughened Zirconia (ATZ) has proved to be very interesting for applications in the biomedical field **[62-64]**.

Recently, the addition of small amount of ATZ to Ultra High Molecular Weight Polyethylene (UHMWPE) has been proven as a promising way to enhance Young modulus, yield stress and hardness, without compromising the other mechanical parameters **[65,66]**. Surprisingly, small amount of ATZ was able to enhance hydrophobicity and cell interaction (adhesion and viability) with respect to those of the unfilled polymer **[65,66]** extending the possible applications of UHMWPE in the biomedical field.

In this light, materials at different concentration of ATZ in High Density Polyethylene (HDPE), cheaper and easy to process than UHMWPE, have been prepared by melt extrusion technique with the aim to achieve a bioactive composite material with good mechanical properties (young modulus, storage modulus, wear behavior) intended as a material for prosthetic device.

With the same rationale, chitosan **[67]** has been explored as possible filler for bioactive composites intended for bone replacement applications. Among the many interesting properties that chitosan can give to a material designed for the biomedical field, its proven antibacterial activity can play a fundamental role to avoid possible complication due to infections onset in the surgical site. **[68]**. In order to explore the effect of chitosan on the mechanical properties of the HDPE, two set of materials were prepared with

two kind of chitosan, which differ from each other in particle size and morphology.

In the last part of this thesis work, radiation-induced grafting of HDPE-ATZ composites with chitosan has been probed to induce a surface modification of these composites, in order to match the reinforcing effect of the ATZ with the antimicrobial activity of the chitosan. The grafting was initiated by irradiation with a low energy electron beam system **[69]**.

Among the materials prepared in this work, the most interesting composites have been subjected to biological assays, in order to evaluate the influence of ATZ, chitosan and radiation processing on the biological behavior of the HDPE.

1.4.1 Thesis structure

The preparation of HDPE/ATZ composites containing different amount of ATZ by melt extrusion process will be described in Chapter 2. A morphological investigation was carried out to find a correlation between the mechanical properties of the materials with the distribution and the dispersion of ATZ into the HDPE. Also the thermal properties of the composites and their thermo-degradation were investigated.

Chapter 3 is focused on the study of the HDPE/chitosan composites, obtained by melting extrusion. Two type of chitosan (labeled as Chitosan M and Chitosan N, related their Micrometer or Nanometer dimensions) have been considered to prepare set of composites HDPE/chitosan at different concentration of chitosan. The thermal properties, thermal degradation and morphology of the raw chitosan have been investigated. The phase morphology occurring in HDPE/chitosan system has been investigated by Scanning Electron Microscopy and XRD powder diffraction to evaluate their

compatibility. Also, mechanical and thermomechanical behavior has been studied.

In Chapter 4 the study about the surface modification of HDPE/ATZ composites with chitosan, induced by irradiation with a low energy electron beam system is reported. Chitosan grafting was conducted on HDPE and HDPE filled samples, exploring different reaction conditions with the aim to find the most efficient. The process feasibility was followed measuring the change of surface wettability by contact angle measurements. ATR spectroscopy was performed to provide further evidence about this surface modification process. The influence of irradiation on the mechanical properties of the bulk materials was also evaluated.

The biological response of the HDPE-based composites is discussed in chapter 5. Cell adhesion and cell viability assays were conducted with a cell line of fibroblasts. The morphology of the cells attached after 24h was observed by SEM. Biological assays results have been compared with the surface wettability in order to understand the main features affecting the cells response.

Each chapter will consist of a brief introduction and a discussion about the obtained results and finally some conclusions. The materials, the methods of preparation of the composites and the characterization techniques will be reported in the Appendix 1 and 2.

1.5 Bibliography

[1] Hildebrand H. F. Biomaterials – a history of 7000 years *BioNanoMat* **(2013)** 14(3-4); 119–133.
[2] Park J.B., Lakes R.S. Biomaterials: an introduction, 3th ed. New York: Springer, **(2007)**.
[3] Definitions in biomaterials: proceedings of a consensus conference of the European Society for Biomaterials, Chester, England, March 3-5, 1986.
[4] Williams D.F. On the nature of biomaterials *Biomaterials* **(2009)** 30; 5897–5909.
[5] Breme H.J., Biehl V., Helsen J.A. Metal as biomaterials, Chichester: Wiley, **(1998)**.
[6] Variola F., Brunski J.B., Orsini G., de Oliveira P.T., Wazen R., Nanci A. Nanoscale surface modifications of medically relevant metals: state-of-the art and perspectives *Nanoscale* **(2011)** 3; 335–353.
[7] Liu X., Chu P.K., Ding C. Surface modification of titanium, titanium alloys, and related materials for biomedical applications *Mater Sci Eng R* **(2004)** 47; 49–121.
[8] Teo A.J.T., Mishra A., Park I., Kim Y.J., Park W.T, Yoon Y.J. Polymeric biomaterials for medical implants and devices *ACS Biomater. Sci. Eng.* **(2016)** 2; 454−472
[9] Duraccio D., Mussano F., Faga M.G. Biomaterials for dental implants: current and future trends, *J Materials Science* **(2015)** 50; 4779-4812.
[10] Hench L.L., Wilson J. An Introduction to Bioceramics Singapore: World Scientific **(1993)** Vol. 1.
[11] Shi J., Votruba A.R., Farokhzad O.C., Langer R. Nanotechnology in drug delivery and tissue engineering: From discovery to applications. *Nano. Lett.* **(2010)** 10; 3223–3230
[12] Ramakrishna S., Mayer J., Wintermantel E., Leong K.W. *Compos Sci Technol* **(2001)** 61; 1189–224.
[13] Christel P., Claes L., Brown S.A. Carbon reinforced composites in orthopedic surgery. In: Szycher M. editor High Performance Biomaterials: A comprehensive Guide to Medical and Pharmaceutical Applications. Lancaster (USA): *Technomic* **(1991)** 499-518.
[14] Huiskes R. Some fundamental aspects of human-joint replacement *Acta Orthop Scand* **(1980)** 185.
[15] Bonfield W., Grynpas M.D., Tully A.E., Bowman J., Abram J. Hydroxyapatite reinforced polyethylene - a mechanically compatible implant material for bone replacement *Biomaterials* **(1981)** 2; 185-186
[16] Bonfield W., Wang M., Tanner K.E. Interfaces in analogue biomaterials *Acta Mater* **(1998)** 46; 2509–18
[17] Hull D., Clyne T.W. An introduction to composite materials, 2nd Ed. Cambridge: *Cambridge University Press* **(1996)**.

[18] Rho J.Y., Kuhn-Spearing L., Zioupos P. Mechanical properties and the hierarchical structure of bone *Medical Engineering & Physics* **(1998)** 20; 92–102.
[19] Baidya K.P., Ramakrishna S., Rahman M., Ritchie A. Quantitative radiographic analysis of fiber reinforced polymer composites *J Biomater Appl* (2001) 15; 279-289.
[20] Guild F.J., Bonfield W. Predictive modelling of hydroxyapatite-polyethylene composite *Biomaterials* **(1993)** 14; 985-993
[21] Swain R.E., Wang M., Beale B., Bonfield W. HAPEX (TM) for otologic applications *Biomed Eng: Appl Basis Commun* **(1999)** 11; 315-20
[22] Wang M., Hench L. L., Bonfield W. Bioglass®/high density polyethylene composite for soft tissue applications: preparation and evaluation *J Biomed Mater Res* **(1998)** 42; 577-586
[23] Bakar M.S.A., Cheang P., Khor K.A. Tensile properties and microstructural analysis of spheroidized hydroxyapatite – poly (etheretherketone) biocomposites *Mater Sci Eng A* **(2003)** 345; 55–63.
[24] Wang M. Developing bioactive composite materials for tissue replacement *Biomaterials* **(2003)** 24; 2133–215.
[25] Kokubo T., Takadama H. How useful is SBF in predicting in vivo bone bioactivity? *Biomaterials* **(2006)** 27; 2907-2915
[26] Black J., Hastings G.W. Handbook of biomaterials properties London: *Chapman and Hall* **(1998).**
[27] Pukánszky B., in: J. Karger-Kocsis Editors, Polypropylene. Structure, Blends and Composites, London: *Chapman and Hall*, **(1995)** p. 1.
[28] Pukánszky B., Móczó J. Morphology and properties of particulate filled polymers *Macromol. Symp.* **(2004)** 214; 115-134.
[29] Fekete E., Molnár Sz., Kim G.M., Michler G.H., Pukánszky B. Aggregation, fracture initiation, and strength of PP/CaCO3 composites *J. Macromol. Sci. Phys.* **(1999)** B38; 885.
[30] Hornsby P.R., in: Rothon R.N. Editors, Particulate-Filled Polymer Composites, Shrewsbury: *Rapra Technology*, **(2003).**
[31] Schwartz C.J., Bahadur S. The role of filler deformability, filler–polymer bonding, and counterface material on the tribological behavior of polyphenylene sulfide (PPS) *Wear* **(2001)** 251; 1532–1540.
[32] Samuels R.J., Structured Polymer Properties, New York: *John Wiley* **(1974)**.
[33] Tanniru M., Misra R.D.K. On enhanced impact strength of calcium carbonate-reinforced high-density polyethylene composites *Mater Sci Eng A* **(2005)** 405; 178–193.
[34] Yuan Q., Misra R.D.K. Impact fracture behavior of clay–reinforced polypropylene nanocomposites *Polymer* **(2006)** 47; 4421-4433.
[35] Fujiyama M., Wakino T. Structures and properties of injection moldings of crystallization nucleator-added polypropylenes. I. Structure–property relationships *J. Appl. Polym. Sci.* **(1991)** 42; 2739.
[36] Maiti P., Nam P.H., Okamoto M., Hasegawa N., Usuki A. Influence of crystallization on intercalation, morphology, and mechanical properties of polypropylene/clay nanocomposites *Macromolecules* **(2002)** 35; 2042-2049.
[37] Móczó J., Pukánszky B. Polymer micro and nanocomposites: Structure, interactions, properties *J. Ind. Eng. Chem.* **(2008)** 14; 535–563.

[38] Callister W.D. Materials science and engineering: an introduction, 4th ed. New York: *Wiley* **(1997)**.
[39] Allen K.W. Physics and adhesion *Phys. Technol.* **(1988)** 19; 234.
[40] Berthier J. Microdrops and Digital Microfluidics: Processing, Development, and Applications 2nd Ed. *William Andrew Publishing* **(2017)** p. 41.
[41] Paxton N.C., Allenby M.C., Lewis P.M., Woodruff M.A. Biomedical applications of polyethylene *Eur. Polym. J.* **(2019)** 118; 412–428.
[42] Lam M.T., Wu J.C. Biomaterial applications in cardiovascular tissue repair and regeneration, *Expert Rev. Cardiovasc. Ther.* **(2012)** 10; 1039–1049.
[43] Sevin K., Askar I., Saray A., Yormuk E. Exposure of high-density porous polyethylene (Medpor®) used for contour restoration and treatment *Br J Oral Maxillofac Surg* **(2000)** 38; 44–49.
[44] Downes R.N., Vardy S., K. Tanner K.E., Bonfield W., Hydroxyapatite-polyethylene composite in orbital surgery *Bioceramics*, **(1991)** 4; 239-246.
[45] Dornhoffer J.L. Hearing results with the Dornhoffer ossicular replacement prostheses *The Laryngoscope* **(1998)** 108; 531–536.
[46] Hofmann D., Kurek A., Thomann R., Schwabe J., Mark S., Enders M., Hees T., Mülhaupt R. Tailored Nanostructured HDPE Wax/UHMWPE Reactor Blends as Additives for Melt-Processable All-Polyethylene Composites and in Situ UHMWPE Fiber Reinforcement *Macromolecules* **(2017)** 50; 8129-8139.
[47] Kurtz S.M., UHMWPE Biomaterials Handbook: Ultra High Molecular Weight Polyethylene in Total Joint Replacement and Medical Devices *Academic Press* **(2015)**.
[48] Wang M., Porter D., Bonfield W.. Processing, characterization, and evaluation of hydroxyapatite reinforced polyethylene composites. *Br Ceram Trans* **(1994)** 93; 91–95.
[49] Juhasz J.A., Best S.M., Brooks R., Kawashita M., Miyata N., Kokubo T., Nakamura T., Bonfield W. Mechanical properties of glass-ceramic A–W-polyethylene composites: effect of filler content and particle size *Biomaterials* **(2004)** 25; 949–955.
[50] Peacock A.J., Handbook of Polyethylene: Structures, Properties and Applications New York: *Marcel Dekker* **(2000)**.
[51] Boor J. Ziegler-Natta catalysts and polymerizations *Academic Press* **(1979)**.
[52] Gibon E., Córdova L.A., Lu L., Lin T.H., Yao Z., Hamadouche M., Goodman S.B. The biological response to orthopedic implants for joint replacement. II: Polyethylene, ceramics, PMMA, and the *foreign body reaction, J. Biomed. Mater. Res. – Part B Appl. Biomater.* **(2017)** 105; 1685–1691.
[53] Chew C., The mechanism of polyethylene oxidation, *J. Appl. Polym. Sci.* **(1959)** 2; 281–288.
[54] Gardette M., Perthue A., Gardette J.L., Janecska T., Földes E., Pukánszky B., Therias S. Photo- and thermal-oxidation of polyethylene: comparison of mechanisms and influence of unsaturation content *Polym. Degrad. Stab.* **(2013)** 98; 2383–2390.
[55] Affatato S., Freccero N., Taddei P. The biomaterials challenge: a comparison of polyethylene wear using a hip joint simulator *J. Mech. Behav. Biomed. Mater.* **(2016)** 53; 40–48.

[56] Devane P.A., Horne J.G., Ashmore A., Mutimer J., Kim W., Stanley J. Highly cross-linked polyethylene reduces wear and revision rates in total hip arthroplasty: a 10-year double-blinded randomized controlled trial *J. Bone Joint Surg. Am.* **(2017)** 99; 1703–1714.
[57] Kang K.T., Son J., Kim H.J., Baek C., Kwon O.R., Koh Y.G. Wear predictions for UHMWPE material with various surface properties used on the femoral component in total knee arthroplasty: a computational simulation study *J. Mater. Sci. Mater. Med.* **(2017)** 28;
[58] Ardestani M.M., Amenabar Edwards P.P, Wimmer M.A. Prediction of polyethylene wear rates from gait biomechanics and implant positioning in total hip replacement *Clin. Orthop. Relat. Res.* **(2017)** 475; 2027–2042.
[59] Nath S., Bodhak S., Basu B. HDPE-Al2O3-HAp Composites for Biomedical Applications: Processing and Characterizations *J Biomed Mater Res Part B: Appl Biomater* **(2009)** 88B; 1–11.
[60] Yari Sadi A., Homaeigohar S.S.,Khavandi A.R., Javadpour J. The effect of partially stabilized zirconia on the mechanical properties of the hydroxyapatite–polyethylene composites *J Mater Sci Mater Med* **(2004)** 15; 853-858.
[61] Yari Sadi A., Shokrgozar M.A., Homaeigohar S.S.,Khavandi A.R. Biological evaluation of partially stabilized zirconia added HA/HDPE composites with osteoblast and fibroblast cell lines *J Mater Sci Mater Med* **(2008)** 19; 2359-2365.
[62] Piconi C., Maccauro G. Zirconia as a ceramic biomaterial *Biomaterials* **(1999)** 20; 1-25.
[63] Piconi C., Burger W., Richter H.G., Cittadini A., Maccauro G., Covacci V., Bruzzese N., Ricci G.A., Marmo E. Y–TZP ceramics for artificial joint replacements. *Biomaterials* **(1998)** 19; 1489–9.
[64] Kohal R. J., Baechle M., Han J. S., Hueren D., Huebner U., Butz F. In vitro reaction of human osteoblasts on alumina-toughened zirconia *Clin Oral Implants Res* **(2009)** 20; 1265–71.
[65] Duraccio D., Strongone V., Malucelli G., Auriemma F., De Rosa C., Mussano F.D., Genova T., Faga M.G. The role of alumina-zirconia loading on the mechanical and biological properties of UHMWPE for biomedical applications *Composites Part B* **(2019)** 164; 800–808.
[66] Duraccio D., Strongone V., Faga M.G, Auriemma F., Mussano F., Genova T., Malucelli G. The role of different dry-mixing techniques on the mechanical and biological behavior of UHMWPE/alumina-zirconia composites for biomedical applications *European Polymer Journal* **(2019)** 120; 109274.
[67] Kean T., Thanou M. Biodegradation, biodistribution and toxicity of chitosan *Adv. Drug Delivery Rev.* **(2010)** 62; 3–11.
[68] Anitha A., Sowmya S., Kumar P.T.S., Deepthi S., Chennazhi K.P., Ehrlich H., Tsurkan M., Jayakumar R. Chitin and chitosan in selected biomedical applications Prog. Polym. Sci. **(2014)** 39; 1644–1667.
[69] Ferry M., Ngono-Ravache Y., Aymes-Chodur C., Clochard M.C., Coqueret X., Cortella L., Pellizzi E., Rouif S., Esnouf S. Ionizing radiation effects in polymers: Reference Module in Materials Science and Materials Engineering Oxford: *Elsevier* **(2016).**

Chapter 2

Alumina toughened Zirconia (ATZ) as filler of HDPE-based composites for biomedical purpose

2.1 Introduction

2.1.1 Zirconia as biomaterial: the Alumina Toughened Zirconia (ATZ)

Zirconia is the zirconium dioxide, one of the most studied ceramic materials, whose use in biomedical field has been explored since the 1960s. In particular, Helmer et al. **[1]** published the first paper concerning the use of zirconium oxide as biomaterial in 1969. As main application field, zirconia was employed to manufacture ball heads for Total Hip Replacement (THR) as a possible alternative to Alumina **[2]** and most recently it is used as material for dental implants. **[3]**. The interest about the use of zirconia in biomedical field is justified by its excellent mechanical properties, in particular high strength, high toughness (if

compared to other ceramic materials) and a young modulus comparable to the that of stainless steels **[3]**.

Zirconia shows three different crystalline structures: monoclinic, tetragonal and cubic. At room temperature, zirconia exists in the monoclinic phase, stable up to 1170°C **[3]**. In the monoclinic phase, zirconia shows lower mechanical performances compared to those of tetragonal zirconia, which is not stable at room temperature **[3]**. With the aim to stabilize the tetragonal form of zirconia, several metal oxides (as example MgO, Y_2O_3, CaO and CeO_2) have been added to pure zirconia. In particular, the system ZrO_2-Y_2O_3 leads to the formation of tetragonal form only, called tetragonal zirconia polycrystals (TZP) **[4]**. Despite the presence of yttria, the tetragonal form of zirconia evolves to the monoclinic one between 200 and 300 ° C, and, at lower temperatures, the process is strongly catalysed by the presence of water, widely present *in vivo* **[5,6]**. This behavior leads to an increase of the volume of TZP, which could lead to a rupture of the zirconia structure and to a dramatic loss of its mechanical performance **[7]**. For this reason, the suitability of TZP to replace alumina in THR has been strongly reconsidered.

Recently, the development of new ceramic composites materials, constituted by alumina and TZP, has resulted in a renewed interest in the use of these materials in the biomedical field. In particular, TZP reinforced with alumina, named as Alumina toughened Zirconia (ATZ) has been developed for biomedical purpose **[8,9]**.

The presence of alumina hinders the transition from the tetragonal to the monoclinic phase, owing mainly to the formation of a stiff matrix able to cage the zirconia particles in a metastable tetragonal state, thus acting as mechanical stabilizer **[8]**. Furthermore, the combination between the hard and stiff alumina and the high strength and tough zirconia leads to the formation of a material with a remarkable resistance to crack growth **[10]**. The ATZ mechanical properties, compared with those of monolithic alumina and TZP, are reported in Table 2.1.

Table 2.1: Physical and mechanical properties of ATZ, TZP and alumina. Values extracted from [10]

	ATZ	TZP	Alumina
Density (g/cm^3)	5.5	6.1	4
Microhardness (Vickers)	1000-1200	1000-1300	2300
Young's modulus (GPa)	220	200	420
Bending Strength (MPa)	2000	1200	500
Toughness KIC ($MPa*m^{1/2}$)	8	9-10	4

As discussed in chapter 1, good mechanical performance are not the only requirement for bone replacement materials. In fact, a key role is played by biocompatibility and bioactivity **[24]** (section 1.1.2), the last one necessary for the osseointegration of the prosthetic device. In this respect, ATZ has proved to be a biocompatible material, showing a good interaction with the biological environment **[11,12]**. Furthermore, the addition of a small amount of ATZ to Ultra High Molecular Weight Polyethylene (UHMWPE) has been proven as a promising way to enhance Young modulus, yield stress and hardness, without compromising the other mechanical parameters **[13]**. A small amount of ATZ is able to enhance hydrophobicity and cell interaction (adhesion and viability) with respect to those of the unfilled polymer **[13]**.

For these reasons, ATZ represents a promising candidate as a filler able to endow HDPE with enhanced mechanical properties and biological response.

2.1.2 Description of the chapter work

This chapter deals with the preparation and the characterization of the HDPE/ATZ composites, aimed at understanding the role of ATZ amount, distribution and dispersion on the structural and mechanical properties of the composites. Several composites were prepared by melt extrusion technique using different amount of ATZ (1, 2, 3, 5, 7 and 12wt%). The morphological and structural properties of the composites were studied by means of scanning electron microscopy (SEM) and wide angle x-rays diffraction scattering (WAXS). Mechanical properties were evaluated at room temperature during stress-strain experiments as well as in temperature using dynamical mechanical thermal analysis (DMTA). Also the thermo-degradation of the filled matrix was investigate by thermogravimetric analysis (TGA). The ATZ influence on the wear behavior of the matrix was investigated by tribological tests.

2.2 Results and discussions

2.2.1 Morphological and structural analysis of ATZ

The morphology of the ATZ particles is shown in the micrographs reported in Figure 2.1. The particles size is about 30nm (Figure 2.1A) but they form spherical agglomerates of dimensions ranging from 10 to 70 μm (Figure 2.1B).

Figure 2.2 shows the XRD pattern of ATZ. The diffraction peaks related to both tetragonal and monoclinic phase of the zirconium oxide are present. In particular, the most intense peaks at 2θ=30° (*hkl* 111), 2θ=34° (*hkl* 002) and 2θ=50° (*hkl* 202) are assigned to the tetragonal phase, whereas 2θ=26° (*hkl* 111) and 2θ=32° (*hkl* -111) are related to the monoclinic one. Furthermore, it is possible to observe also the peaks related to the α-phase of alumina (Al_2O_3) at 2θ=26° (*hkl* 012), 2θ=43° (*hkl* 113) and 2θ=57° (*hkl* 116).

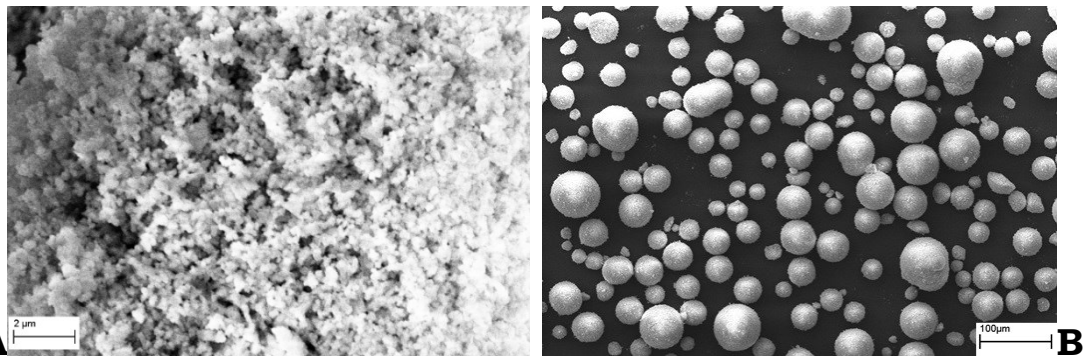

Figure 2.1: SEM micrographs of alumina toughened zirconia powder obtained at different magnifications.

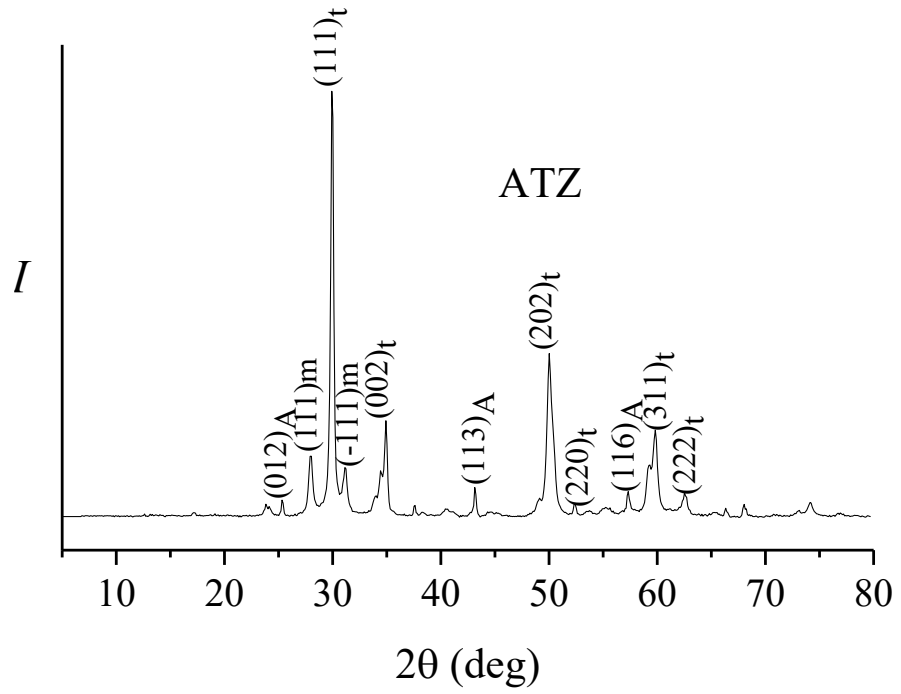

Figure 2.2: XRD patterns of ATZ. Spectra were obtained by XRD using a continuous scan of 0.04°/s, working at 45 kV and 40 mA.

2.2.2 Morphological and structural analysis of HDPE/ATZ composites

The cross section of the HDPE/ATZ composites with different amount of ATZ (99/1, 98/2, 97/3, 95/5, 93/7, and 88/12) are shown in Figure 2.3. A good distribution of ATZ particles is observed in the HDPE matrix for all the compositions. ATZ dimension varies from 200 to 500 nm, indicating that the process used for preparing composites destroy the initial ATZ micrometric aggregates, leading to sub-micrometric particles. However, by increasing the ATZ content, a few aggregates of bigger dimensions are visible.

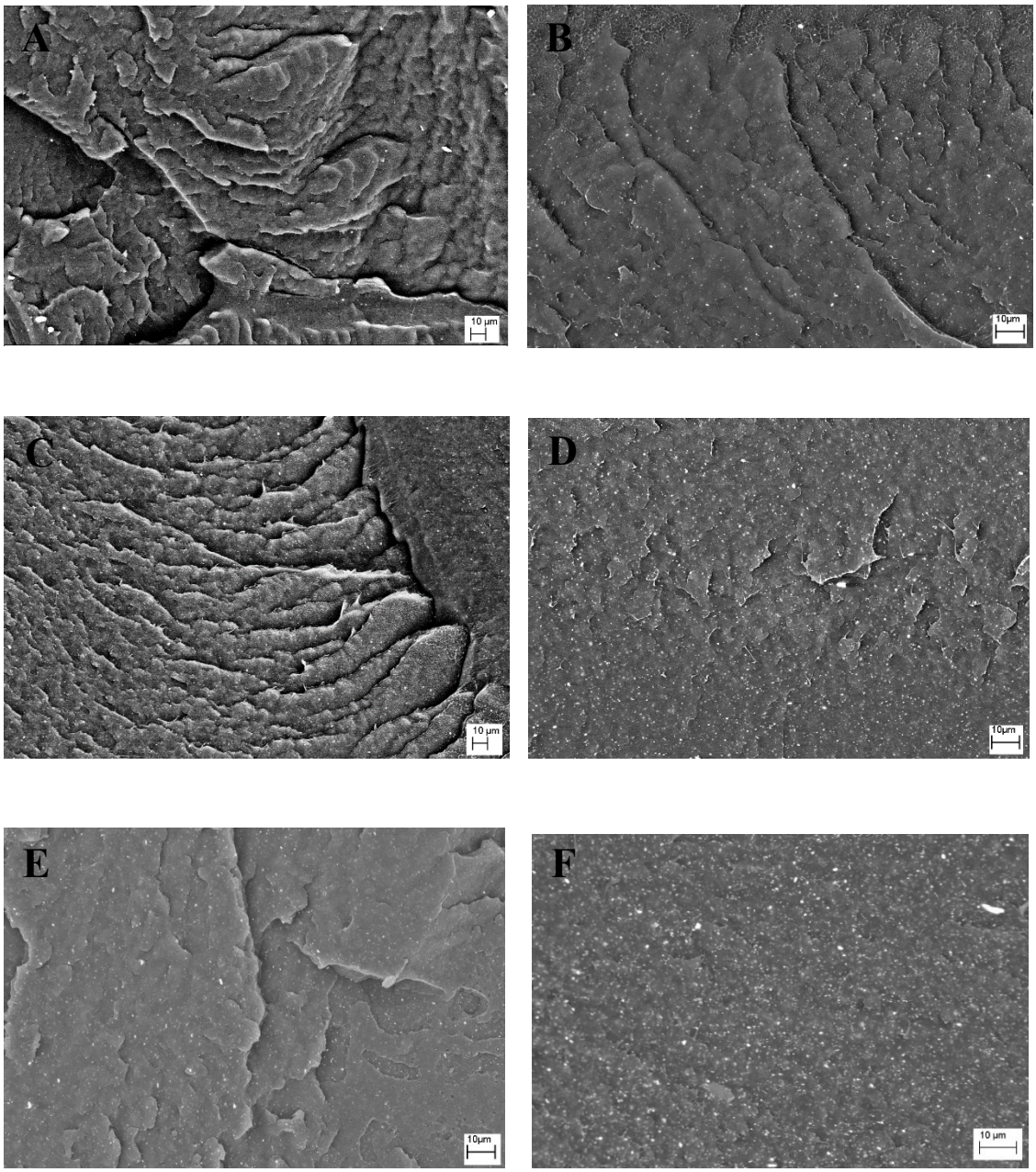

Figure 2.3: SEM micrographs of a) HDPE/ATZ 99/1, b) HDPE/ATZ 98/2, c) HDPE/ATZ 97/3, d) HDPE/ATZ 95/5, e) HDPE/ATZ 93/7, f) HDPE/ATZ 88/12.

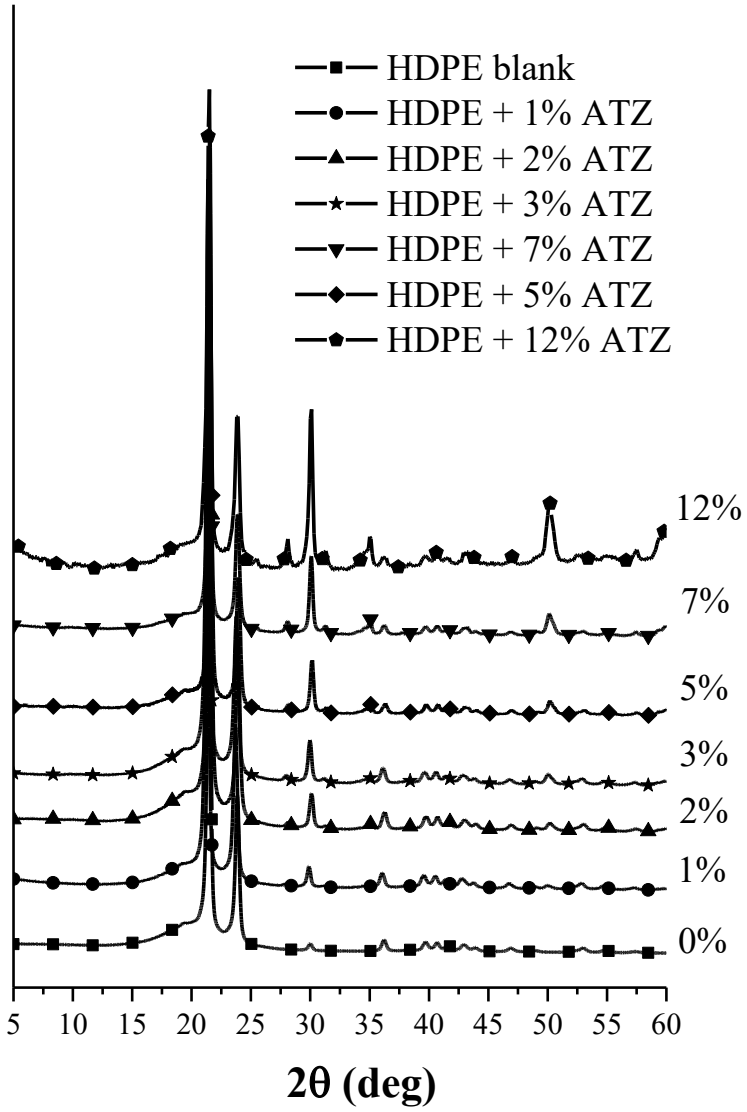

Figure 2.4: XRD patterns of the HDPE/ATZ composites. Spectra were obtained by XRD using a continuous scan of 0.04°/s, working at 45 kV and 40 mA.

Figure 2.4 reports the WAXS profiles of HDPE/ATZ composites. All the samples show the presence of the 110, 200 and 020 reflections at 2θ = 21°, 24° and 36° respectively, typical of the orthorhombic form of polyethylene **[9],** highlighting that ATZ presence does not influence the crystalline structure of the HDPE. Also, the most intense peaks related to the ATZ are detected. In particular, the peaks at 2θ = 50° (hkl 202), related

to the tetragonal form of zirconium oxide, increase with the increment of the ATZ content.

The crystallinity degree (x_c) of the composites, reported in Table 2.3, increases with the increment of ATZ until the ATZ reaches the amount of 7%wt. Indeed, the x_c of the 88/12 composites is comparable with the value obtained for the 93/7 one. This result suggests that ATZ act as nucleating agent, leading an increase of the crystallinity in particular at lower concentration of the filler.

Table 2.3: Cristallinity degree (x_c) of the HDPE/ATZ composites, calculated by XRD.

Materials	x_c
HDPE blank	69.3%
HDPE/ATZ 99/1	70.6%
HDPE/ATZ 98/2	72.7%
HDPE/ATZ 97/3	73.1%
HDPE/ATZ 95/5	73.9%
HDPE/ATZ 93/7	75.0%
HDPE/ATZ 88/12	74.6%

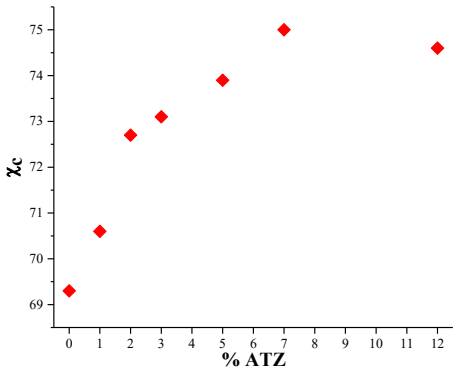

The contribution of ATZ crystals (blue curve) and polymer amorphous phase (red curve) for each diffraction pattern is shown in Figure 2.5.

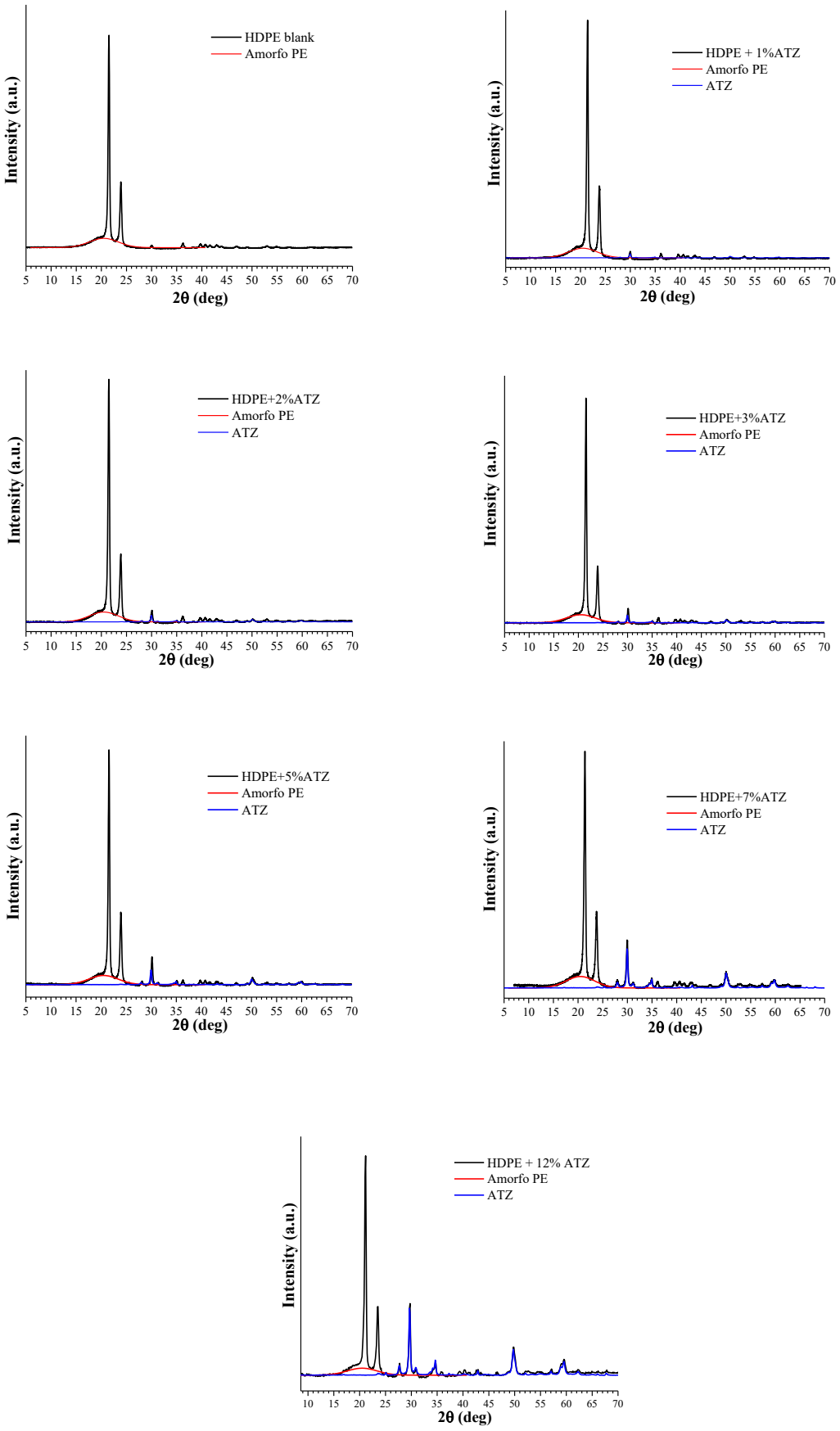

Figure 2.5: XRD spectra of the composites, showing the overall diffractometric profile (black), the amorphous phase (red) and the ATZ one (blue).

2.2.3 Mechanical properties of HDPE/ATZ composites

Figure 2.6A shows the storage modulus as a function of temperature for all the investigated systems. The main effect exerted by the presence of the ATZ is a slightly increase of the storage moduli E' in all the temperature range. The value of the E' at 40°C is reported in Figure 2.6B, as this temperature approaches the mean body temperature. Although the data dispersion, an increasing of E' value of the composites is quite evident, especially for ATZ concentration in the 5-12wt% range.

Figure 2.7 displays the stress strain curves, obtained at room temperature according to the standard test method ASTM D882. All the tensile properties of composites obtained by stress – strain experiments are reported in Table 2.4.

HDPE 97/3 (green curve), 98/2 (blue curve) and 99/1 (red curve) are more ductile with respect to the other composites and the neat HDPE (i.e. their elongation at break is significantly higher with respect the neat HDPE). A reasonable interpretation of this behavior is related to the nucleating effect of ATZ that leads to a ri-crystallization of the polymer with formation of crystals smaller than those of the neat HDPE. The size of the crystallites depends from the nucleation density: higher nucleation density leads to the formation of smaller crystals. Indeed, HDPE/ATZ 97/3 is more ductile than HDPE/ATZ 98/2, which is more ductile than HDPE/ATZ 99/1. At concentration upper than 3% of ATZ, the formation of aggregates leads to a decrease of the ductility.

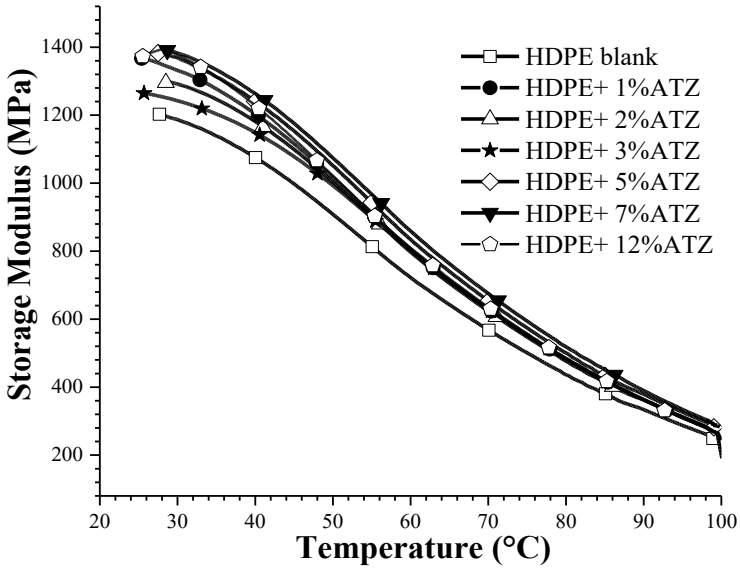

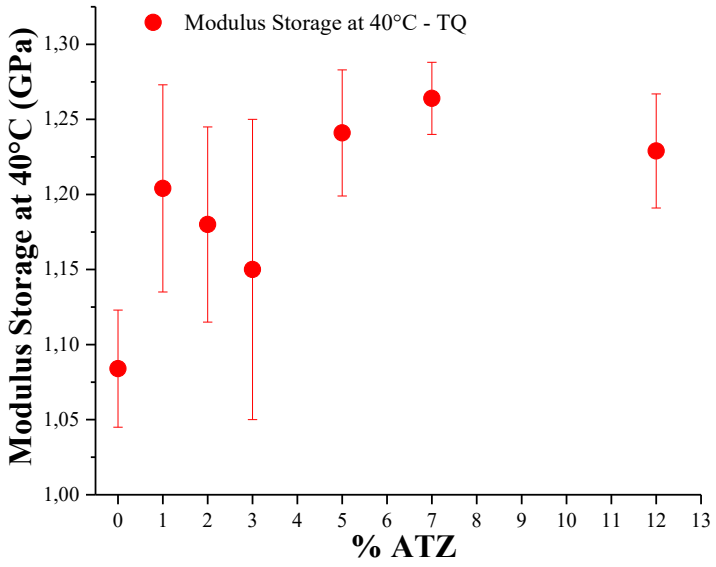

Figure 2.6: a) Storage modulus (E') of HDPE/ATZ composites obtained by DMTA analysis performed from 25 to 100 °C, heating rate of 3 °C/min, 1 Hz frequency and 0.05% of oscillation amplitude in strain-controlled mode b) Storage modulus (E') of the HDPE/ATZ composites at 40°C.

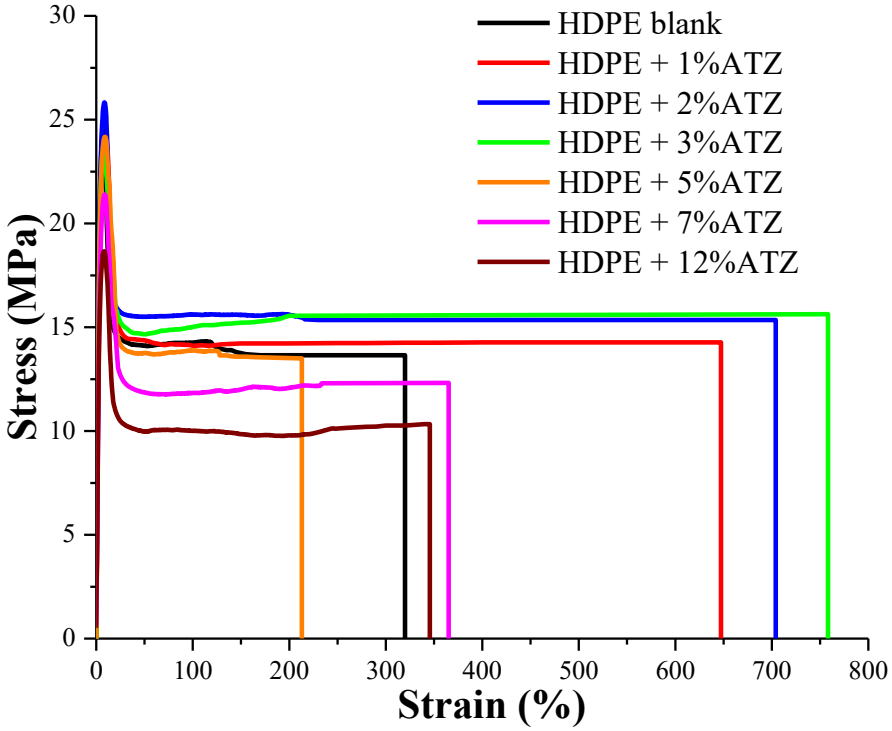

Figure 2.7: Stress-strain curves of HDPE/ATZ composites obtained at room temperature according to the standard test method ASTM D882.

In Figure 2.8 the Young modulus and tensile strength of the composites, obtained by stress-strain tests, are reported.

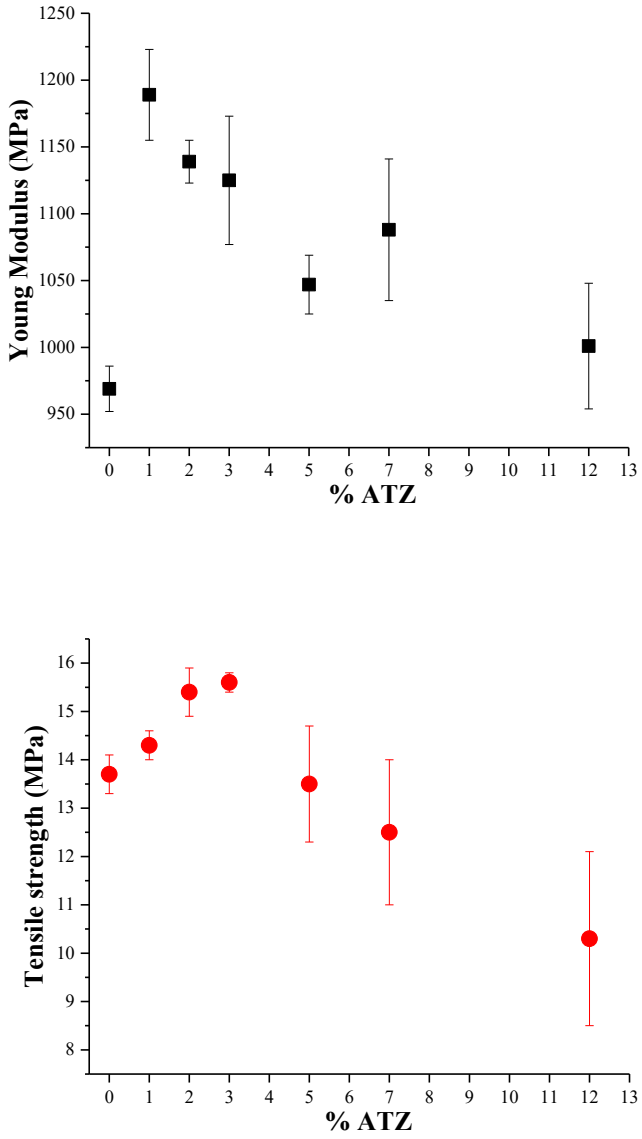

Figure 2.8: a) Young modulus and b) Tensile strength of HDPE/ATZ composites obtained by stress – strain experiments conducted at room temperature according to the standard test method ASTM D882.

The Young modulus of the composites is always higher with respect to that of the neat HDPE. However, for ATZ concentration of 12 wt%, the data dispersion does not allow to state a real E increment Moreover, for the composites at lower concentration of ATZ (99/1, 98/2 and 97/3) the

modulus is significantly higher than that of neat HDPE. Tensile strength increases for the composites by increasing ATZ amount till 3wt%, and then it starts to decrease. It becomes even lower than that of neat HDPE at the concentration of 12%wt.

These results indicate that at low ATZ content (>3%) the filler is able to re-enforce the polymer matrix (also thanks to the crystallinity increase), whereas at higher ATZ content (>3%) the presence of aggregates of big dimensions (as supported by SEM) leads to the formation of crack initiation sites, which induces a premature rupture of the material and a fall in the mechanical parameters **[15]**.

Table 2.4: Tensile properties of composites obtained by stress – strain experiments. Young modulus (**E**), elongation at break (ε_b) and tensile strength at break (σ_b) have been reported.

Sample	**E (MPa)**	**ε_b (%)**	**σ_b (MPa)**
HDPE blank	969 ± 17	320 ± 100	13.7 ± 0.4
HDPE + 1% ATZ	1189 ± 34	647 ± 28	14.3 ± 0.3
HDPE + 2% ATZ	1139 ± 16	704 ± 85	15.4 ± 0.5
HDPE + 3% ATZ	1125 ± 48	758 ± 44	15.6 ± 0.2
HDPE + 5% ATZ	1047 ± 22	213 ± 57	13.5 ± 1.2
HDPE + 7% ATZ	1088 ± 53	365 ± 145	12.5 ± 1.5
HDPE + 12% ATZ	1001 ± 47	346 ± 103	10.3 ± 1.8

The Charpy impact energy obtained according with ISO 179/1 standard is reported in Table 2.5. The fracture resistance of the composites is slightly reduced respect to that of the neat HDPE.

Table 2.5: Charpy impact energy obtained by V-notch test (ISO 179-1)

Samples	E CVN (kJ/m²)
HDPE blank	10.3 ± 0.5
HDPE + 1% ATZ	9.0 ± 0.8
HDPE + 2% ATZ	8.6 ± 0.7
HDPE + 3% ATZ	9.4 ± 0.4
HDPE + 5% ATZ	9.3 ± 0.6
HDPE + 7% ATZ	9.2 ± 0.6
HDPE + 12% ATZ	9.4 ± 0.9

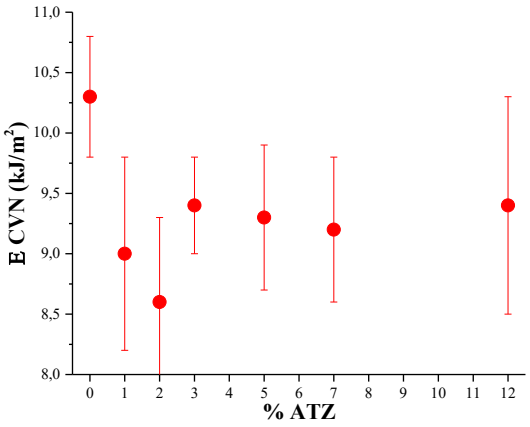

2.2.4 ATZ influence on the wear behavior of the HDPE

The wear behavior plays a key role for a material intended for bone replacement application. In order to investigate this property, tribological tests were performed on the composites to evaluate the friction coefficient (COF) and the wear rate of the composites.

Figure 2.9 displays the friction coefficient of neat HDPE, HDPE/ATZ 93/7 and 88/12. The graph shows that the COF of the composites is lower with respect the COF of the neat HDPE. This behavior is more evident for the HDPE/ATZ 88/12 composite, suggesting that ATZ presence strongly reduces this property. In Table 2.6 the friction coefficient and the wear rate, obtained by the evaluation of the wear volume loss (V) after the tribological test, are reported. The wear rate obtained for the composite HDPE/ATZ 88/12 is significantly lower than that of the neat HDPE and HDPE/ATZ 93/7.

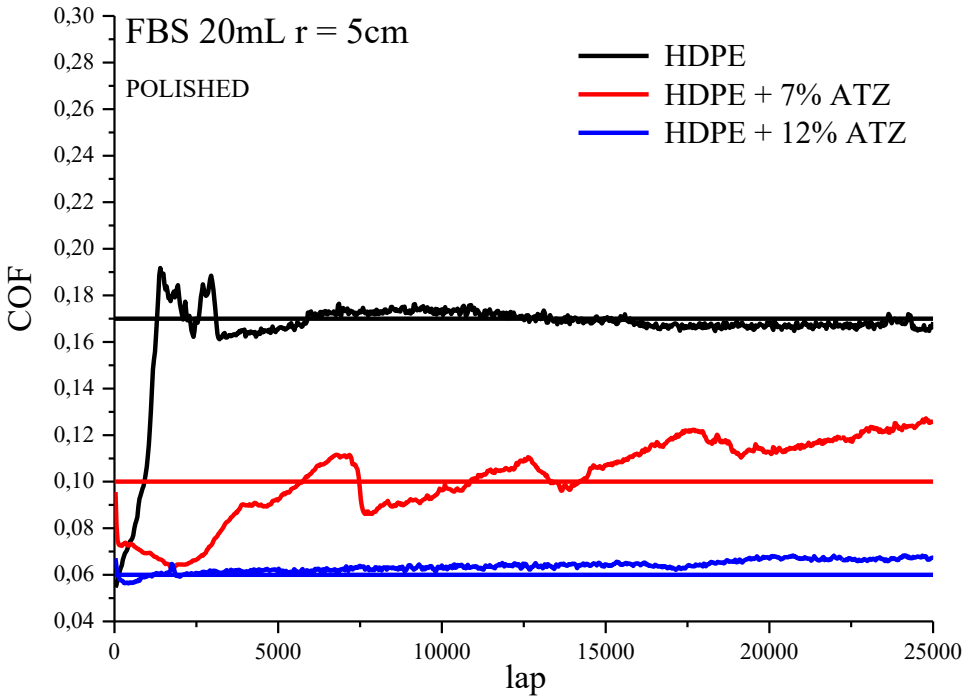

Figure 2.9: Friction coefficient (COF) evolution of the neat HDPE and its composites in function of the sliding distance.

Table 2.6: Friction coefficient and wear rate of neat HDPE and its composites

Samples	COF	Wear k 10^{-5} (mm^3/(N*m)
HDPE blank	0.17	2.9
HDPE + 7% ATZ	0.10	2.7
HDPE + 12% ATZ	0.06	1.2

2.2.5 Thermo-degradative behavior of HDPE/ATZ composites

The thermal and thermo-oxidative stability of HDPE and its composites were carried out by TGA. Figure 2.10 reports TG and dTG curves recorded in N_2 (2.10A) and air (2.10B). T_{10} and T_{max}, (i.e. the temperatures corresponding to a 10% weight loss and at the maximum of the derivative curves, respectively), together with the char content at 700 °C are listed in Table 2.7.

In inert atmosphere, HDPE thermally degrades by a single step centered around 420-500°C. In air, a multistep decomposition is evident and all the pyrolysis products are released as volatile species and no species are converted into a stable residue (char is equal to 0). HDPE/ATZ composites show the same behavior of neat HDPE, both in N_2 and in air, however the thermal process is influenced by the ATZ contents. This influence is more evident in air for HDPE/ATZ 95/5 and 93/7 whose T_{max} is 12 and 22 °C higher respect to that of neat HDPE. The increase in thermal stability is generally attributed to the filler that can act as a barrier for the degradation of the HDPE also slowing the diffusion of the degradation products of the polymer matrix **[16,17]**.

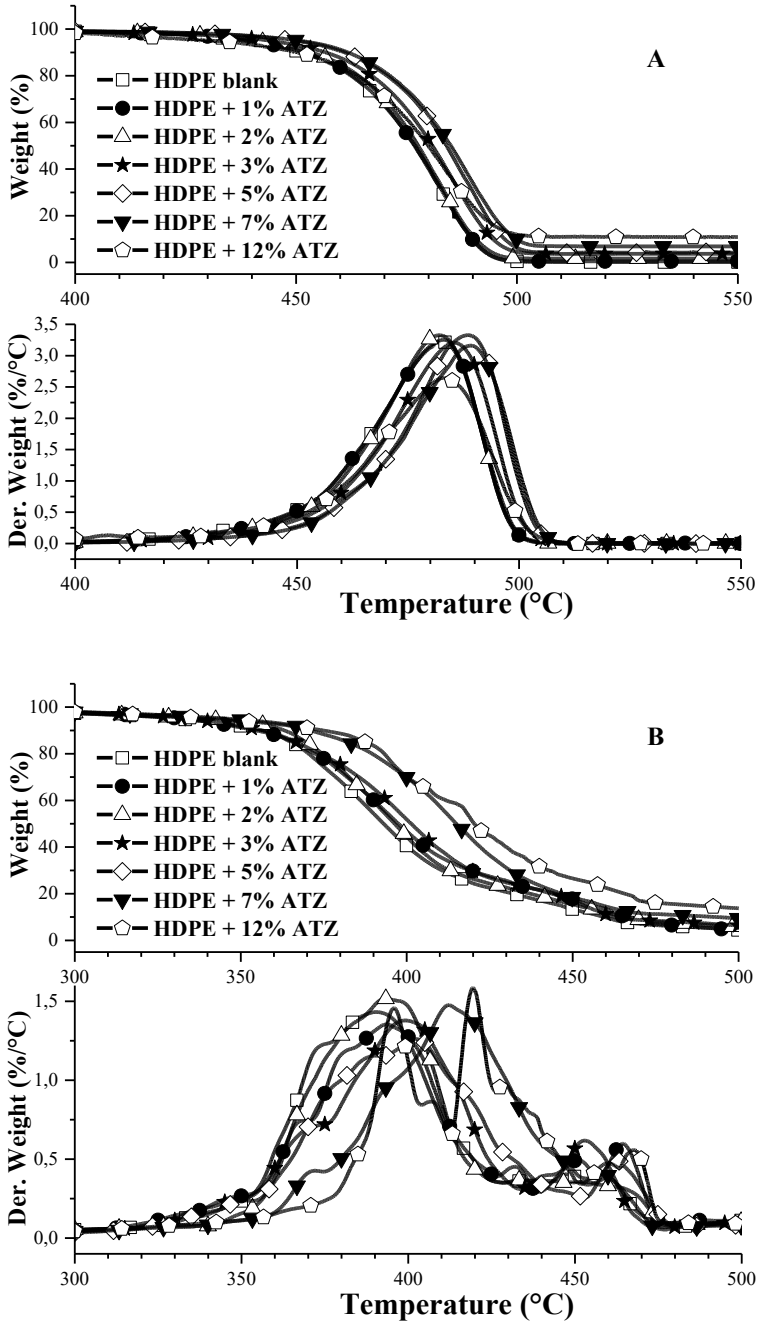

Figure 2.10: TG and dTG curves of HDPE and HDPE composites in nitrogen (A) and air (B).

Table 2.7: Thermogravimetric parameters of HDPE/ATZ composites

	N_2			Air		
	T_{10} (°C)	T_{max} (°C)	Residue (@700°C)	T_{10} (°C)	T_{max} (°C)	Residue (@700°C)
HDPE	451.0	482.4	0.0	356.9	390.3	0
HDPE/ATZ 99/1	451.8	483.1	0.4	354.6	393.5	0.9
HDPE/ATZ 98/2	453.4	482.0	1.6	363.1	393.3	1.8
HDPE/ATZ 97/3	463.0	491.9	2.0	356.7	399.2	2.4
HDPE/ATZ 95/5	461.0	488.6	4.0	362.0	402.5	4.2
HDPE/ATZ 93/7	461.7	489.1	6.9	371.1	412.1	6.7
HDPE/ATZ 88/12	450.3	482.8	10.9	374.9	419.4	11.7

2.3 Conclusions

Several composites HDPE/ATZ with different amount of ATZ were prepared by melt extrusion technique (i.e. 99/1, 98/2, 97/3, 95/5, 93/7 and 88/12). SEM and WAXS measurements were performed to investigate respectively the morphology and structure of the starting materials and their composites. The mechanical properties were evaluated by DMTA, stress-strain experiments and Charpy impact tests. Also the influence of ATZ on the wear behavior of HDPE was investigated by tribological test. Finally, the thermodegradative behavior of the composites was reported.

ATZ appeared well dispersed in the polymer matrix, especially at low concentrations. For amount of ATZ ranging between 5 and 12wt% aggregates of bigger dimensions were observed, suggesting, however, that the processing procedure was suitable to obtain a good dispersion of the filler in the composites at the concentration used in this work. Furthermore, ATZ does not affect the crystalline structure of HDPE but its presence leads to an increase in the crystallinity degree of the composites, due to the nucleating effect of the filler. This increase of the crystallinity degree contributes to improve the mechanical performance of the composites, in particular the 99/1, 98/2 and 97/3 HDPE/ATZ composites. Stress-strain experiments evidence a decrease of the tensile strength for the composites at higher concentration of ATZ (<5%) probably do to the formation of ATZ aggregates and voids. Furthermore, ATZ proved to be able to significantly reduce the COF of composites and simultaneously enhance the wear resistance of the polymer matrix. Finally, ATZ proved to be able to improve slightly the thermal stability of the polymer matrix, whereas it did not affect significantly the fracture resistance of the composite

2.4 Bibliography

[1] Helmer J.D., Driskell T.D. Research on Bioceramics *Symp. On Use of Ceramics as Surgical Implants.* Clemson University **(1969)** South Carolina (USA).
[2] Christel P., Meunier A., Dorlot J.M., Crolet J.M., Witvoet J., Sedel L., Boutin P. Biomechanical compatibility and design of ceramic implants for orthopedic surgery. *Ann NY Acad Sci* **(1988)** 523; 234-256.
[3] Manicone P.F., Rossi Iommetti P., Raffaelli L. An Overview of Zirconia Ceramics: Basic Properties and Clinical Applications. *J. Dent.* **(2007)** 35; 819–826.
[4] Gupta T.K., Bechtold J.H., Kuznickie R.C., Cadoff L.H., Rossing B.R. Stabilization of tetragonal phase in polycrystalline zirconia. *J. Mat. Sci.* **(1978)** 13; 1464.
[5] Deville S, Guenin G., Chevalier J. Martensitic transformation in zirconia part II. Martensite growth. *Acta Materialia.* **(2004)** 52; 5709-5721.
[6] Guo X. On the degradation of zirconia ceramics during low-temperature annealing in water or water vapor *J. Phys. Chem. Solids* **(1999)** 60(4); 539-546.
[7] Chevalier J., Gremillard L., Deville S. Low-temperature degradation of Zirconia and implications for biomedical implants *Annu. Rev. Mater. Res.* **(2007)** 37; 1-32.
[8] Fabbri P., Piconi C., Burresi E., Magnani G., Mazzanti F., Mingazzini C. Lifetime estimation of a zirconia-alumina composite for biomedical applications *Dent Mater* **(2014)** 21(5); 454-463.
[9] Hallmann L., Ulmer P., Reusser E., Louvel M., Hämmerle C.H.F. Effect of dopants and sintering temperature on microstructure and low temperature degradation of dental Y-TZP-zirconia *J. Eur. Ceram. Soc.* **(2013)** 32; 4091-4104.
[10] Mussano F., Genova T., Munaron L., Faga M.G., Carossa S. Ceramic biomaterials for dental implants: Current use and future perspectives. In Dental Implantology and Biomaterial, 2nd ed. *Intech: London, UK*, **(2016)** 63–90.
[11] Schierano G., Mussano F., Faga M.G., Menicucci G., Manzella C., Sabione C. An alumina toughned zirconia composite for dental implant application: in vivo animal results. *Biomed. Res. Int.* **(2015)** 2015:157360.
[12] Spies B.C., Balmer M., Patzelt S.B.M., Vach K., Kohal R.J. Clinical and patient-reported outcomes of a zirconia oral implant: three-year results of a prospective cohort investigation *J. Dent. Res.* **(2015)** 94; 1385-1391.
[13] Duraccio D., Strongone V., Malucelli G., Auriemma F., De Rosa C., Mussano F.D., Genova T., Faga M.G. The role of alumina-zirconia loading on the mechanical and biological properties of UHMWPE for biomedical applications *Composites Part B* **(2019)** 164; 800–808.
[14] Kawai Y., Uo M., Wang Y., Kono S., Ohnuki S., Watari F. Phase transformation of zirconia ceramics by hydrothermal degradation *Den. Mat. J.* **(2011)** 30; 286–292.
[15] Pukánszky B., in: J. Karger-Kocsis Editors, Polypropylene. Structure, Blends and Composites, London: *Chapman and Hall*, **(1995)** p. 1.
[16] Chrissafis K., Paraskevopoulos K.M., Pavlidou E., Bikiaris D. Thermal degradation mechanism of HDPE nanocomposites containing fumed silica nanoparticles *Thermochim Acta* **(2009)** 485; 65-71.

[17] Sinha Ray S., Bousmina M. Biodegradable polymers and their layered silicate nanocomposites: in greening the 21st century materials world *Prog. Mater. Sci.* **(2005)** 50; 962-1079.

Chapter 3

Chitosan as filler of HDPE-based composites for biomedical purpose

3.1 Introduction

3.1.1 Chitin and chitosan: general aspects

Chitosan (Figure 3.1) is the deacetylated form of chitin, a well known natural polymer, widely present in nature as component of the shell of a large amount of insects and crustaceans. After the cellulose, chitin is the most abundant biopolymer in nature **[1]**. Chitosan is a semi-crystalline polymer and its crystallinity degree is a function of its deacetylation degree (i.e. a more deacetylated chitosan is more crystalline).

Chitosan is soluble in aqueous solution at pH ≈ 5, when the amino groups are protonated, so it becomes easy to process in different dimension and shape, such as microparticles **[2]**, nanoparticles **[3]** and nanofibers **[4]**.

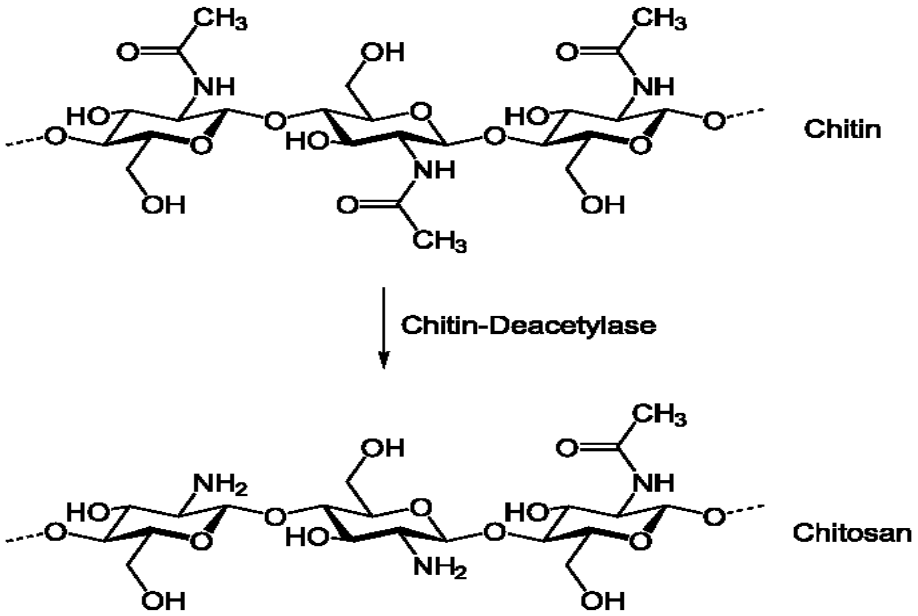

Figure 3.1: Chitin and chitosan molecular structure.

Chitosan shows unique biological properties, such as biocompatibility and biodegradability and it is nontoxic for the biological environment. In addition, chitosan has shown a proven antibacterial activity **[5].**

For these reasons, chitosan represents a very promising material for biomedical applications **[1,5]**. As example, a large amount of studies concerns the use of chitosan as component in devices for tissue engineering **[6-8]** and as excipient for drug **[9]** and gene **[10]** delivery. Chitosan has been also considered as polymer matrix of composites filled with a large variety of particles with the aim to obtain scaffolds for tissue engineering. Some examples include the use of silica **[11,12]**, titania **[13]** and zirconia **[14,15]** with the aim to induce bioactivity and osseointegration.

Among the large amount of chitosan properties, its antimicrobial activity appears very interesting for bone replacement application. Indeed, an important aspect to carefully control during orthopedic procedures dealing with prosthetic implants is the possible complication due to infections onset in the surgical site. The mean rates of infections related to

surgery that involves implants are in the range of 1.5% in the case of total knee implantation and 6.8% for femur head replacement, where HDPE is widely used **[16]**. For these reasons, the use of chitosan as filler of HDPE-based composites for bone replacement application has been considered in this work.

3.1.2 Description of the chapter work

This chapter deals with the preparation and the characterization of HDPE-based composites filled with two kind of chitosan: chitosan microparticles and chitosan nanoparticles (labeled as Chitosan M and N). Two set of composites (i.e. a set for each type of chitosan) were prepared by melt extrusion technique with different amount of filler.

Firstly, a morphological, thermal and structural analysis were carried out on the chitosan, using thermogravimetric analysis (TGA), Differential Scanning Calorimetry (DSC), scanning electron microscopy (SEM), and wide angle X ray scattering (WAXS). Morphological and structural investigation was carried out also on the composites. Mechanical properties of the materials were evaluated at room temperature during stress-strain experiments and in the range -150°C to 80°C using dynamical mechanical thermal analysis (DMTA). The mechanical properties were explained based on the morphological and structural analysis. Also the thermo-degradation of the filled matrix was investigated, using thermogravimetric analysis (TGA).

3.2 Results and discussion

3.2.1 Morphological, structural and thermal analysis of chitosan M and N

The morphology of the chitosan particles is shown in the micrographs reported in Figure 3.2. Chitosan M (Figure 3.2A) is a powder characterized by the presence of particles with very wide size distribution (from 100 to 600 μm) whereas chitosan N (Figure 3.2B) consists of particles of smaller size, from a few micrometers up to a maximum of 100 μm).

Figure 3.3 shows the XRD pattern of chitosan M and N. Chitosan M (black curve) shows two relative sharp peak at 10.4° (*hkl* 020) and 20.1° (*hkl* 110) indicating the presence of crystals in the material. Chitosan N (red curve) shows two broad peaks at the same positions of chitosan M. The position, intensity and width of the peaks would seem to indicate that chitosan M and N have a different degree of deacetylation **[17]**.

Figure 3.4 displays the thermal stability of chitosan M (black curve) and N (red curve). Both chitosan particles show a loss of weight around 100°C due to water. Over this temperature, chitosan M and N are thermally stable until 300°C, indicating that they are processable at HDPE processing temperature (190°C).

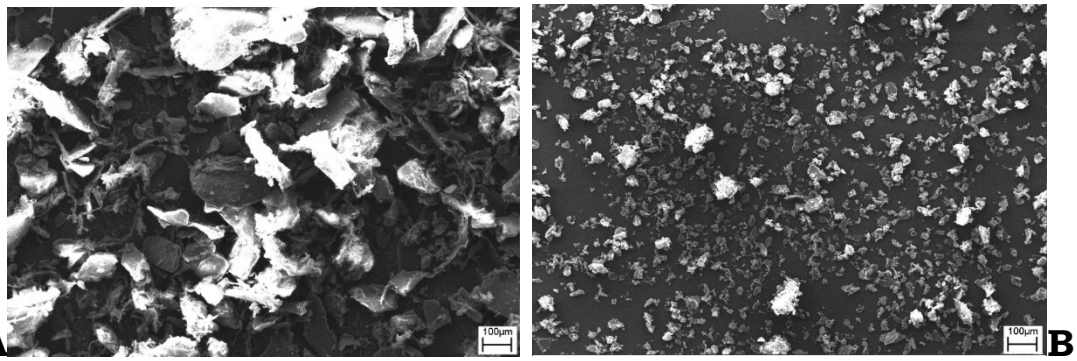

Figure 3.2: SEM micrographs of A) chitosan microparticles (Chitosan M) and B), chitosan nanoparticles (Chitosan N).

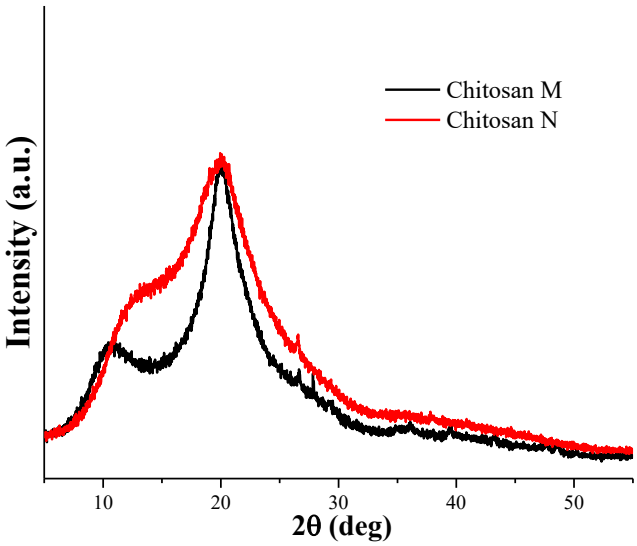

Figure 3.3: XRD patterns of chitosan M (black curve) and N (red curve). Spectra were obtained by XRD using a continuous scan of 0.04°/s, working at 45 kV and 40 mA.

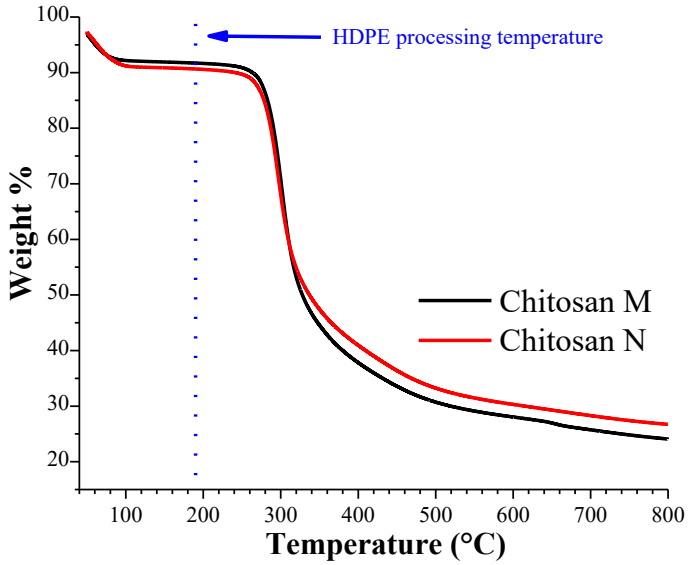

Figure 3.4: TG curves of chitosan M (black curve) and N (red curve), performed in N_2 at 10°C/min.

3.2.2 Morphological and structural analysis of HDPE/Chitosan composites

The cross section of HDPE/chitosan composites, with different amount of M and N chitosan (99/1, 98/2 and 95/5) are shown in Figure 3.5. The morphology of the composites with both type of chitosan is different. In particular, in both materials big chitosan aggregates are visible. However, these aggregates are elongated in composites with Chitosan M and almost spherical for chitosan N.

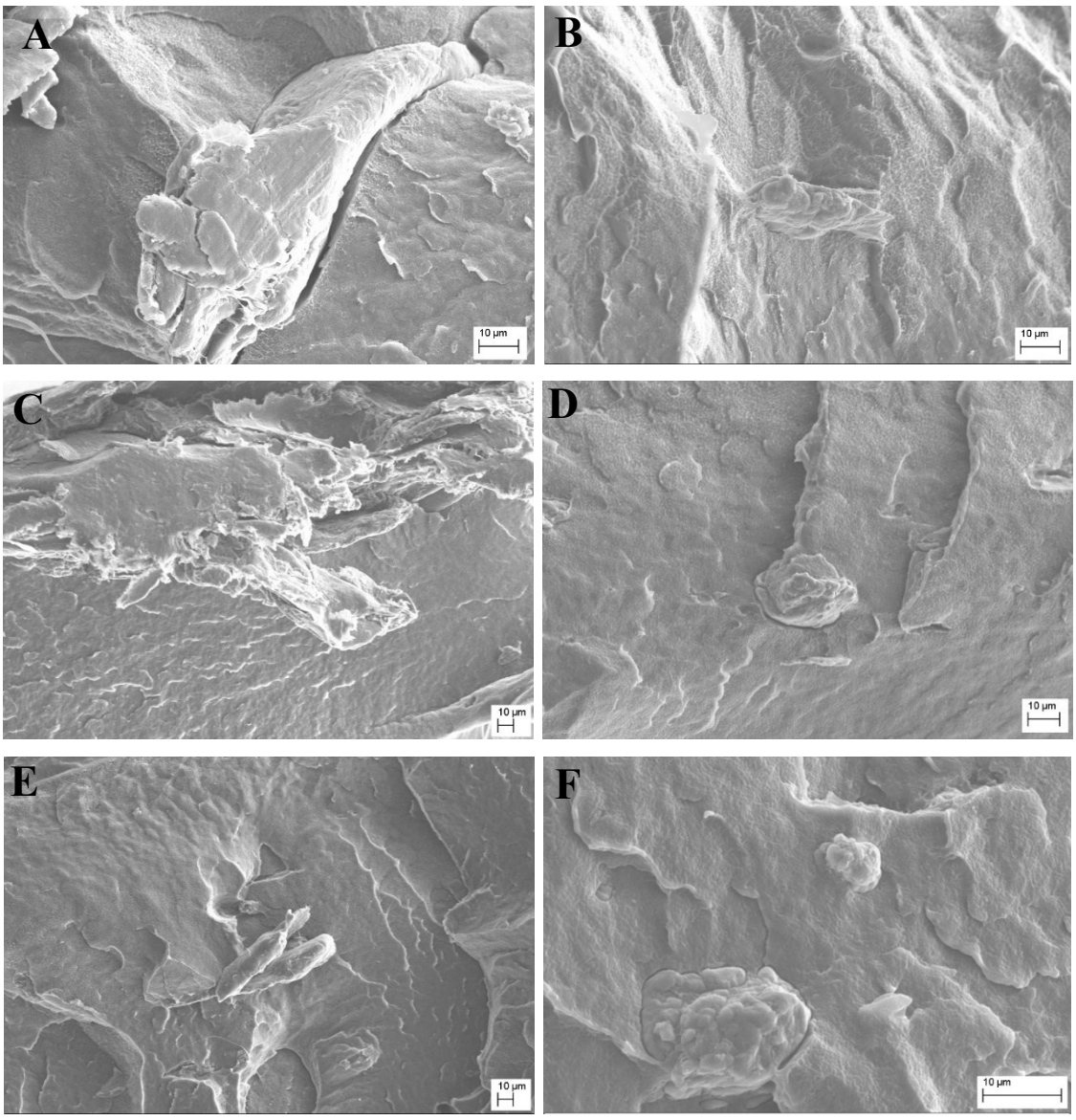

Figure 3.5: SEM micrographs of A) HDPE/Chitosan M 99/1, B) HDPE/Chitosan N 99/1, C) HDPE/Chitosan M 98/2, D) HDPE/Chitosan N 98/2, E) HDPE/Chitosan M 95/5, F) HDPE/Chitosan N 95/5.

In Figure 3.6A and B, XRD patterns of HDPE composites with chitosan M and N are reported. The presence of the chitosan does not influence the crystalline structure of the HDPE, which shows the typical pattern of the orthorhombic form of polyethylene (section 2.3.2). No Chitosan-related peaks are detected.

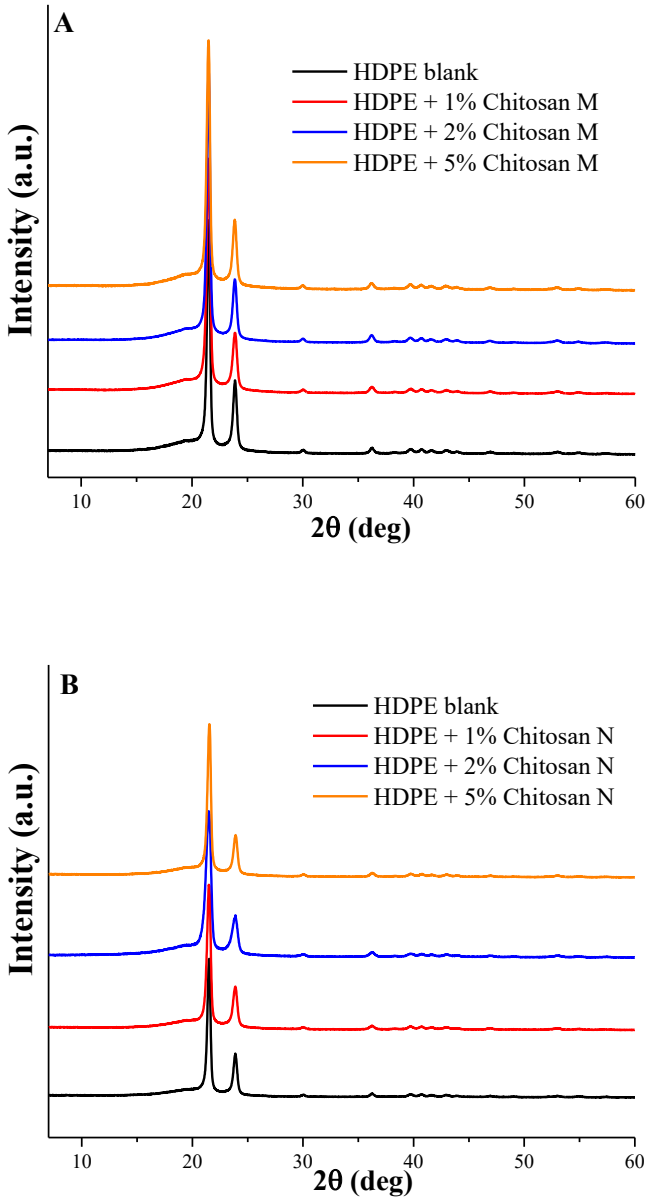

Figure 3.6: XRD patterns of A) HDPE/Chitosan M composites and B) HDPE/Chitosan N composites. Spectra were obtained by XRD using a continuous scan of 0.04°/s, working at 45 kV and 40 mA.

Due to the difficulty to separate the contribution of chitosan from that of the polymer matrix the crystallinity degree of the composites was evaluated by DSC experiments. Table 3.1 shows the values of cristallinity calculated by the ratio between the ΔH_f of the samples and that of a 100% crystalline PE, corresponding to 293 J g^{-1}. The results shown in the Table indicate the absence of a clear influence of the type of chitosan on the crystallinity degree. Also the amount of chitosan does not result in any evident influence on the crystallinity degree.

Table 3.1: Cristallinity degree of the HDPE/Chitosan composites evaluated by DSC.

Chitosan M	$\mathbf{x_c}$	**Chitosan N**	$\mathbf{x_c}$
HDPE blank	59 %	HDPE blank	59 %
HDPE + 1% Chitosan	57%	HDPE + 1% Chitosan	58%
HDPE + 2% Chitosan	60%	HDPE + 2% Chitosan	57%
HDPE + 5% Chitosan	56%	HDPE + 5% Chitosan	61%

3.2.3 Mechanical properties of HDPE/chitosan composites

Figure 3.7 shows the storage modulus as a function of the temperature for HDPE/chitosan M and HDPE/chitosan N systems. The presence of both type of chitosan strongly improves the storage modulus of the HDPE, reaching the best results at 2% for both kind of chitosan (blue curve). Chitosan M has a higher effect than chitosan N. No reinforcing effect has been detected for HDPE + 1% Chitosan N (Figure 3.7B, red curve).

Figure 3.8 shows tan δ curves for both the set of composites. Tan δ is the phase lag between the stress and the strain and it corresponds to the ratio between the loss and the storage modulus (E"/E'). PE shows the γ transitions around -110°C **[18]** and this transition, easily detected by DMTA analysis, corresponds to the maximum of the tan δ curve. The

temperature corresponding to the γ transitions is the T_g of the PE **[18]**. Figure 3.8A and 3.8B display tan δ curves of HDPE/Chitosan M and HDPE/Chitosan N composites respectively. For both the set of composites, chitosan does not affect the T_g of HDPE that occur at -113°C. This result excludes a possible miscibility between the two polymers, also at the lowest amount of chitosan. The lack of miscibility can account for the uneven distribution of the filler into the matrix observed by SEM.

The values of the tensile properties of HDPE/Chitosan composites at 40°C are reported in Table 3.2.

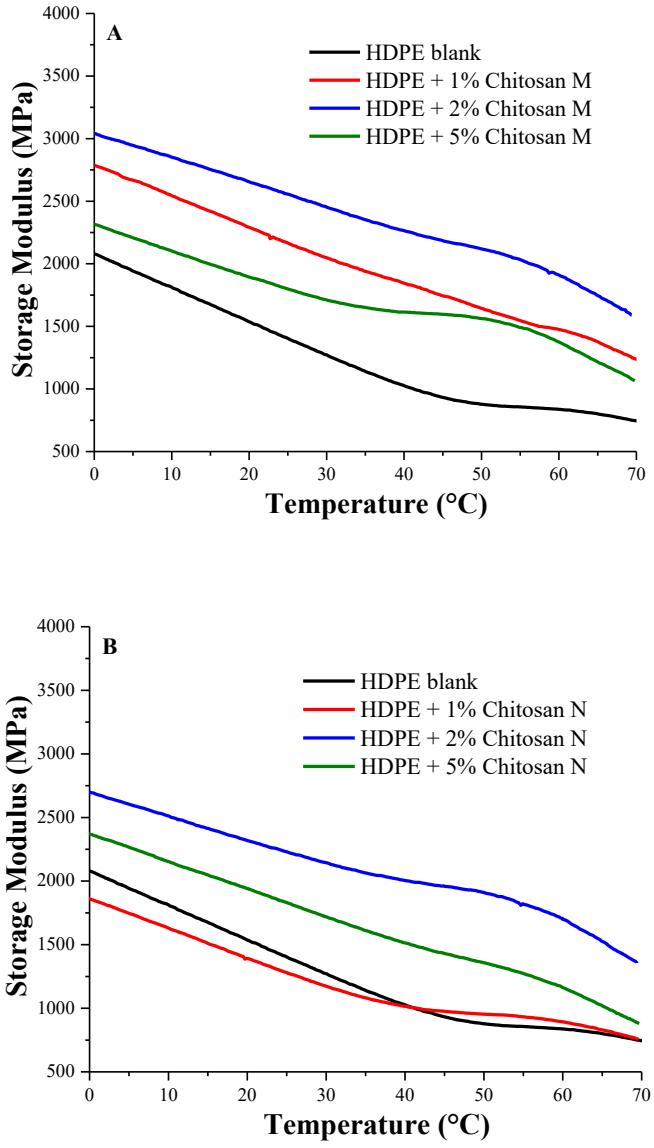

Figure 3.7: A) Storage modulus (E') of HDPE/Chitosan M composites B) Storage modulus (E') of HDPE/Chitosan N composite.

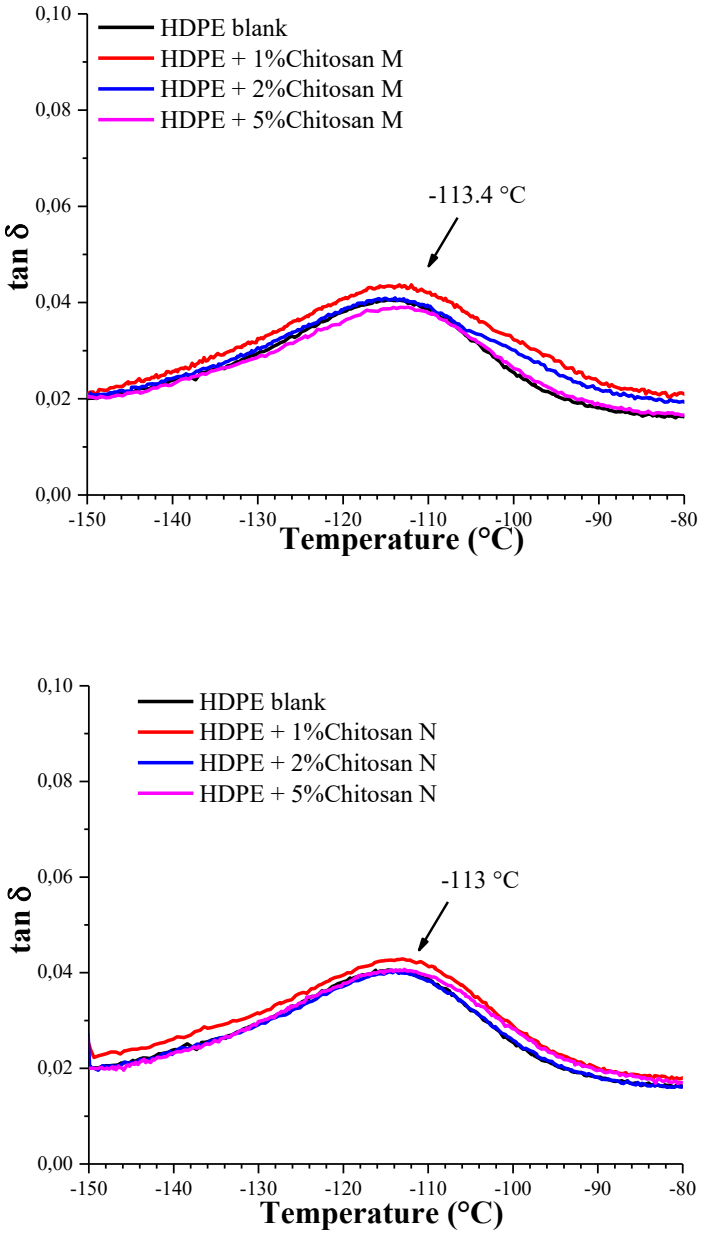

Figure 3.8: A) Tan δ of HDPE/Chitosan M composites B) Tan δ of HDPE/Chitosan N composites.

Table 3.2: Tensile properties at 40°C of HDPE/Chitosan composites obtained by DMTA analysis.

	CHITOSAN M				**CHITOSAN N**		
	Storage modulus (MPa)	Loss modulus (MPa)	Tan δ		Storage modulus (MPa)	Loss modulus (MPa)	Tan δ
0%	1029	159.2	0.154	**0%**	1029	159.2	0.154
1%	1845	247.0	0.134	**1%**	1017	162.8	0.160
2%	2265	288.7	0.127	**2%**	2006	267.3	0.133
5%	1614	219.5	0.136	**5%**	1511	208.7	0.138

In table 3.3 the tensile properties obtained by stress-strain experiments, performed at room temperature, are reported. Both the kind of chitosan enhance the young modulus of the neat HDPE. The increment goes with the amount of chitosan. The reinforcing effect is more relevant in the case of chitosan M. Tensile strength increases with the increment of the fillers for both the kind of materials, showing again a greater reinforcing effect for the chitosan M. On the contrary, the presence of chitosan particles leads to a dramatic reduction of the composites ductility. Indeed, the composites with the higher chitosan content are the less ductile.

Table 3.3: Tensile properties of HDPE/chitosan composites obtained by stress – strain experiments. Young modulus (**E**), elongation at break ($\boldsymbol{\varepsilon_b}$) and tensile strength at break ($\boldsymbol{\sigma_b}$) have been reported.

	CHITOSAN M				**CHITOSAN N**		
	Young modulus (E) (MPa)	Tensile Strength (σ_b) (MPa)	Elongation at break (ε_b) (%)		Young modulus (E) (MPa)	Tensile Strength (σ_b) (MPa)	Elongation at break (ε_b) (%)
0%	969 ± 17	13.7 ± 0.4	320 ± 100	**0%**	969 ± 17	13.7 ± 0.4	320 ± 100
1%	1057 ± 49	14.8 ± 4.2	22 ± 6	**1%**	1071 ± 54	15.2 ± 0.4	148 ± 53
2%	1069 ± 45	15.2 ± 1.8	19 ± 4	**2%**	1088 ± 36	15.0 ± 1.0	29 ± 11
5%	1219 ± 74	19.7 ± 2.4	10 ± 2	**5%**	1117 ± 34	15.7 ± 1.5	17 ± 2

3.2.4 Thermo-degradative behavior of HDPE/Chitosan composites

Figure 3.9 reports TG and dTG curves recorded in N_2 of HDPE/Chitosan M (3.9A) and HDPE/Chitosan N (3.9B). For both the composites set, T_{10} and T_{max} are listed in Table 3.4.

In nitrogen atmosphere, HDPE thermally degrades by a single step centered around 420-500°C. Thermal stability of the polymer matrix is enhanced by the presence of both type of chitosan. This effect is more evident for the T_{max} of degradation and does not seem to be related to the amount of the filler. Both the materials are able to improve the T_{max} of the HDPE by about 18°C.

Table 3.4: Thermogravimetric parameters of HDPE/Chitosan composites.

	CHITOSAN M					CHITOSAN N			
	Blank	1%	2%	5%		Blank	1%	2%	5%
T_{10}	451.2	463.2	461.9	457.6	T_{10}	451.2	458.6	462.8	459.1
T_{max}	476.7	493.3	492.2	491.8	T_{max}	476.7	487.7	492.4	491.4

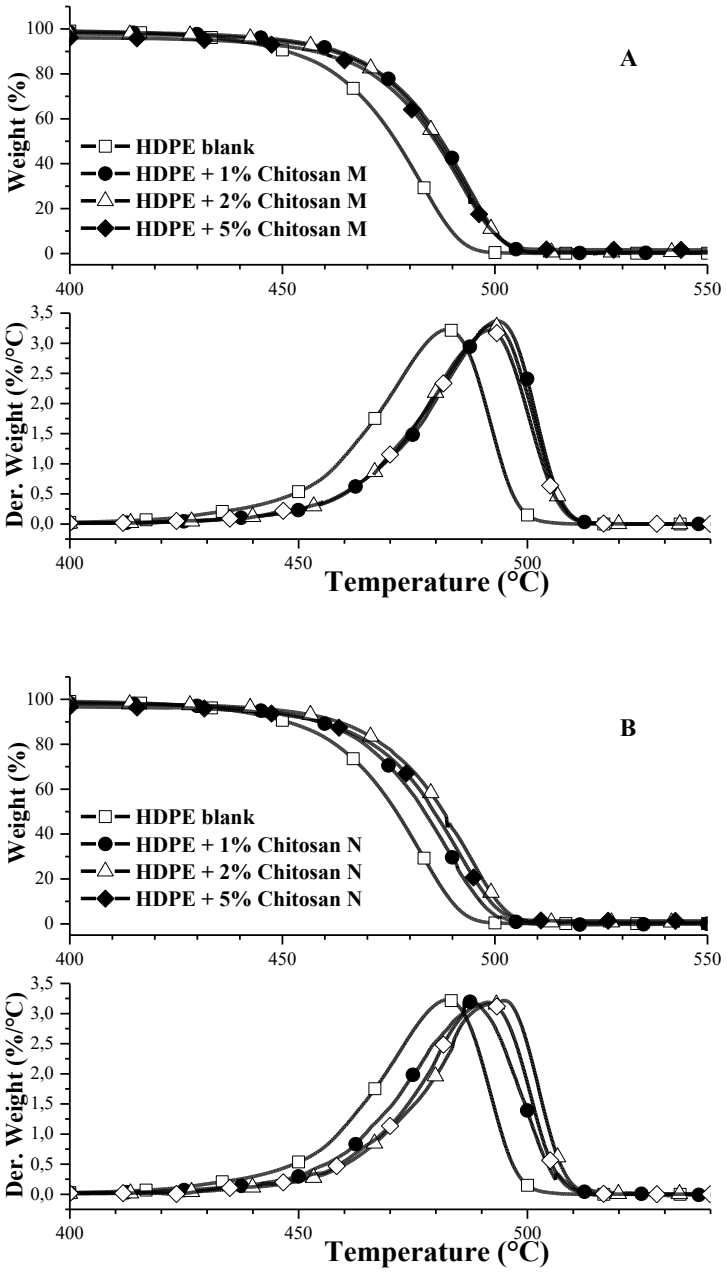

Figure 3.9: a) TG and dTG curves of the HDPE/Chitosan M composites (50 °C to 800°C – 10 °C/min in Nitrogen with a TA Discovery) b) TG and dTG curves of the HDPE/Chitosan N composites (50 °C to 800°C – 10 °C/min in Nitrogen with a TA Discovery)

3.3 Conclusions

Two set of HDPE/chitosan composites with different amount of micrometric chitosan (chitosan M) and nanometric chitosan (chitosan N) were prepared by melt extrusion technique (i.e. 99/1, 98/2 and 95/5 wt%). SEM, WAXS and TGA measurements were performed to investigate morphology, structure and thermo-stability of both starting materials and composites. Mechanical properties of the composites were evaluated by DMTA and stress-strain experiments. Finally, the thermodegradative behavior of the composites was discussed.

Chitosan M and N are two semi-crystalline polymers, stable at the HDPE processing temperature. Particles size of chitosan M ranges between 100 and 600 μm whereas chitosan N consists of particles of smaller size, from a few micrometers up to a maximum of 100 μm. The chitosan distribution in the HDPE matrix appears inhomogeneous, regardless the filler used (M or N). Indeed, in some areas of the samples chitosan aggregates are present, in form of elongated particles in the case of chitosan M and as spherical one for chitosan N. Furthermore, neither chitosan M or N influence the crystal structure of PE. The increase in crystallinity, observed for some composites, cannot be related to a particular effect of the type of filler.

Both chitosan M and N lead to an improving of the mechanical properties. In particular, the storage modulus at 40°C for the HDPE/Chitosan 98/2 strongly increases with respect to the neat HDPE. Chitosan M and N do not affect the T_g of the PE.

Stress-strain experiments, performed at RT, evidence an increase of the young modulus and the tensile strength for the composites. Such increase is higher at higher filler amount, for both chitosan M and N. On the contrary, both the fillers reduce the HDPE ductility.

Finally, chitosan M and N slightly improve the thermal stability of the polymer matrix.

3.4 Bibliography

[1] Prashanth K.V.H., Tharanathan R.N. Chitin/Chitosan: modifications and their unlimited application potential – an overview *Trends Food Sci Technol* **(2007)** 18; 117-131.
[2] Prabaharan M., Mano J.F. Chitosan-based particles as controlled drug delivery systems *Drug Deliv* **(2005)** 12; 41–57.
[3] Anitha A., Deepagan V.G., Divya R.V.V., Deepthy M., Nair S.V., Jayakumar R. Preparation, characterization, in vitro drug release and biological studies of curcumin loaded dextran sulphate-chitosan nanoparticles *Carbohydr Polym* **(2011)** 84; 1158–1164.
[4] Jayakumar R., Prabaharan M., Nair S.V., Tamura H. Novel chitin and chitosan nanofibers in biomedical applications *Biotechnol Adv* **(2010)** 28; 142–150.
[5] Kong M., Chen X.G., Xing K., Park H.J. Antimicrobial properties of chitosan and mode of action: A state of the art review *Int J Food Microbiology* **(2010)** 144; 51-63
[6] Venkatesan J., Kim S.K. Chitosan composites for bone tissue engineering – an overview *Mar Drugs* **(2010)** 8; 2252-2266.
[7] Ragetly G.R., Slavik G.J., Cunningham B.T., Schaeffer D.J., Griffon D.J. Cartilage tissue engineering on fibrous chitosan scaffolds produced by a replica molding technique *J. Biomed. Mater. Res. A* **(2010)** 93; 46-55.
[8] Suh J.K.F., Matthew H.W.T. Application of chitosan-based polysaccharide biomaterials in cartilage tissue engineering: a review *Biomaterials* **(2000)** 21; 2589-2598.
[9] Sashiwa H., Aiba S. Chemically modified chitin and chitosan as biomaterials *Prog Polym Sci* **(2004)** 29; 887-8.
[10] Yi H., Wu L.Q., Bentley W.E., Ghodssi R., Rubloff G.W., Culver J.N., Payne G.F. Biofabrication with chitosan *Biomacromolecules* **(2005)** 6; 2881-2894.
[11] Toskas G., Cherif C., Hund R.D., Laourine E., Mahltig B., Fahmi A., Heinemann C., Hanke T. Chitosan (PEO)/silica hybrid nanofibers as a potential biomaterial for bone regeneration *Carbohydr Polym* **(2013)** 94; 713–722.
[12] Madhumathi K., Sudheesh Kumar P.T., Kavya K.C., Furuike T., Tamura H., Nair S.V., Jayakumar R. Novel chitin/nanosilica composite scaffolds for bone tissue engineering applications *Int J Biol Macromol* **(2009)** 45; 289–292.
[13] Jayakumar R., Ramachandran R., Divyarani V.V., Chennazhi K.P., Tamura H., Nair S.V. Fabrication of chitin–chitosan/nano TiO_2-composite scaffolds for tissue engineering applications *Int J BiolMacromol* **(2011)** 48; 336–344.
[14] Ehrlich H., Simon P., Motylenko M., Wysokowski M., Bazhenov V.V., Galli R., Stelling A.L., Stawski D., Ilan M., Stöcker H., Abendroth B., Born R., Jesionowski T., Kurzydłowskii K.J., Meyera D.C. Extreme biomimetics: formation of zirconium dioxide nanophase using chitinous scaffolds under hydrothermal conditions. *J Mater Chem B* **(2013)** 1; 5092–5099.
[15] Jayakumar R., Ramachandran R., Sudheesh Kumar P.T., Divya R.V.V., Sowmya S., Chennazhi K.P., Tamura H., Nair S.V. Fabrication of chitin–chitosan/nano ZrO_2 composite scaffolds for tissue engineering applications *Int J Biol Macromol* **(2011)** 49; 274–280.
[16] Kalmeijer M.D., Coertjens H., Van Nieuwland-Bollen P.M., Bogaers-Hofman D., de Baere G.A.J., Stuurman A., van Belkum A., Kluytmans J.A.J.W. Surgical site infections in orthopedic surgery: the effect of mupirocin nasal ointment in a

double-blind, randomized, placebo-controlled study *Clin Infect Dis* **(2002)** 35; 353–358.
[17] Zhang Y., Xue C., Xue Y., Gao R., Zhang X. Determination of the degree of deacetylation of chitin and chitosan by X-ray powder diffraction *Carbohydr. Res.* **(2005)** 340; 1914– 1917.
[18] Stehling F.C. Mandelkern L. The Glass Temperature of Linear Polyethylene, *Macromolecules* **(1970)** 3; 242-252.

Chapter 4

Radiation-induced grafting of HDPE-ATZ composites with chitosan for biomedical purpose

4.1 Introduction

4.1.1 Radiation-induced grafting: general aspects

In polymer sciences, grafting is a process consisting in the surface modification of a polymer material by reaction of the polymer backbones with a monomer having functional groups, such as –OH, -NH_2, -COOH an, aiming at changing the surface properties without influence on the bulk material. Usually this process is not spontaneous and, in order to obtain the reaction, radiations can be used to generate on the surface free radicals able to react with the monomers to achieve a graft copolymer **[1,2]**. Gamma rays and electron beam are typical techniques used to induce the grafting process **[1,2]**.

The electronic excitation induced by irradiation gives highly excited molecules that may relax to give radicals through homolytic bond cleavage **[3]**. The resulting radicals can migrate along the polymer chain, and

easily recombine to give cross-linking, or can react with the oxygen to give surface oxidation. These radicals could also represent the reactive sites for a grafting reaction **[3]**. In the case of semi-crystalline polymers, like polyethylene, radicals can be identified in both the amorphous and crystalline phases. Radicals trapped in the crystalline phase have longer lifetimes due to their restricted mobility among the crystalline lamellae **[3]**. A diagram of a generic grafting process is shown in Figure 4.1.

The degree of grafting can be adjusted by changing the reaction conditions (reaction temperature, monomer concentration and type of solvent) and the radiation treatment parameters (dose of irradiation).

In solution, grafting is controlled by diffusion laws, so the rate of grafting increase with the increment of the reaction temperature. In addition, increasing of temperature leads to the decomposition of peroxides on the surface, forming active centers for the propagation of the grafting reaction **[4,5]**.

Another important factor that influences the rate of grafting is the absorbed irradiation dose. Absorbed dose (D) is the energy absorbed by material. Its unit is the gray (Gy) and 1 Gy corresponds to 1 Joule of energy deposited in 1 kg of material (1 Gy = 1 J kg^{-1}). The higher the dose, the greater the amount of radicals generated in the polymeric material, which has a direct impact on the degree of grafting **[3]**. Also the dose rate affects the distribution, the possible surface oxidation and the lifetime of the radicals. At the same dose, higher dose rate results in lower efficiency of grafting, because the resulting high concentration of radicals increases their combination, leading to a rapid termination process **[3]**.

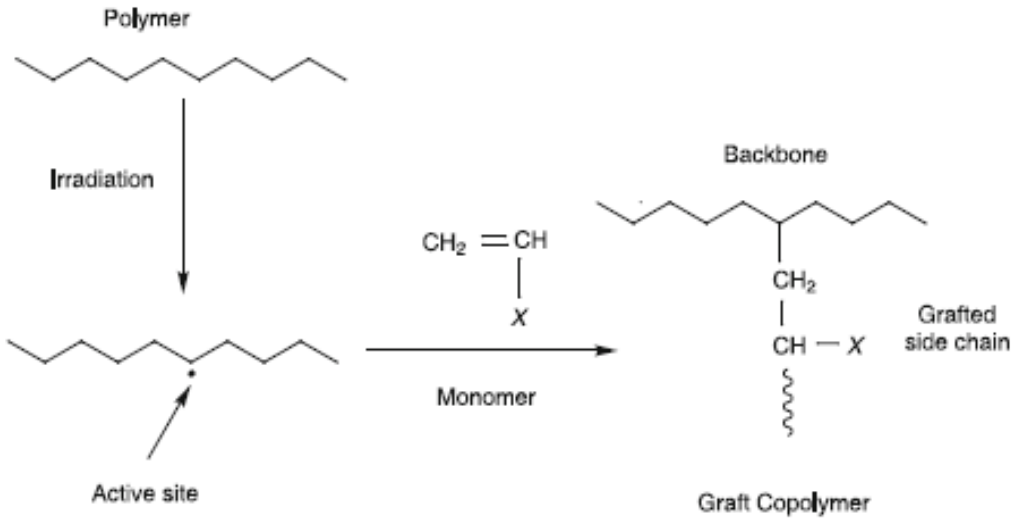

Figure 4.1: Generic process of a surface grafting process with a vinylic monomer.

Surface modification by radiation-induced grafting method has numerous advantages. It is a relatively simple and repeatable process, exploitable for the treatment of a wide range of synthetic polymers in any form (fiber, film or powder), on which surface a large amount of monomers can be grafted. Moreover, no initiator or related impurities remain on the treated material.

Among the polymers whose surfaces were modified by radiation grafting, the largest group are polyolefins, such as polyethylene (PE), polypropylene (PP) and polystyrene (PS). Radiation-induced grafting can be used to get tailored materials that could be employed for several industrial uses, like for biomedical and environmental field. In particular, graft surface modification can improve or reduce polymer hydrophobicity, then inducing surface properties able to extend the application fields of the starting materials. **[6]**.

4.1.2 Low energy electron beam system for surface materials grafting

The application of low energy electron beam systems (operating at 100-300 keV) can be quite effective in some technological processes, among which the grafting process is one of the most relevant.

These systems can be classified into linear or planar cathode accelerator and scanning accelerators. Figure 4.2 shows a schematic representation of a linear cathode electron beam accelerator.

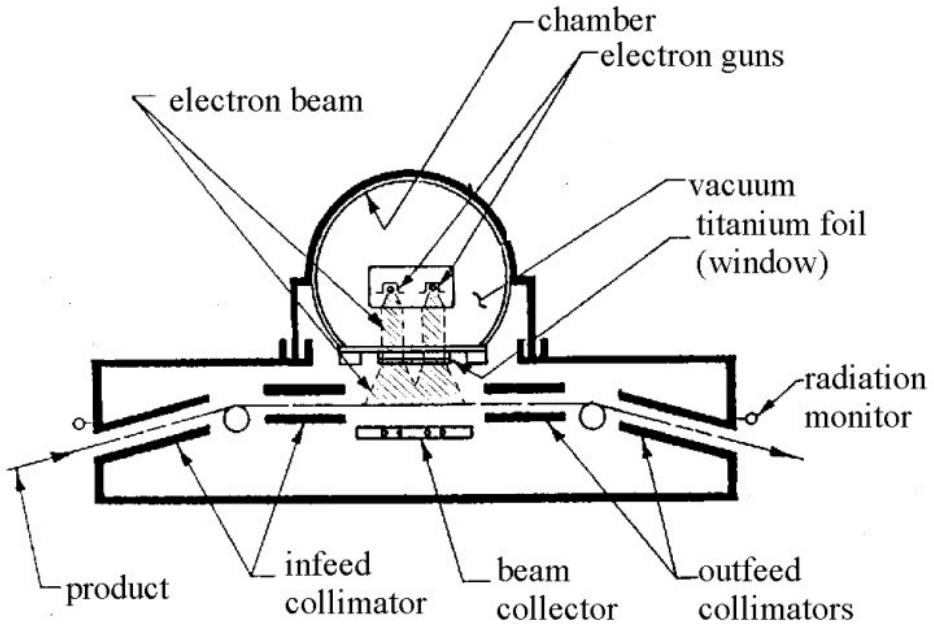

Figure 4.2: Schematic representation of a linear cathode electron beam accelerator.

The film, or sheet, of material pass under the electron beam on a conveyor belt. The electron beam is generated in a vacuum chamber and after pass through a thin metal film (for example a titanium film), due to its high energy. All the system is carefully shielded, in order to avoid exposure of workers to X-rays generated by the impact of high energy electrons with the matter. For a low energy electron beam, a vacuum

chamber is required, because low energy electrons have a low mean free path in air **[7]**.

4.1.3 Description of the chapter work

Radiation-induced grafting of chitosan on HDPE-ATZ composites was considered, with the purpose to introduce another functionality without modifying the bulk properties (e.g. antimicrobial properties). The grafting was initiated by irradiation with a low energy electron beam system, available at *Institut de Chimie Moléculaire de Reims*, in the laboratories of the group Polymères Fonctionnels et Réseaux (PFR), directed by Professor Xavier Coqueret.

The first step of this activity concerned the setup of the best working conditions to graft the materials with chitosan. In order to optimize the reaction conditions, two doses of irradiation were used on the blank HDPE (50kGy and 100kGy). After irradiation, the grafting process was conducted in a chitosan solution at 70°C under stirring for different reaction time. Chitosan was purified twice by solubilization in a 1% aqueous acetic acid solution, filtered with filter paper, precipitated with a 1% aqueous sodium hydroxide solution, and washed extensively with deionized water until neutral pH was reached **[8].** This way, the best reaction conditions were assessed and applied to ATZ/HDPE composites. Three different type of samples were selected for grafting process (1/99, 2/98 and 7/93 ATZ/HDPE) under the most efficient reaction time (1 hours and 3 hours). The process feasibility was followed measuring the change in surface wettability by contact angle measurements. ATR spectroscopy were performed to provide further evidence of the surface modification process.

In order to evaluate the influence of the irradiation on the bulk properties, morphology and mechanical properties of the irradiated materials were also investigated.

4.2 Results and discussions

4.2.1 Characterization of low molecular weight chitosan.

The morphology of the chitosan used for the grafting reaction is shown in Figure 4.3. Chitosan (LMWC) used for grafting is a powder characterized by the presence of particles with wide size distribution (from 1 to 200 μm).

The IR spectrum of the sample (4000 – 400 cm^{-1}), reported in figure 4.4, shows the typical N-H, C-O-H and C=O amidic groups belonging to chitosan **[9,10]**. The peaks related to the stretching of amidic C=O bond at 1600 cm^{-1} and to the stretching of C-O bond at 1081 cm^{-1} can be used to identify the chitosan grafted on the composites surface.

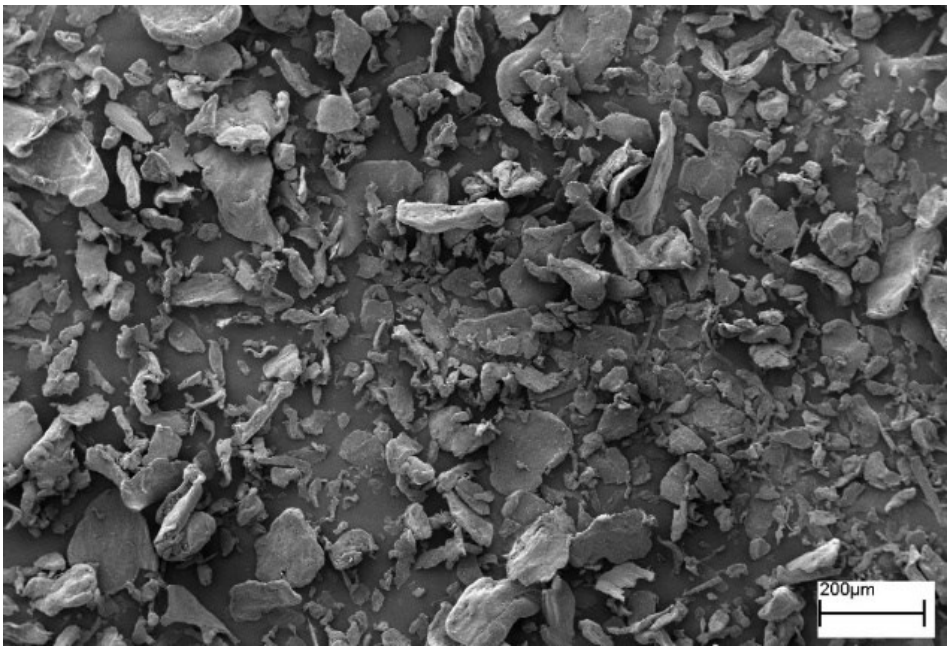

Figure 4.3: SEM micrographs of Chitosan purchased by Sigma Aldrich.

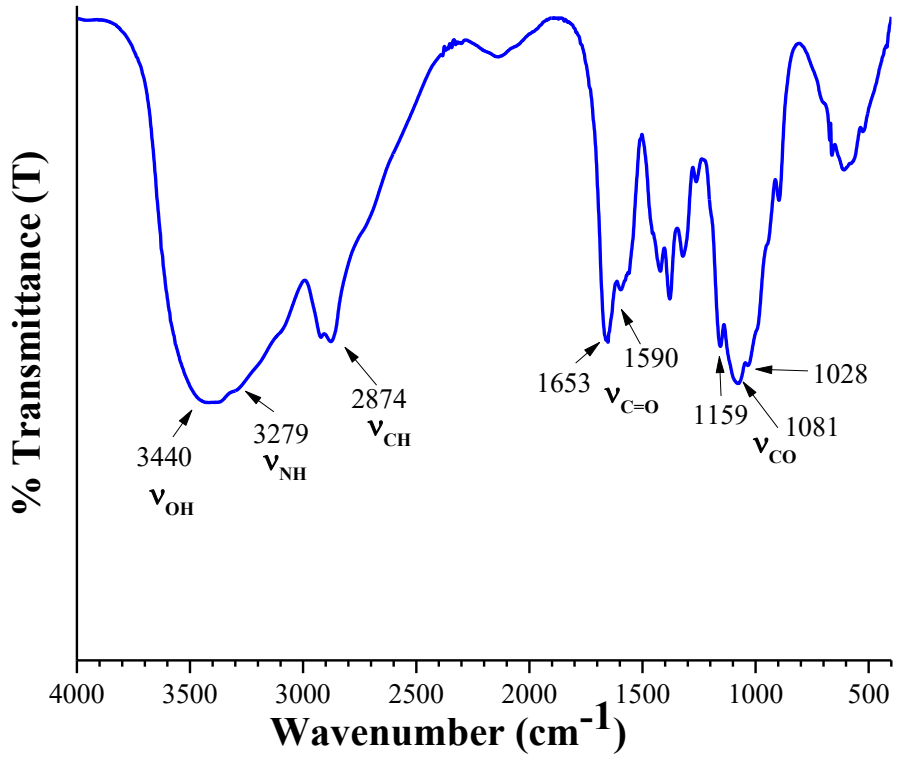

Figure 4.4: IR spectrum of Chitosan used for the grafting process.

4.2.2 Structural analysis and mechanical behavior of irradiated composites

The influence of irradiation on the morphological structure and the consequent mechanical properties are a key issue for the evaluation of the process application. With this purpose, an investigation on the crystallinity index due to the irradiation process was necessary.

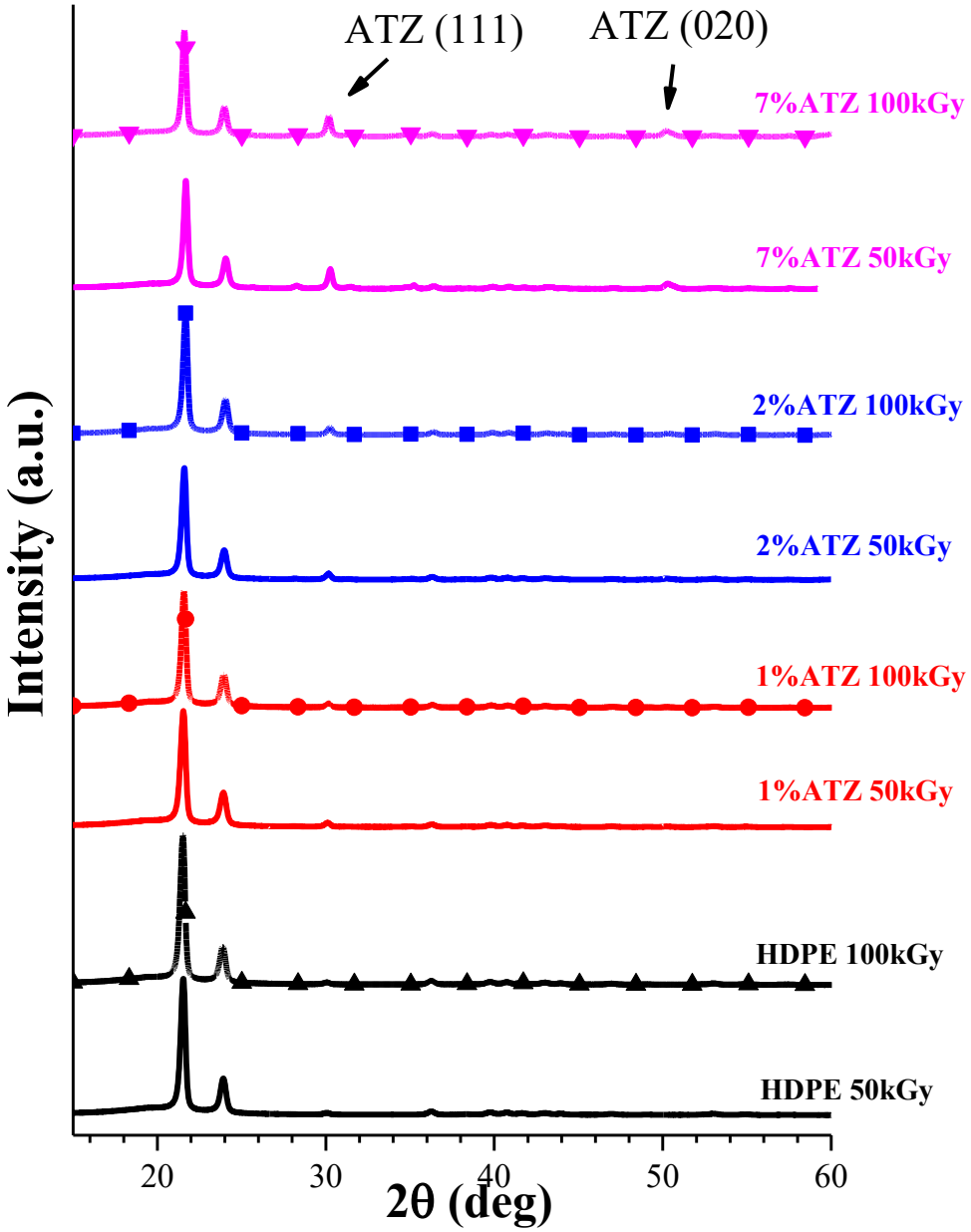

Figure 4.5: XRD patterns of the irradiated materials. Spectra were obtained by XRD powder diffraction experiments using a continuous scan of 0.04°/s, working at 45 kV and 40 mA.

Figure 4.5 reports the X-ray diffraction profiles of irradiated HDPE and HDPE/ATZ composites. All the samples show the presence of the 110, 200 and 020 reflections at 2θ = 21°, 24° and 36° respectively, typical of the orthorhombic form of polyethylene **[11]**. Also the most intense peaks related to the ATZ are detected. In particular, the peaks at 2θ = 30° and 50° (111 and 202 reflections) are related to the tetragonal and monoclinic form of the Zirconium Oxide.

The crystallinity degree (x_c) of the irradiated materials, obtained by the ratio between the intensity of the crystalline phase diffraction and the intensity of the total sample diffraction, is shown in Table 4.1. According with literature **[12]**, x_c increases after the irradiation. This is due to the crystallization of tie chain molecules that undergo scission in the amorphous region during the process. The increase in crystallinity is more relevant at 100kGy and for neat HDPE and 7/93 ATZ/HDPE.

Table 4.1: Cristallinity degree (x_c) of the irradiated composites, calculated by XRD, compared to the untreated materials.

	Cristallinity degree x_c		
Materials	0kGy	50kGy	100kGy
HDPE blank	69.3%	74.6%	78.4%
1/99 ATZ/HDPE	70.6%	76.0%	78.5%
2/98 ATZ/HDPE	72.7%	76.5%	78.6%
7/93 ATZ/HDPE	75.0%	87.5%	85.0%

Table 4.2 reports the tensile properties of irradiated and untreated materials obtained by stress – strain test. The Young modulus of irradiated materials increases after irradiation in most of the cases. The increase is more evident for neat HDPE and for 7/93 ATZ/HDPE, although it does not seem related to the radiation dose. For all the composites, the elongation at break decreases after irradiation, whereas the tensile

strength is not affected in a relevant way. The increase of elastic modulus and the decrease of elongation at break can be ascribed to the increase of material crystallinity **[11]**.

In the case of the HDPE, the irradiation process at leads to an increment of the tensile strength and to an increment of the elongation at break.

Table 4.2: Young modulus (***E***), tensile strength at break (σ_b) and elongation at break (ε_b) of irradiated composites obtained by stress – strain experiments performed at room temperature.

Young modulus (*E*) (MPa)			
Materials	0kGy	50kGy	100kGy
HDPE blank	969 ± 17	1147 ± 80	1052 ± 75
1/99 ATZ/HDPE	1189 ± 34	1090 ± 18	1202 ± 65
2/98 ATZ/HDPE	1139 ± 16	1210 ± 18	1152 ± 50
7/93 ATZ/HDPE	1088 ± 53	1245 ± 36	1271 ± 24
Tensile Strength (σ_b) (MPa)			
Materials	0kGy	50kGy	100kGy
HDPE blank	13.7 ± 0.4	16.4 ± 0.4	15.3 ± 0.6
1/99 ATZ/HDPE	14.3 ± 0.3	12.0 ± 0.4	13.9 ± 0.5
2/98 ATZ/HDPE	15.4 ± 0.5	14.2 ± 0.9	13.7 ± 1.5
7/93 ATZ/HDPE	12.5 ± 1.5	13.9 ± 0.7	13.0 ± 0.9
Elongation at break (ε_b) (%)			
Materials	0kGy	50kGy	100kGy
HDPE blank	320 ± 100	735 ± 268	79 ± 81
1/99 ATZ/HDPE	647 ± 28	138 ± 118	97 ± 105
2/98 ATZ/HDPE	704 ± 85	131 ± 58	254 ± 140
7/93 ATZ/HDPE	365 ± 145	92 ± 65	100 ± 6

4.2.3 Characterization of the grafted materials

With the purpose to find the most efficient conditions to graft the materials with chitosan, different reaction times were used on the neat HDPE, treated at 50kGy and 100kGy. The grafting process feasibility was followed measuring the change of surface wettability by contact angle measurements. Figure 4.6 displays representative images of 3μL water droplet profile on the grafted HDPE sheets, treated at different reaction time. Different contact angles can be observed, indicating the different degree of hydrophilicity of the materials. In particular, an unexpected variation of the contact angle as a function of the grafting time in presence of chitosan was observed: the hydrophilicity, initially enhanced by grafting, was gradually lost for longer grafting times. For both irradiation doses, the lowest value of contact angle (i.e. the most efficient reaction time) was obtained after 3 hours of grafting reaction.

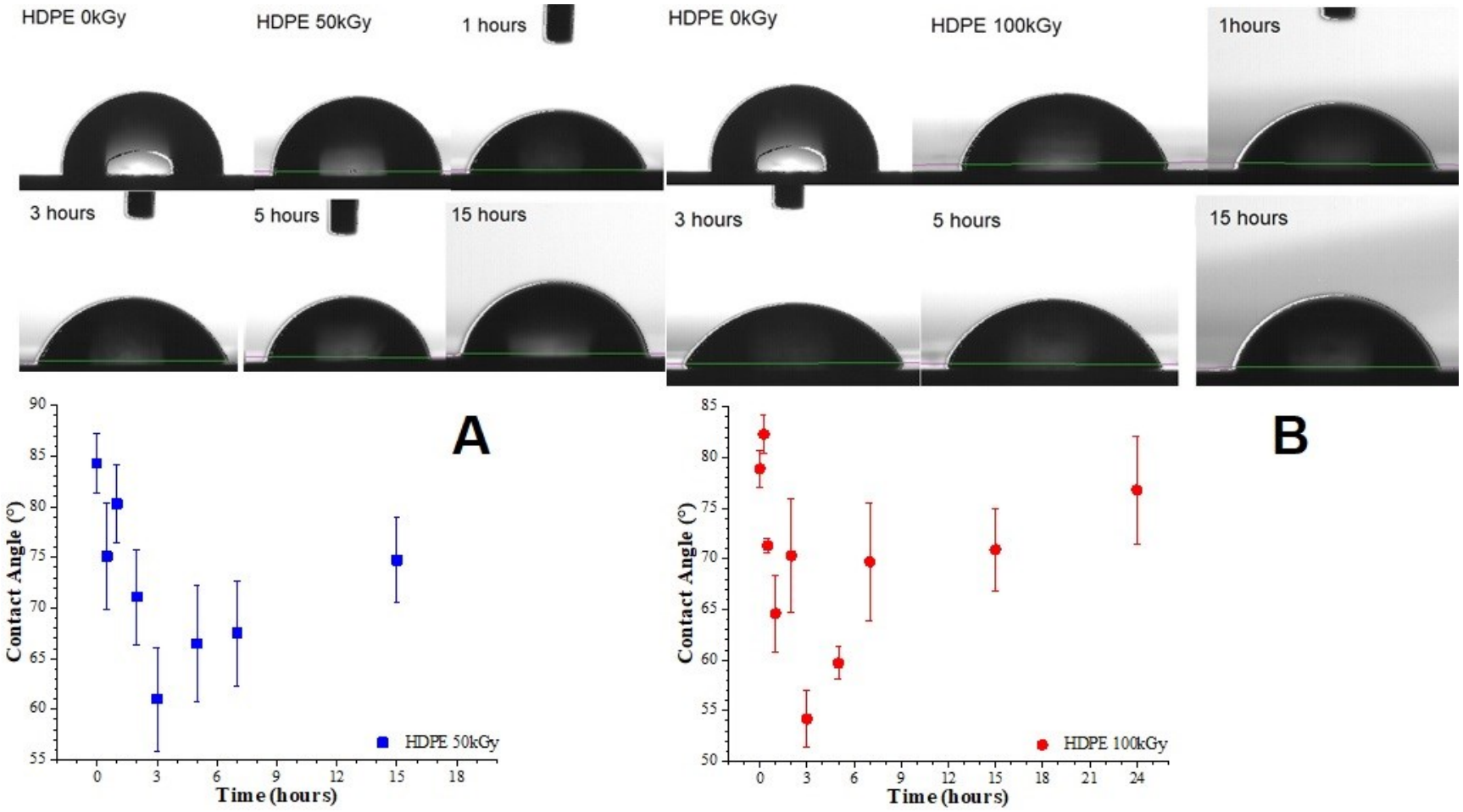

Figure 4.6: a) Contact angle measurements of HDPE treated at (a) 50kGy and (b) 100kGy and grafted for different reaction time

ATR spectra, reported in Figure 4.7, show the presence of C=O amidic bond on HDPE surface after chitosan grafting. For both the set of materials (treated at 50 and 100 kGy), the intensity of the peaks is higher for the samples with the highest wettability. Indeed, the materials for which the grafting time was 1h and 3h present the highest intensity of the C=O amidic peak, then roughly confirming the wettability results.

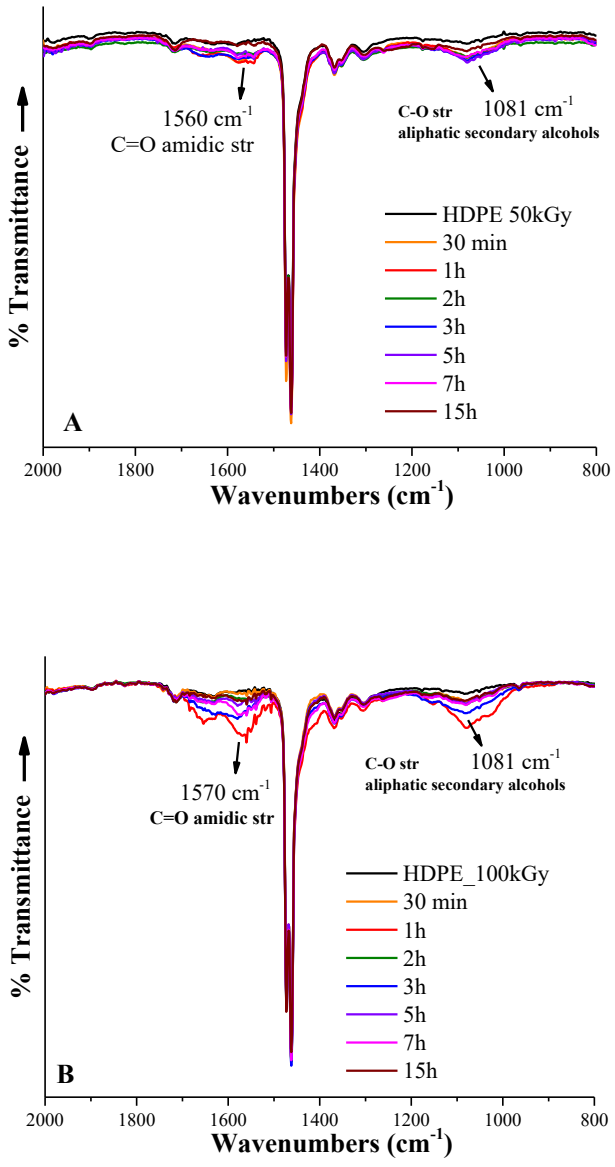

Figure 4.7: ATR spectra of HDPE treated at (A) 50kGy and (B) 100 kGy grafted at different reaction time

According to these results, ATZ/HDPE composites (i.e. 1/99, 2/98 and 7/93), activated by irradiation at 50 and 100kGy, were grafted with chitosan at two reaction time (i.e. 1 hours and 3 hours). Contact angle measurements were measured after the grafting process. Tables 4.3 and 4.4 show the contact angle values obtained for irradiated samples at 50 kGy and 100 kGy respectively. Only 1/99 ATZ/HDPE sample, treated at 100kGy and grafted for 3 hours, shows a significant decrease of the contact angle with respect to the simply-irradiated sample (i.e. 66.0 ± 4.7 respect to 71.6 ± 2.3). For all the other samples, the wettability of the materials grafted with chitosan does not decrease with respect to the irradiated samples. Even, in some cases the contact angle value increases with respect to that of the irradiated samples. ATR spectra, reported in figure 4.8A, B and C, show an increase of the peaks related to amidic C=O and alcoholic C-O bond only for the 1/99 ATZ/HDPE sample, explaining the reason for the contact angle decrease. In brief, the grafting process for composites with an ATZ content of 2 and 7 wt% is not feasible at the same conditions of neat HDPE. On the contrary, the process would seem feasible for the 1/99 ATZ/HDPE composite.

Table 4.3: Contact angle average values obtained using the sessile drop method for neat HDPE, 1/99, 2/98 and 7/93 ATZ/HDPE composites irradiated at 50kGy and grafted for 1 hour and 3 hours

Samples	**Contact angle**	**Samples**	**Contact angle**	**Samples**	**Contact angle**	**Samples**	**Contact angle**
HDPE untreated	95.5 ± 2.1	1/99 ATZ/HDPE blank	83.1 ± 3.0	2/98 ATZ/HDPE blank	96.3 ± 3.0	7/93 ATZ/HDPE blank	95.5 ± 3.2
HDPE 50kGy	84.3 ± 2.9	1/99 ATZ/HDPE 50kGy	74.8 ± 2.7	2/98 ATZ/HDPE 50kGy	73.4 ± 2.7	7/93 ATZ/HDPE 50kGy	71.2 ± 2.6
HDPE 50kGy Grafted 1h	80.3 ± 3.9	1/99 ATZ/HDPE 50kGy Grafted 1h	81.2 ± 5.0	2/98 ATZ/HDPE 50kGy Grafted 1h	69.9 ± 5.6	7/93 ATZ/HDPE 50kGy Grafted 1h	79.7 ± 3.9
HDPE 50kGy Grafted 3h	61.6 ± 5.1	1/99 ATZ/HDPE 50kGy Grafted 3h	73.6 ± 3.8	2/98 ATZ/HDPE 50kGy Grafted 3h	73.1 ± 1.7	7/93 ATZ/HDPE 50kGy Grafted 3h	79.2 ± 5.0

Table 4.4: Contact angle average values obtained using the sessile drop method for neat HDPE, 1/99, 2/98 and 7/93 ATZ/HDPE composites irradiated at 100kGy and grafted for 1 hour and 3 hours

Samples	**Contact angle**	**Samples**	**Contact angle**	**Samples**	**Contact angle**	**Samples**	**Contact angle**
HDPE untreated	95.5 ± 2.1	1/99 ATZ/HDPE untreated	83.1 ± 3.0	2/98 ATZ/HDPE untreated	96.3 ± 3.0	7/93 ATZ/HDPE untreated	95.5 ± 3.2
HDPE 100kGy	78.9 ± 1.8	1/99 ATZ/HDPE 100kGy	71.6 ± 2.3	2/98 ATZ/HDPE 100kGy	72.4 ± 3.9	7/93 ATZ/HDPE 100kGy	66.8 ± 3.7
HDPE 100kGy Grafted 1h	74.5 ± 4.3	1/99 ATZ/HDPE 100kGy Grafted 1h	74.5 ± 4.3	2/98 ATZ/HDPE 100kGy Grafted 1h	81.9 ± 5.5	7/93 ATZ/HDPE 100kGy Grafted 1h	75.3 ± 5.3
HDPE 100kGy Grafted 3h	66.0 ± 4.7	1/99 ATZ/HDPE 100kGy Grafted 3h	66.0 ± 4.7	2/98 ATZ/HDPE 100kGy Grafted 3h	73.0 ± 3.0	7/93 ATZ/HDPE 100kGy Grafted 3h	70.4 ± 4.1

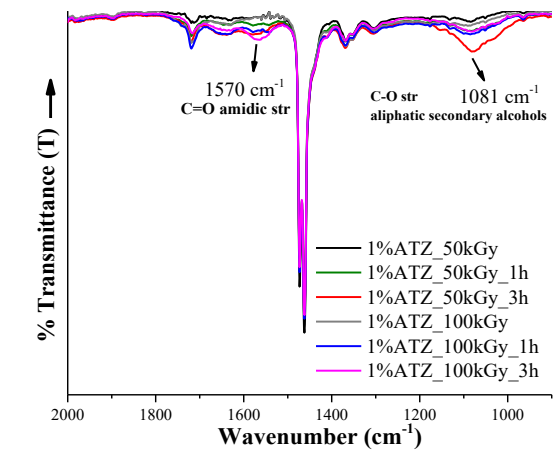

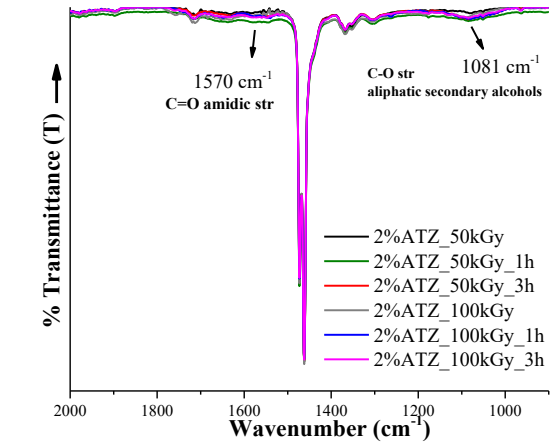

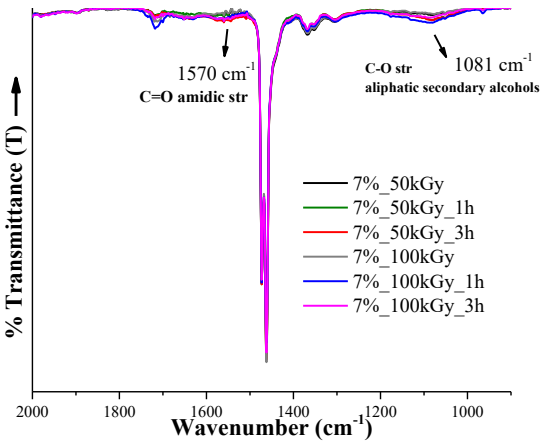

Figure 4.8: a) ATR spectra of 1/99 ATZ/HDPE treated at 50 and 100kGy and grafted with Chitosan for 1 and 3 hours. b) ATR spectra of 2/98 ATZ/HDPE treated at 50 and 100kGy and grafted with Chitosan for 1 and 3 hours. c) ATR spectra of 7/93 ATZ/HDPE treated at 50 and 100kGy and grafted with Chitosan for 1 and 3 hours.

4.3 Conclusions

An explorative study, dealing with the grafting of the ATZ/HDPE composites with chitosan, induced by pre-irradiation is discussed in this chapter.

The work was divided in two parts: the first step was devoted to the optimization of the grafting reaction conditions, carried out on the neat HDPE. For this purpose, the grafting reactions were conducted at different time on HDPE slabs after the irradiation treatment at 50 and 100kGy. All the experiments were carried out at 70°C, in a 1wt% solution of purified chitosan, under argon atmosphere. The grafting process was followed by contact angle measurements and ATR spectroscopy.

The experiments revealed that radiation-induced grafting of chitosan on HDPE was effective using under 50 and 100kGy of irradiation and 1 and 3 hours of reaction time.

According to the results obtained on the neat HDPE, ATZ/HDPE composites (i.e. 1/99, 2/98 and 7/93), irradiated at 50 and 100kGy, were grafted with chitosan at 1 and 3 hours. Both contact angle and ATR measures reveal that only 1/99 ATZ/HDPE composite shows evidence of successful grafting process. On the contrary, 2/98 and 7/93 ATZ/HDPE does not show increase of wettability as a consequence of surface modification. Indeed, for these composites, ATR spectra do not reveal the presence of C=O amidic bond on the surface.

The influence of irradiation on materials morphology and mechanical properties was investigated. An increase of the crystallinity degree as a consequence of irradiation process was observed: such increase leads to a general increment of the young modulus of the composites, in particular in the case of 7/93 ATZ/HDPE, and to a decrease of the elongation at break for all the samples.

4.4 Bibliography

[1] Stannet V. T. Radiation grafting – State-of-the-art *Int J Radiat Appl Instrum, Part C* **(1990)** 35; 82-87.

[2] Uyama Y.,Kato K., Ykada Y. Surface modification of polymers by grafting *Adv Polym Sci* **(1998)** 137; 1-39.

[3] Ferry M., Ngono-Ravache Y., Aymes-Chodur C., Clochard M.C., Coqueret X., Cortella L., Pellizzi E., Rouif S., Esnouf S. Ionizing radiation effects in polymers: Reference Module in Materials Science and Materials Engineering Oxford: *Elsevier* **(2016).**

[4] Walo M. Radiation-induced grafting. In Y. Sun, & A. G. Chmielewski Applications of ionizing radiation in materials processing *Warzsawa* **(2017)** vol. 1 p. 193.

[5] Brack P., Buhrer H.G., Bonorand L., Scherer G.G. Grafting of pre-irradiated poly (ethylene-alt-tetrafluoroethylene) films with styrene: influence of base polymer film properties and processing parameters *J. Mater. Chem.* **(2000)** 10; 1795-1803.

[6] Nasef M.M, Guven O. Radiation-grafted copolymers for separation and purification purposes: Status, challenges and future directions *Prog. Polym. Sci.* **(2012)** 37(12); 1597-1656.

[7] Garbassi F., Morra M., Occhiello E. Polymer Surfaces: From Physics to Technology Chichester (UK): Wiley **(1998)** p. 245.

[8] dos Santos D.S., Goulet P.J.G., Pieczonka N.P.W., Oliveira O.N., Aroca R.F. Gold nanoparticle embedded, self-sustained chitosan films as substrates for surface-enhanced Raman scattering *Langmuir* **(2004)** 20; 10273-10277.

[9] Pearson F.G., Marchessault R.H., Liang C.Y. Infrared spectra of crystalline polysaccharides. V. Chitin *J Polym Sci* **(1960)** 43; 101.

[10] Shigemasa Y., Matsuura H., Sashiwa H., Saimoto H. Evaluation of different absorbance ratios from infrared spectroscopy for analyzing the degree of deacetylation in chitin *Int. J. Biol. Macromol.* **(1996)** 18; 237-242

[11] Bunn C.W. The crystal structure of long-chain normal paraffin hydrocarbons. The “shape” of the CH2 group, *Trans. Faraday Soc.* **(1939)** 35; 482–491.

[12] Bhateja S.K., Andrews E.H., Young R.J. Radiation-Induced crystallinity changes in linear polyethylene *J. Polym. Sci., Polymer Phys. Ed.* **(1983)** 21; 523–536.

Chapter 5

Biological response of HDPE-based composites

5.1 Introduction

5.1.1 Biological behavior of materials intended for biomedical applications: cell adhesion and cell viability assays

An important feature that a material designed for biomedical applications should possess is to interact positively with the biological environment. Generally, fillers have the role of improving the response to the cellular environment of bioinert materials, such as PE, as well to reinforce the mechanical properties of the polymer matrix. **[1]**.

In order to evaluate the biological behavior of materials for biomedical applications and to avoid possible cytotoxicity of the fillers, variety of in vitro biological assays are usually performed on these systems.

Among the available methods, cell adhesion and cell viability assays are the most frequently employed. In fact, cell adhesion, the binding of a

cell to the extracellular matrix (ECM), other cells, or a specific surface **[2]**, plays a key role in a wide number of biological processes and is essential in cell communication and regulation. The amount of cells able to interact with a material is an index of its affinity with the biological environment. Cell attachment and detachment events are taken into consideration in these assays. Cell detachment could be related to the accumulation of toxins, drugs or nanoparticles, which lead to the cell death and which could represent a sign of cytotoxicity. On the contrary, high viability and cell proliferation indicate a good biological response of the materials.

5.1.2 Description of the chapter work

Cell adhesion and cell viability assays were performed with the aim to investigate the influence of ATZ and chitosan (mixed in the polymer matrix and grafted on the surface) on the biological behavior of the composites. For this purpose, the cell adhesion after 10 minutes and the number of viable cells still presents at 24 hours on the samples surface were evaluated. The samples wettability and the cells morphology were studied in order to understand the main features affecting the cells response.

5.2 Results and discussions

Biological assays were conducted on the following composites:

1) Neat HDPE, as a control sample;
2) HDPE/ATZ (99/1, 98/2 and 93/7) HDPE/ATZ 99/1 and 98/2 have been selected because they show higher young modulus and an improved tensile strength respect to neat HDPE. HDPE/ATZ 93/7 has been selected because, despite the worse dispersion of ATZ in the polymer matrix, it shows the highest storage modulus at 40°C.
3) HDPE/chitosan M and N (98/2 and 95/5), with the purpose to evaluate the effect of the type and amount of chitosan on the biological response of the composites.
4) HDPE, HDPE/ATZ 99/1, HDPE/ATZ 98/2 and HDPE 93/7 irradiated at 100kGy and grafted with chitosan for 3 hours, that was the best reaction condition to graft chitosan on the composites surface (section 4.3.2).

5.2.1 ATZ influence on the biological response of HDPE/ATZ composites

Figure 5.1 shows cell adhesion at 10min (A) and cell viability after 24h (B) of the composites HDPE/ATZ (99/1, 98/2 and 93/7). As clearly seen in Figure 5.1A, ATZ presence in low amount improves the cell adhesion of the composites. More interesting is the cell viability, shown in Figure 5.1B, where the composite with 2% of ATZ shows a higher efficiency in promoting the cell viability with respect to neat HDPE and the other composites. This result is consistent with the cell viability obtained

for UHMWPE/ATZ composites **[3-5]**, for which the composite at 2.5% of ATZ has shown the higher cell viability with respect to the composites at higher amount of ATZ. However, unlike what is discussed in **[4]**, in this case no relation between cell viability and wettability of the composites can be observed. As shown in Figure 5.2 the pattern of wettability does not appear similar to the pattern of the cell viability. In particular, wettability of neat polymer is similar to that of the composite with 2% of ATZ, which is instead the most prone to favor the cell viability.

The enhancement of the cells interaction can be then ascribed to the good dispersion of ATZ in the composites with low filler amount. It can be supposed that 1% of ATZ is not enough to guarantee an improvement in terms of cells viability, for which a percentage of 2% is needed. For higher content (i.e. 7%), the inhomogeneity of ATZ dispersion disadvantages the interaction with cells, that becomes similar to that of the neat polymer.

Micrographs reported in Figure 5.3 show the cell morphology present at the surface after the cell viability assays at 24h. Fibroblasts appear well-spread and spindle-shaped for all the composites and neat HDPE, and they form clear filopodia (Figure 5.3E), according to the well-known morphology of fibroblast. Filopodia are actin-containing structures with an important sensory function in fibroblasts and are required for guidance of neuronal growth cones **[6]**. In this case, their formation is a strong index of cellular mobility and reveals that the materials have a good interaction with the biological environment.

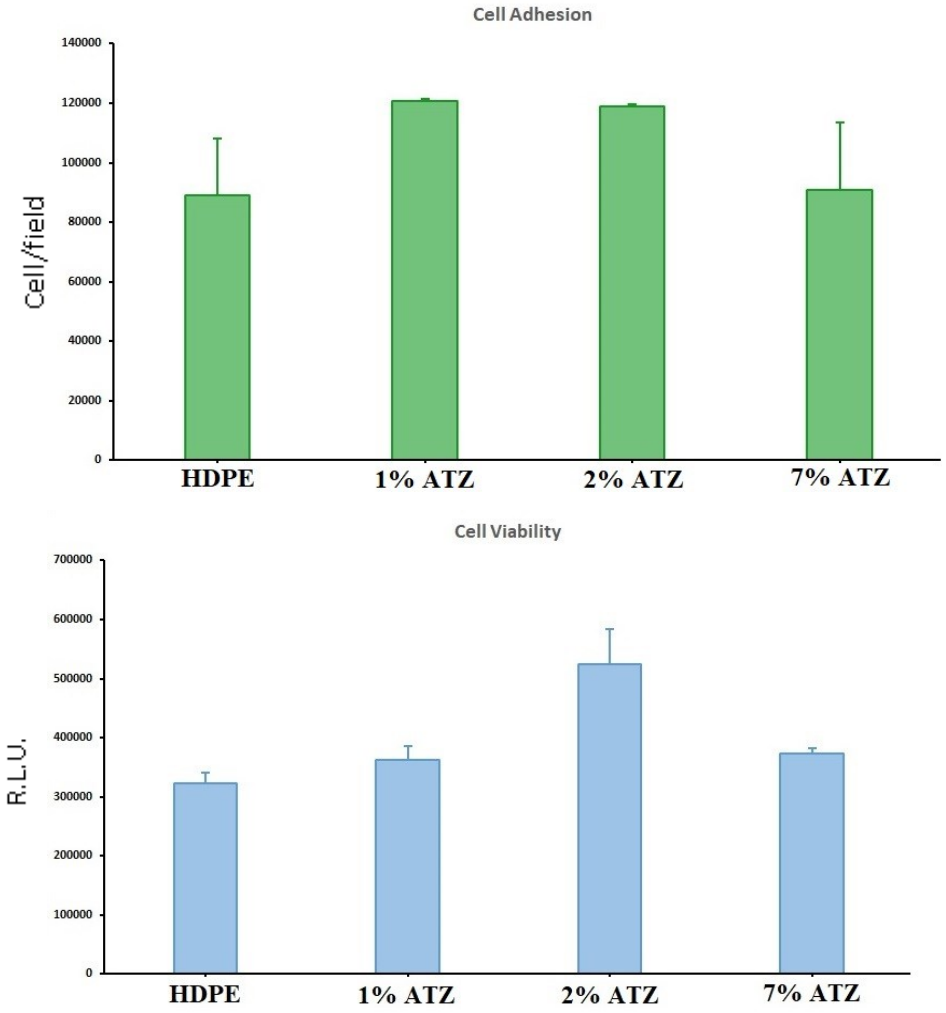

Figure 5.1: Adherent fibroblast per field at 10 min (A) and the viable cells after 24h (B) of HDPE/ATZ composites.

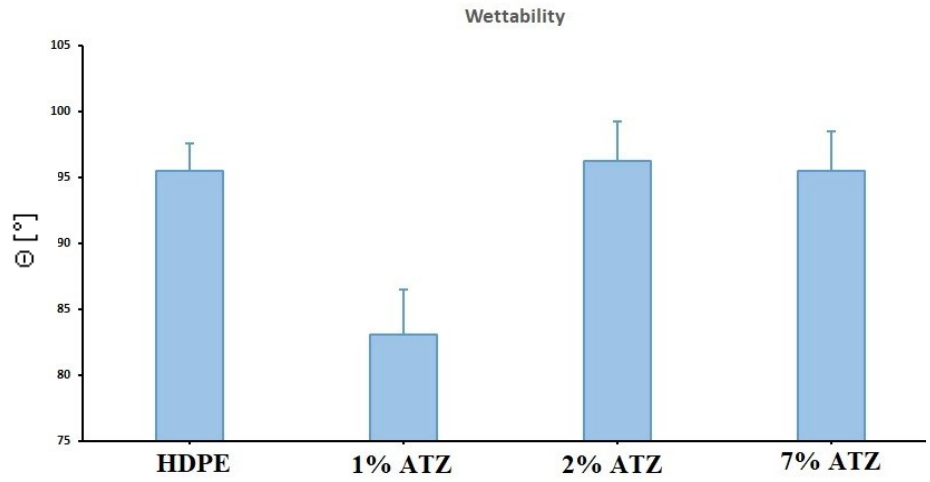

Figure 5.2: Water contact angle values obtained using the sessile drop method for neat HDPE, 1/99, 2/98 and 7/93 ATZ/HDPE composites.

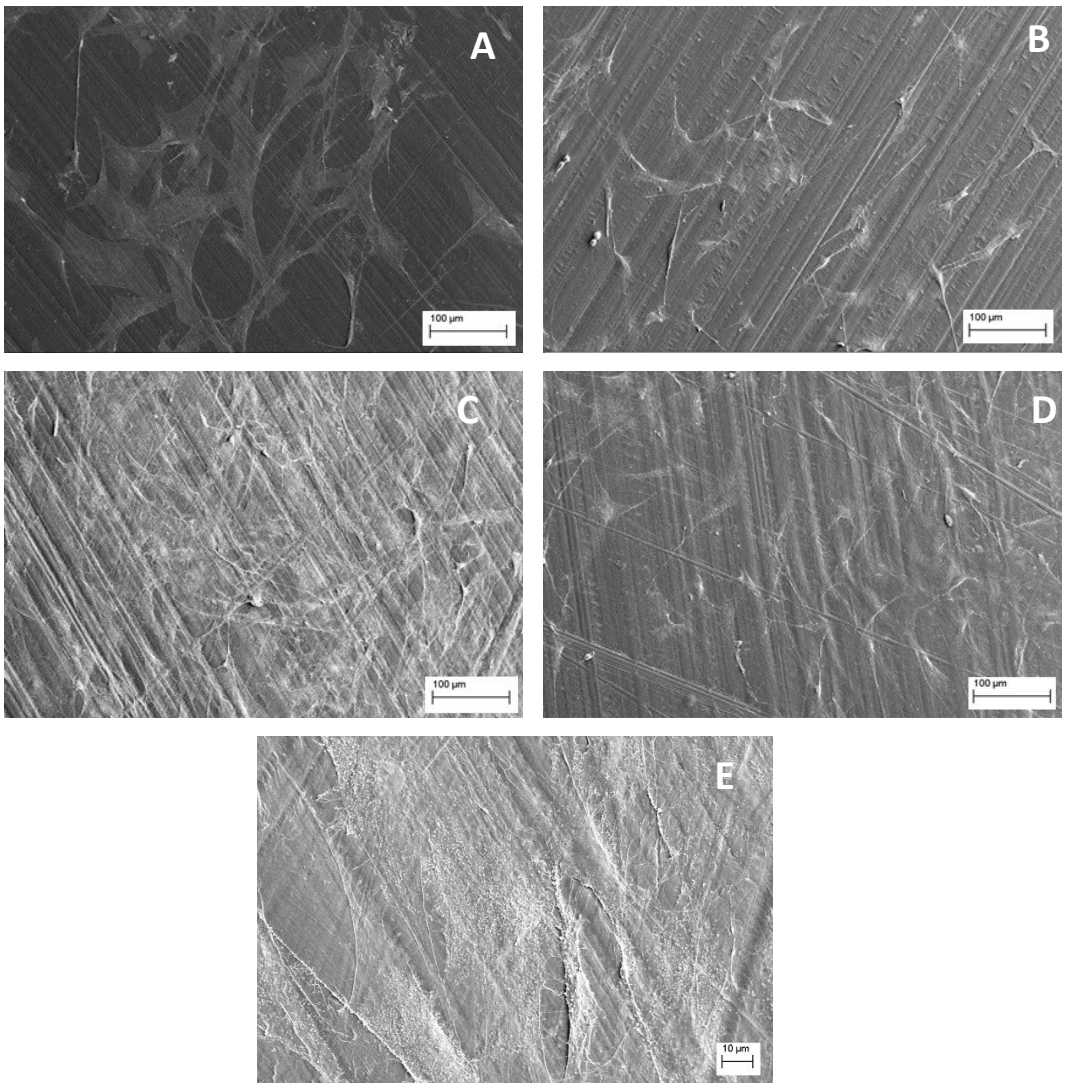

Figure 5.3: Fibroblast morphology observed on neat HDPE (A), 1/99 (B), 2/98 (C) and 7/93 (D) ATZ/HDPE composites at 24h and a representative image of an fibroblast showing the formation of filopodia (E).

5.2.2 Chitosan influence on the biological response of HDPE/chitosan composites

Figure 5.4 shows cell adhesion at 10min (A) and cell viability after 24h (B) of the composites HDPE/chitosan M (98/2 and 95/5) and HDPE/chitosan N (98/2 and 95/5). As for ATZ, chitosan M and N improves the cell adhesion of the composites, with respect the unfilled HDPE. The composites with higher content of chitosan are more efficient to promote the immediate cell adhesion, while show a lower cell viability with respect to the other samples. Indeed, the samples with 2% of chitosan exhibit the best behavior in terms of viability, that is significantly higher with respect to pure HDPE. Chitosan M increases the cell viability more than chitosan N. Figure 5.5 shows the contact angles obtained for the composites with chitosan M and chitosan N. Both chitosan M and N significantly improves the wettability of the composites, regardless their amount. Also in this case, the pattern of the wettability does not follow the cell viability behavior. It is then reasonable to assume that the main effect on cell interaction is given by the chemical effect of chitosan. Indeed, low amount of chitosan promotes a good fibroblasts adhesion but higher concentrations negatively affect cell viability. Probably, when the chitosan percentage overcome an edge value, the cell viability decreases due to the same reason for which chitosan acts as an antibacterial agent **[7]**.

Micrographs reported in Figure 5.6 show the cell morphology, after the viability assay at 24h. As for the composites with ATZ, the morphology of fibroblasts appears spindle-shaped for all the samples. Cells are also well-spread on the surface, in particular in the case of HDPE/chitosan M composites. Fibroblast form clear filopodia, according to the well-known morphology of fibroblast, as reported for the composites containing ATZ.

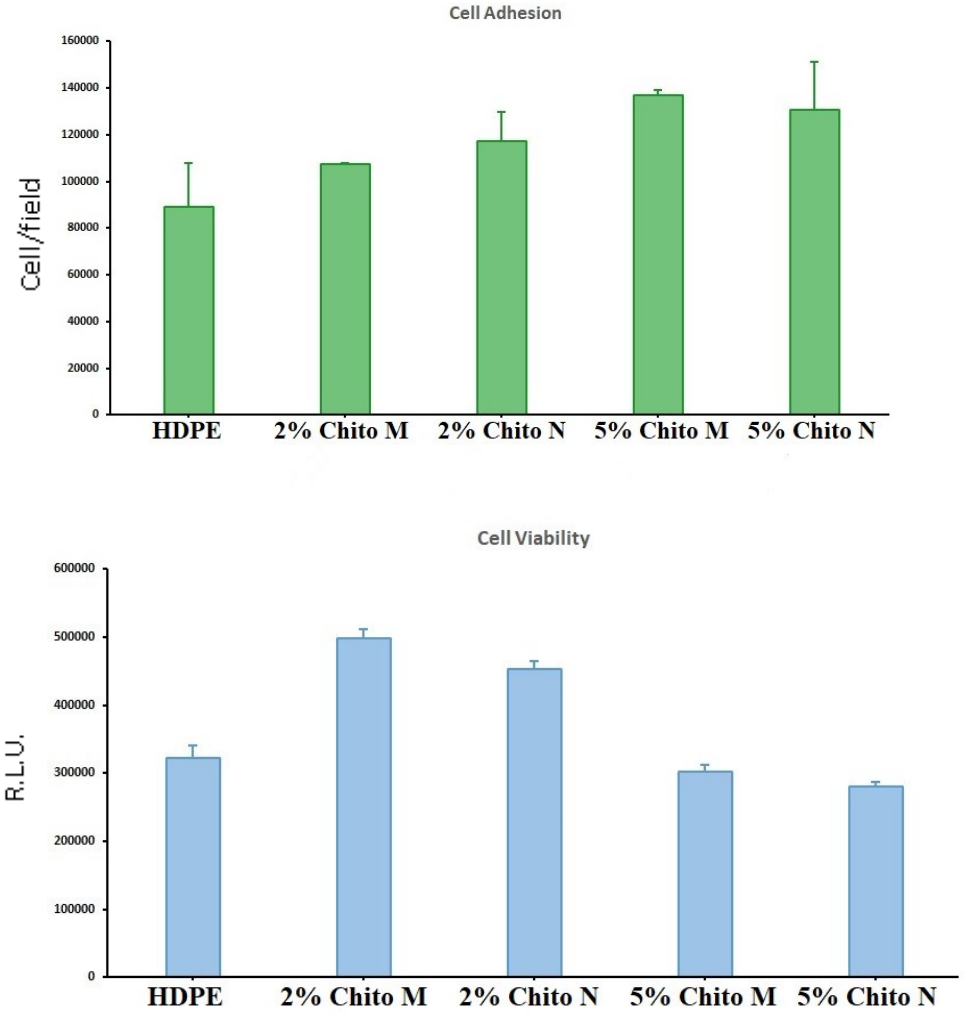

Figure 5.4: Adherent fibroblast per field at 10 min (A) and the viable cells after 24h (B) of HDPE/chitosan composites.

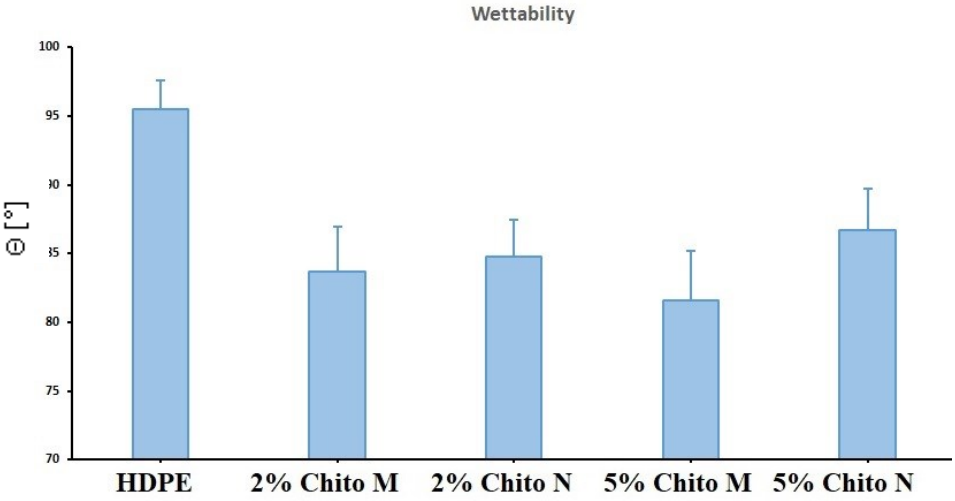

Figure 5.5: Water contact angle values obtained using the sessile drop method for HDPE/chitosan M 98/2 and 95/5 and HDPE/chitosan N 98/2 and 95/5 composites.

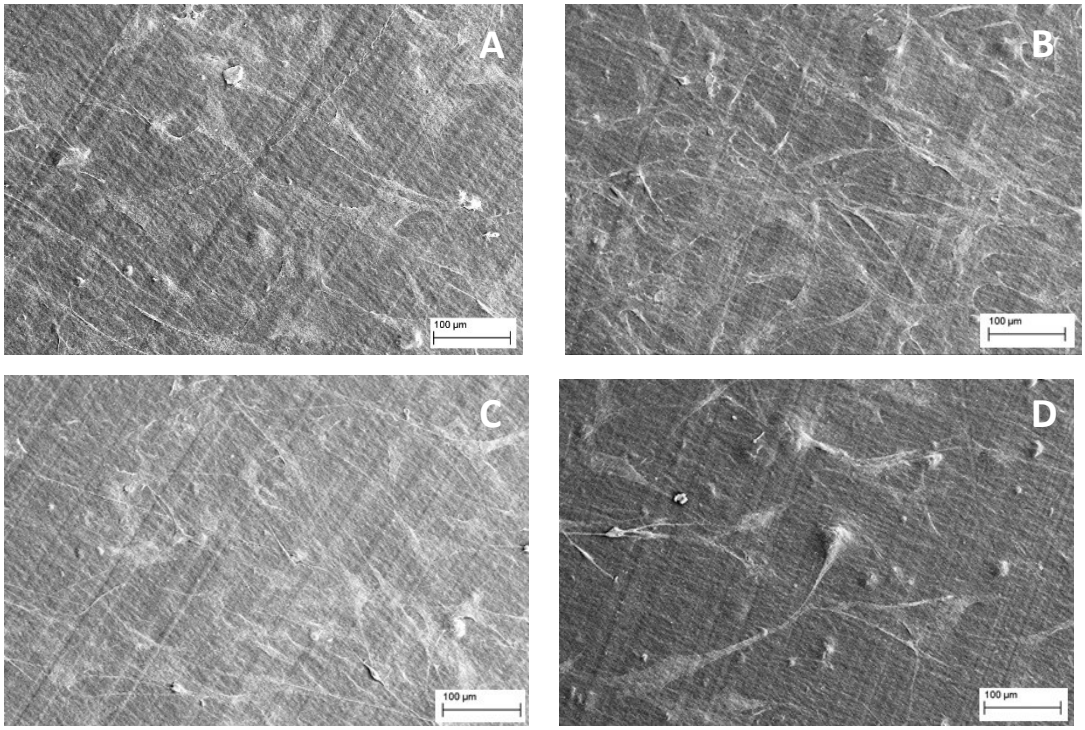

Figure 5.6: Fibroblast morphology observed on HDPE/chitosan M 98/2 (A), HDPE/chitosan M 95/5 (B), HDPE/chitosan N 98/2 and HDPE/chitosan N 95/5 (D) at 24h.

5.2.3 Biological response of HDPE/ATZ composites grafted with chitosan

Figure 5.7 shows cell adhesion at 10min (A) and cell viability after 24h (B) of the composites HDPE/ATZ (99/1, 98/2 and 93/7), irradiated at 100kGy and grafted with chitosan for 3 hours. The immediate adhesion and the cell viability are compared with the results obtained on the untreated composites.

The cell adhesion of the grafted materials is generally a little bit higher than that of the untreated composites, except for the HDPE/ATZ 99/1, that shows an immediate adhesion significantly lower with respect the untreated material. On the contrary, cell viability at 24h significantly decreases for the grafted composites. The higher value of the cell viability was obtained for HDPE/ATZ 93/7. According to the results obtained with HDPE/chitosan composites, the presence of chitosan graft on the surface drastically reduces their cell viability.

Micrographs reported in Figure 5.8 show the cell morphology after cell viability assay at 24h. As for the other composites, the morphology of fibroblasts appears spindle-shaped for all of them and they form clear filopodia, according to the well-known morphology of fibroblast. Fibroblast are well-spread on the grafted HDPE and grafted 2% ATZ and 7% ATZ whereas they appear significantly less spread on the grafted HDPE/ATZ 99/1 (Figure 5.9B).

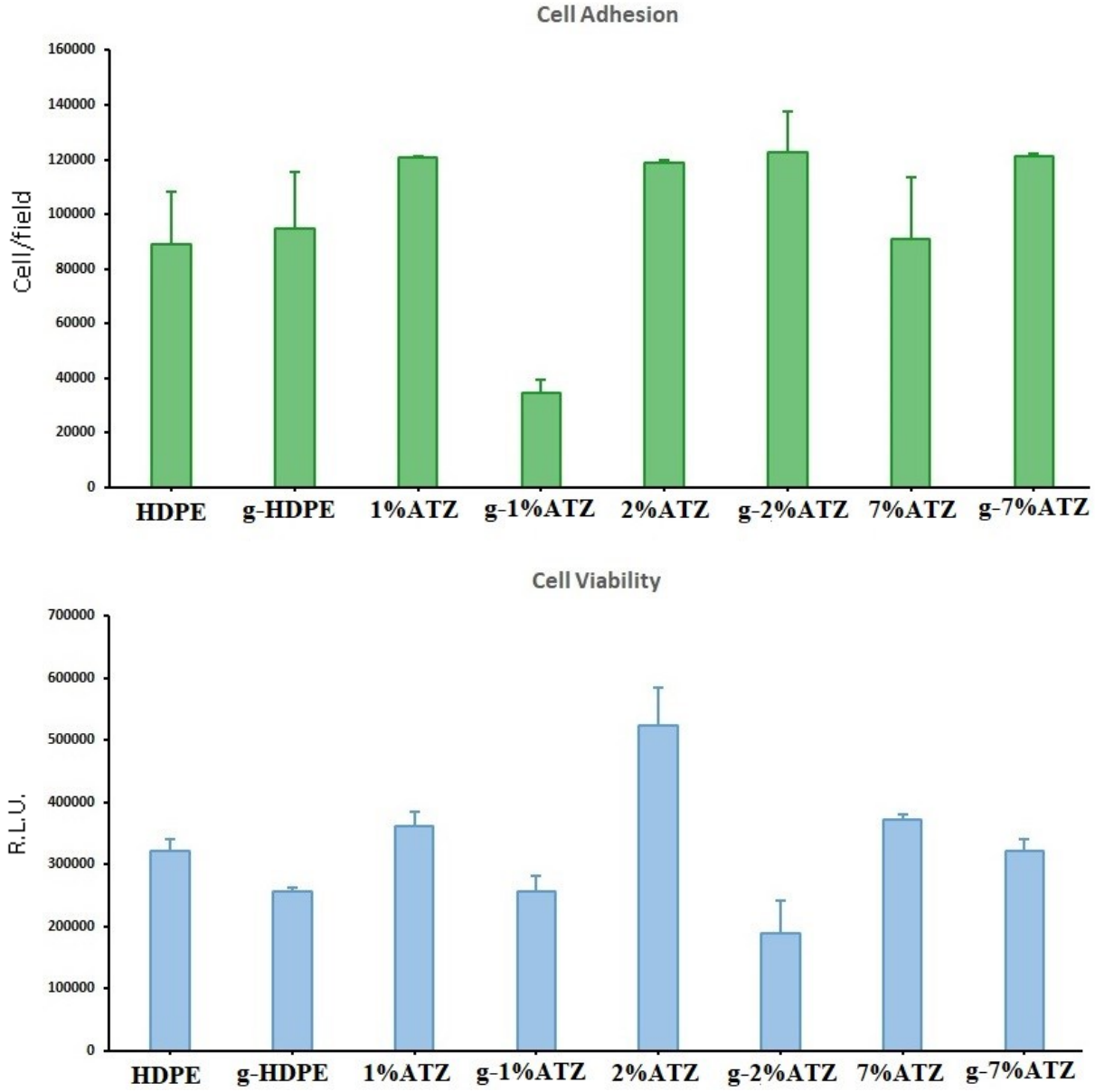

Figure 5.7: Adherent fibroblast per field at 10 min (A) and the viable cells after 24h (B) of HDPE/ATZ composites grafted with chitosan.

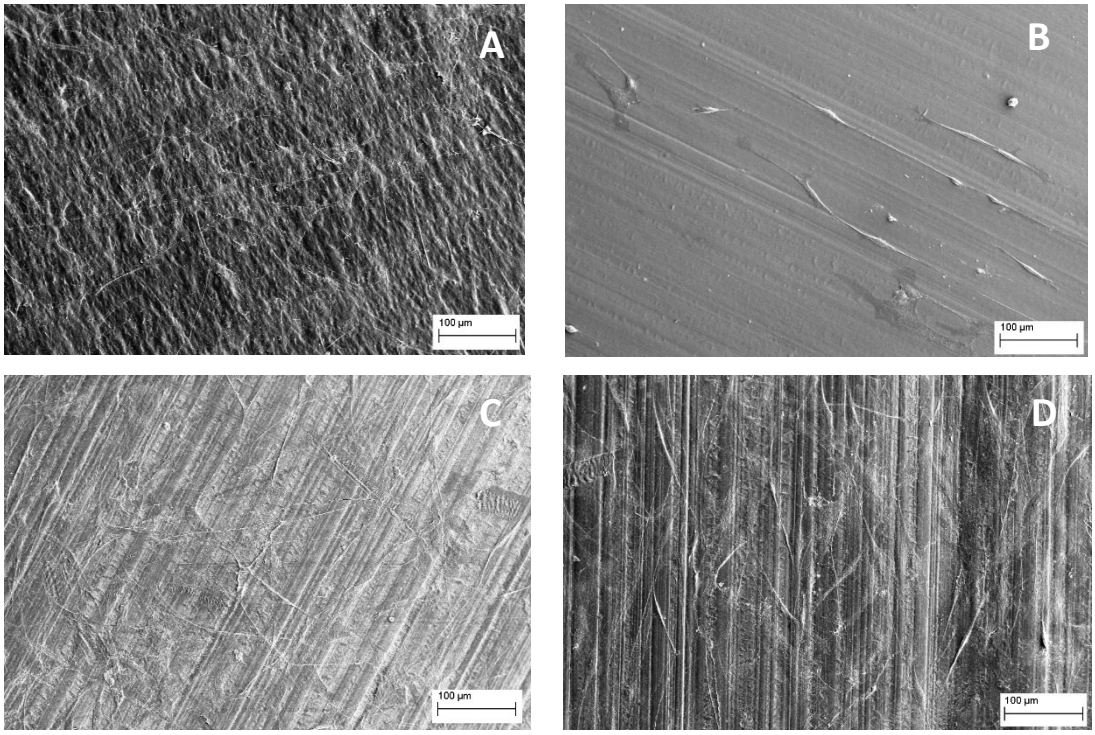

Figure 5.8: Fibroblast morphology observed on neat HDPE grafted with chitosan (A), HDPE/ATZ 99/1 grafted with chitosan (B), HDPE/ATZ 98/2 grafted with chitosan (C) and HDPE/ATZ 93/7 grafted with chitosan (D) at 24h.

5.3 Conclusions

With the aim to compare the results, Figure 5.9 reports a bar chart of immediate cell adhesion and cell viability at 24h for all the composites discussed in this chapter.

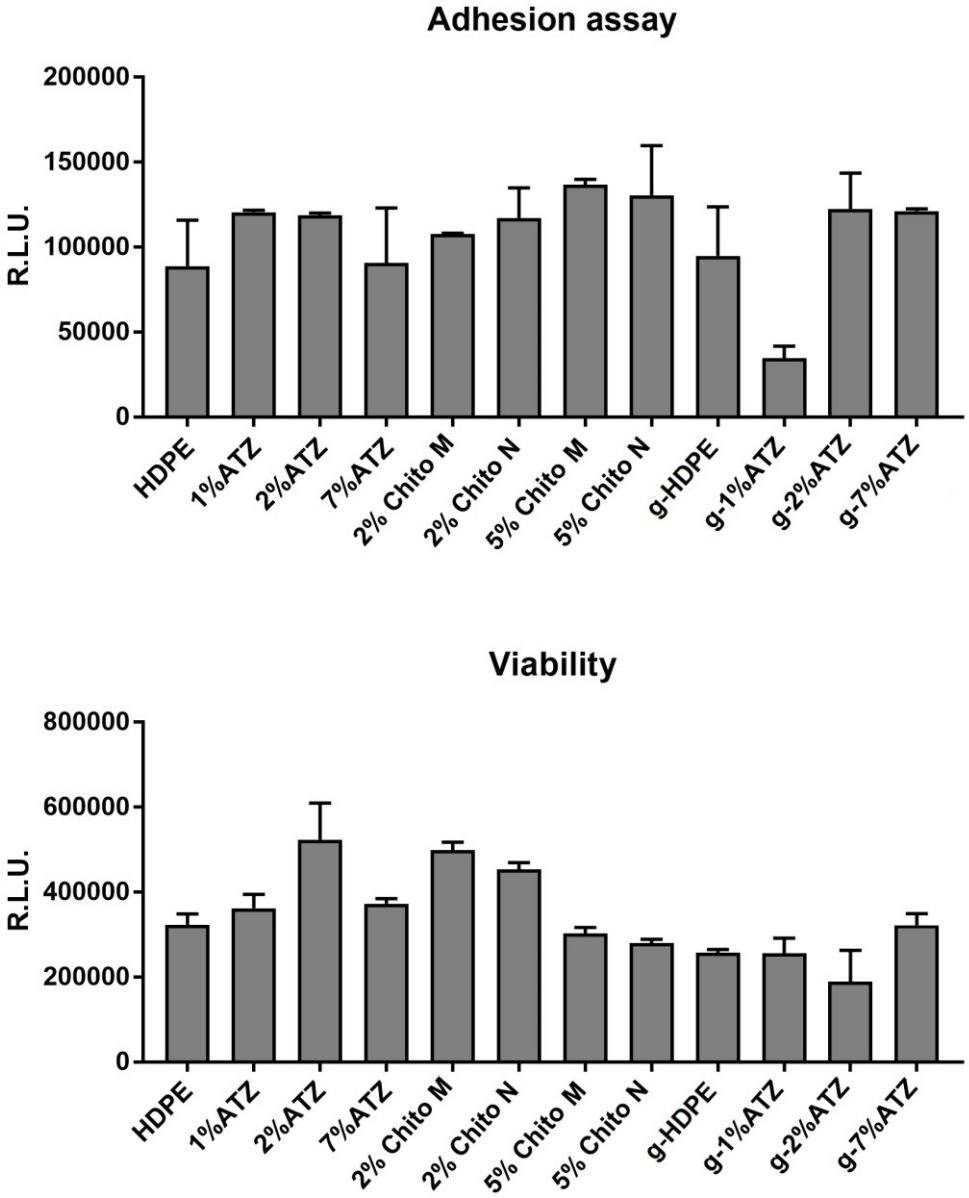

Figure 5.9: Bar chart portraying the number of immediate cell adhesion (A) and the number of viable cells at 24h (B).

As clearly seen in Figure 5.9A, ATZ, chitosan M and chitosan N improve the cell adhesion rate of the material. This effect is higher for the composites with 1 and 2% of ATZ and for the composites with 5% of chitosan, both M and N. The grafting process seems to reduce the immediate cell adhesion of the composites with ATZ, in particular for the HDPE/ATZ 99/1. Also the cell viability at 24h (Figure 5.9B) is higher for the composites with ATZ, chitosan M and N. In particular, the composites with 2% of these fillers show the highest value of viable cells. Chitosan M improves the viability more than chitosan N. Cell viability on the grafted materials appears lower than that observed on the untreated composites.

Fibroblasts attached on the surface of the composites appear with their typical morphology, consisting in spindle-shaped molecules with formation of filopodia, which confirm the good response of the composites with the biological environment. They appear well-spread on the surface of all the composites, except for the HDPE/ATZ 99/1 grafted with chitosan.

Chemical effect of ATZ seems to play the predominant role in the immediate cell adhesion. In fact, the presence of polar fractions of the material (influence of the filler) dispersed into an apolar matrix generates a first interaction between the material and the biological environment. In the case of cell viability, wettability could have some relevance, highlighted in different studies **[4,5,8]**, but in this case such feature does not appear as a significant parameter.

Also the composites with chitosan M and N show a higher cell adhesion with respect the neat HDPE, mainly due to the presence of a more polar molecules dispersed into the matrix. However, at higher concentration chitosan negatively affects the cell viability, which is strongly reduced for the composites at 5% of both chitosan M and N and for the HDPE/ATZ composites grafted with chitosan.

In conclusion, although further research is needed to assess the interaction with more specific cell lines such as osteoblasts and chondrocytes (in order to simulate bones and cartilages), these preliminary results indicate that both ATZ and chitosan are promising fillers for composites intended for biomedical applications. Indeed,

materials with a few amount of filler (2%), are able to improve both cell adhesion and cell viability of the neat HDPE. The filler amount is of paramount importance especially in the case of chitosan, for which a content higher than 2% results in a viability lower that that of the pure polymer. This phenomenon could be related to the ascertained antimicrobial activity of chitosan, that, probably, can results in a detrimental effect on the cells only when the percentage overcomes a threshold value. As for ATZ, the optimal content of 2% appears related to a good compromise between proper amount to interact with cells and dispersion quality.

5.4 Bibliography

[1] Wang M. Developing bioactive composite materials for tissue replacement *Biomaterials* **(2003)** 24; 2133–215.
[2] Khalili A.A., Ahmad M.R. A Review of Cell Adhesion Studies for Biomedical and Biological Applications *Int. J. Mol. Sci.* **(2015)** 16; 18149-18184.
[3] Mussano F., Genova T., Rivolo P., Mandracci P., Munaron L., Faga M.G., Carossa S. Role of surface finishing on the in vitro biological properties of a silicon nitride–titanium nitride (Si3N4–TiN) composite *Journal of Materials Science* **(2017)** 52; 467–477.
[4] Duraccio D., Strongone V., Malucelli G., Auriemma F., De Rosa C., Mussano F.D., Genova T., Faga M.G. The role of alumina-zirconia loading on the mechanical and biological properties of UHMWPE for biomedical applications *Composites Part B* **(2019)** 164; 800–808.
[5] Duraccio D., Strongone V., Faga M.G, Auriemma F., Mussano F., Genova T., Malucelli G. The role of different dry-mixing techniques on the mechanical and biological behavior of UHMWPE/alumina-zirconia composites for biomedical applications *European Polymer Journal* **(2019)** 120; 109274.
[6] Hynes R.O., Lander A.D. Contact and adhesive specificities in the associations, migrations, and targeting of cells and axons *Cell* **(1992)** 68; 303–322.
[7] Prashanth K.V.H., Tharanathan R.N. Chitin/Chitosan: modifications and their unlimited application potential – an overview *Trends Food Sci Technol* **(2007)** 18; 117-131.
[8] Mussano F., Genova T., Laurenti M., Munaron L., Prri C.F., Rivolo P., Carossa S., Mandracci P. Hydrogenated amorphous silicon coatings may modulate gingival cell response *Appl. Surf. Sci.* **(2018)** 436; 603-612.

Conclusions

Alumina Toughened Zirconia (ATZ) and chitosan have been used as filler of High Density Polyethylene (HDPE) with the purpose to obtain novel bio-composites intended for bone replacement applications. The composites have been prepared by melt extrusion technique. A morphological and structural investigation was carried out in order to correlate dispersion of the filler and crystallinity with the mechanical properties of the materials. Also the thermal properties and the thermo-degradation of the composites were studied. The ATZ influence on the wear behavior of the matrix was also investigated by tribological tests.

Composites containing both ATZ and chitosan were prepared in order to analyze the effect of both components on the properties of HDPE. For the preparation of HDPE/chitosan composites, two different chitosan starting powders with different size were used: chitosan microparticles and chitosan nanoparticles (labeled as chitosan M and N). Due to the immiscibility of chitosan and HDPE, the composites HDPE/ATZ/chitosan were prepared by radiation-induced grafting of chitosan on HDPE-ATZ composites.

Finally, a selection of HDPE composites were subjected to fibroblastic cell adhesion and viability, in order to evaluate the influence of ATZ, chitosan and radiation processing on the biological behavior of the HDPE.

Based on the results obtained in this thesis, the following conclusions may be highlighted:

HDPE/ATZ composites presented a good dispersion of ATZ particles, especially at low concentrations of filler (i.e. 99/1, 98/2 and 97/3 HDPE/ATZ), while some aggregates were observed at higher concentrations.

ATZ presence up to 3wt% leads to an increase of the mechanical properties of the matrix (young modulus and tensile strength, elongation at break), whereas for higher amount a decrease of tensile strength was observed. ATZ particles were also effective in reducing the COF and enhancing the wear resistance of the polymer matrix.

As for the chitosan/HDPE composites, an improving of the mechanical properties was observed. In particular, the storage modulus at 40°C for the HDPE/chitosan 98/2 significantly increases with respect to that of neat HDPE. An increase of both Young modulus and tensile strength was observed by stress-strain experiments at room temperature. Such increase was higher at higher filler amount for both chitosan M and N. On the contrary, both the fillers reduce the HDPE ductility.

Radiation-induced grafting of chitosan on HDPE and HDPE-ATZ composites was divided in two part. The first step was devoted to the optimization of the grafting reaction conditions on the neat HDPE (i.e. radiation dose and, reaction time). The best reaction conditions, corresponding to 1 and 3 hours of reaction time on the materials irradiated at 50 and 100kGy, were then applied to 1/99, 2/98 and 7/93 ATZ/HDPE composites.

Both contact angle and ATR measures evidenced that only 1/99 ATZ/HDPE composite was successful grafted. Indeed, for this composite: (i) an increase of the wettability (with respect to untreated composites) was detected and ATR spectra revealed the presence of C=O amidic bond on the surface.

The increase of the crystallinity degree, as a consequence of irradiation process, led to a general increment of the young modulus of the composites, in particular in the case of 7/93 ATZ/HDPE, and to a decrease of the elongation at break for all the samples.

The biological assays indicated that both ATZ and chitosan are promising fillers for composites intended for biomedical applications. Indeed, both cell adhesion and cell viability of the neat HDPE were improved when a few amount of filler (2%) was used.

The filler amount is of paramount importance especially in the case of chitosan, for which a content higher than 2% results in a viability lower than that of the pure polymer.

Regarding the grafted materials, cell adhesion was slightly higher than that of the untreated composites, except for the HDPE/ATZ 99/1. On the contrary, cell viability at 24h significantly decreases for the grafted composites. According to the results obtained with HDPE/chitosan composites, the presence of chitosan grafted on the surface drastically reduces their cell viability, probably due to the ascertained antimicrobial activity of chitosan, which could results in a detrimental effect also on the cell viability.

In conclusion, the results reported in this work indicated that it is possible to tune the mechanical parameters of HDPE by using a proper amount of ATZ and/or chitosan. Moreover, the good results obtained in terms of viability for HDPE/ATZ and HDPE/chitosan confirmed the feasibility of these systems as biomedical supportive materials. However, further research is needed to assess the interaction with more specific cell lines such as osteoblasts and chondrocytes in order to simulate bones and cartilages.

Appendix 1

Materials and preparation methods

A.1.1 Materials

HDPE (HOSTALEN GF 4750), with melt flow index of 0.4g/10min (190°C/2.16Kg), kindly supplied by Lyondell – Basel, was chosen as polymer matrix for all the composites prepared in this thesis work. Main properties of the polymer, obtained by experimental measurements carried out for this thesis work, are summarized in Table 1.

Table 1: Physical properties of neat HDPE GF 4750 used for this work thesis.

Melting temperature (°C)	135
Cristallinity degree by XRD (%)	69.3
Young modulus (MPa)	969 ± 17
Tensile strength (MPa)	13.7 ± 0.4
Impact E CVN (kJ/m^2)	10.3

Alumina Toughened Zirconia (ATZ), labeled with TZ-3Y-S-20A code, was purchased by TOSOH. This material consists of TZP stabilized with 3% of Yttria (Y_2O_3) and containing 20% of Alumina (Al_2O_3).

Chitosan M and N are the name to label HMW-1 (High Molecular Weight Chitosan) and CN001, Chitosan Nanoparticles, respectively. Both the samples was purchased by G.T.C. Bio Corporation (China) and they have been used without further purification.

A.1.2 Composites preparation

HDPE/ATZ composites have been prepared in a twin screw extruder DSM xplore Micro 15cc (Figure 1) at 190°C for 5 minutes. The speed of the extruder screws was 60rpm. The extruder has a capacity of 15 cm^3 and offers a maximum torque of 12 Nm/screw. Before the processing, ATZ was grinded and, after, dried in a vacuum oven at 80°C for 2h. The mixing ratios of HDPE/ATZ (wt/wt) were 100/0, 99/1, 98/2, 97/3, 95/5, and 93/7 and 88/12 wt%. Slabs of HDPE and HDPE/ATZ were obtained by compression molding in a press Collin P200T at 210°C for 2 minutes. The mold had a rectangular shape with dimensions of 100 × 100 mm and a thickness of 0.5 mm.

Figure 1: DSM xplore Micro 15cc twin screw compounder available at Politecnico of Torino, Techonological center of Alessandria (Italy).

HDPE/chitosan composites were prepared by melt extrusion technique by DSM xplore Micro 15cc twin screw compounder working at 190°C and mixed for 5 minutes. The extruded material was compressed with a press Collin P200T at 210°C for 2 minutes to obtain sheets of 0.5mm of thickness at different concentration of chitosan. Three compositions for each type of chitosan were prepared: 99/1, 98/2 and 95/5. Before processing, chitosan M and N were dried in a vacuum oven at 60°C for 12h to avoid hydrothermal degradation.

A.1.3 Irradiation processing

Irradiation step was performed by electron beam irradiation using an Advanced Electron Beam, (Wilmington, USA) operating at 145kV (1.1 mA of the beam with a penetration depth of ca. 150 μm). The samples were placed on a conveyor belt passing under the electron beam source at a speed of 15 m/min. Under these conditions, a dose of 5kGy radiation is absorbed by the samples for each pass. Two doses of irradiation were used on both the blank HDPE and the composites (50kGy and 100kGy). After irradiation, the grafting process was conducted on the treated HDPE sets in aqueous solution containing chitosan at 1wt% under argon atmosphere at 70°C. Several reaction times were used (30 minutes, 1 hour, 2 hours, 3 hours, 5 hours, 7 hours and 15 hours) in order to find the best grafting conditions. The materials were then washed with acetic acid solution, dried and stored at -80°C to avoid any possible crosslinking as a consequence of the generated radicals.

A.1.4 Biological assays

Cell culture

To characterize the biological response in vitro, the fibroblastic cell line NHDF (ECACC, Salisbury, UK) was used. Cells were maintained in DMEM (Dulbecco's Modified Eagle Medium) supplemented with 10% fetal bovine serum (Life Technologies, Milan, Italy), 100 U/ml penicillin, 100 µg/ml streptomycin, were passaged at subconfluency to prevent contact inhibition and were kept under a humidified atmosphere of 5% CO_2 in air, at 37°C.

Cell adhesion

Cell adhesion on grafts was evaluated using a 24 well plate at 10 minutes post seeding. Cells were detached using trypsin for 3 minutes, carefully counted and seeded at 2 x 10^3 cells/disk in 100µl of growth medium on the samples. The 24-well plates were kept at 37°C, 0.5% CO_2 for 15 min. The grafts were carefully washed with Phosphate Buffer Solution (PBS) and then were stained with DAPI (4',6-diamidino-2-phenylindole dihydrochloride) in order to stain the nuclei. The number of adherent cells was determined by counting the number of DAPI-positive nuclei.

Bioreactor

In order to obtain a proper cell growth on different samples, the LiveBox1 bioreactor (IVTech) was employed: it consists of a peristaltic pump, a reservoir and a perfusion chamber. The bioreactor was kept under a humidified atmosphere of 5% CO_2 in air, at 37 °C

Cell viability

Cells were plated at a density of 2500 cells/sample in 24-well and then transferred into the bioreactor. After 24h the viability was assessed by Cell Titer GLO (Promega, Milan, Italy), according to the manufacturer's protocol.

Cell morphology

To study cell morphology, fibroblasts were seeded at a concentration of 5000 cells/sample in a 24-well plate and then transferred into the bioreactor. After 24 hours, cells were fixed in 2.5% glutaraldehyde in Phosphate Buffer Saline (PBS) and then dehydrated using progressive incubation in ethanol. A Scanning Electron Microscope (Zeiss Evo 50 XVP with a LaB_6 source) was employed to observe the cells attached on the samples surface. A gold layer of few nanometers was applied on the samples in order to avoid any charge effect during the SEM analysis.

Appendix 2

Characterization techniques

A.2.1 Raw materials and composites characterization

Morphological and structural analysis

Scanning electron microscopy (SEM)

A scanning electron microscope (Zeiss Evo 50 XVP with LaB_6 source) was used to investigate the morphology of the starting material and the filler dispersion and distribution in the composites. Prior the analysis, the samples were cryogenically fractured in liquid nitrogen to avoid plastic deformation. To avoid electron interaction with gas particles, measurements must be conducted under vacuum. The samples must be conducting and, hence, a non conductive sample, such as polymer, must have a gold layer deposited on its surface to be investigated.

Scanning electron microscope produces images of a sample by scanning the surface with a focused beam of electrons. The volume and depth of penetration of the electron beam increase with an increase of the beam energy and fall with the increasing specimen atomic number. The use

of a high accelerating voltage will result in deep penetration length and a large primary excitation region, but will cause the loss of detailed surface information of the samples. The electrons interact with atoms in the specimen, producing various signals that contain information about the sample's surface topography and composition (Figure1). In particular, backscattered electrons, secondary electrons, x-rays and auger electrons are produced. Secondary electrons and backscattered electrons are commonly used for imaging: the first ones are used to detect the sample surface morphology, on the other hand backscattered are used to investigate different chemical compositions such as in different phases.

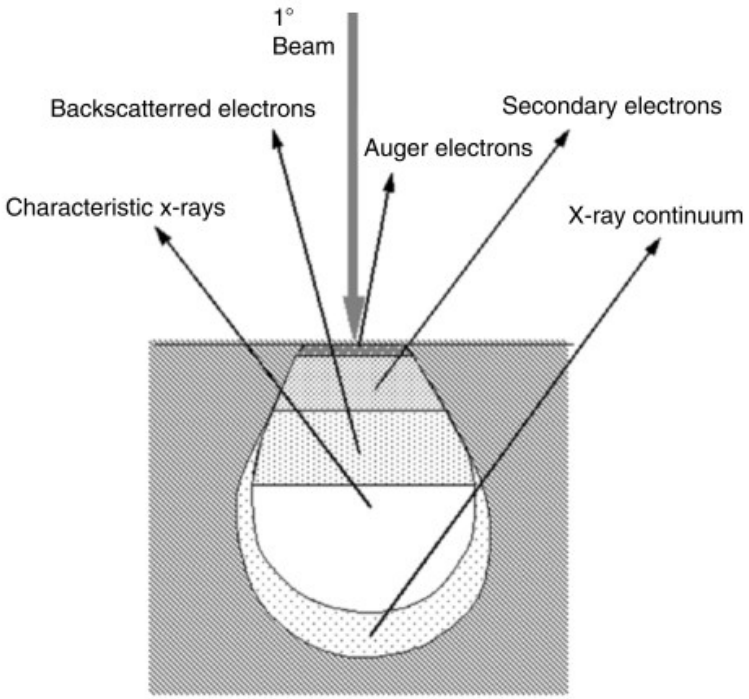

Figure 1: Illustration of several signals generated by the electron beam–specimen interaction and the regions from which the signals can be detected, copy by "Fundamentals of scanning electron microscopy" of Zhou and co-workers.

X-rays signals are emitted when an inner shell electron is displaced by collision with a primary electron and an outer shell electron fall into the inner shell to reinstate the proper charge balance in its orbitals following an ionization event. With the emission of x-ray photon, the ionized atom returns to ground state. The analysis of characteristic x-rays to provide chemical information is the most widely used micro analytical technique coupled to the SEM (Energy Dispersive X-ray Spectrometry).

A schematic diagram of a SEM is shown in Figure 2. SEM system requires that the electron gun produces a stable electron beam with high current, small spot size, adjustable energy and small energy dispersion. SEM based on thermionic emissions are the most diffused instruments. Usually, tungsten or lanthanum hexaboride (LaB_6) cathodes are used. Lanthanum hexaboride has lower work function respect tungsten, then it provides stronger emission of electrons at the same heating temperature. Therefore, LaB_6 electron guns provide greater brightness and a longer lifetime compared with conventional tungsten guns. By increasing the filament current, the electron emission also increases, reaching a saturation point, at which there is the most effective electron emission. Then electrons are focused into a tight bundle by the negative accelerating voltage. After this, the electron beam goes through the condenser lenses, which allows converging and collimating the electron beam into a relatively parallel stream.

A second condenser lens is often used in modern electronic microscopes to provide additional control over the electron beam. This will diverge below the condenser aperture and this is the reason why there are objective lenses used to focus the electron beam into a probe point at the specimen surface and to supply further demagnification. An appropriate choice of lens demagnification and aperture size leads to a reduction of the diameter of electron beam on the specimen surface and enhances the image resolution.

An optimum choice of aperture size can also minimize the detrimental effects of aberrations on the probe size. However, there could be a problem related with the lens defects and contamination on aperture or column. These issues can cause the cross section of the electron beam profile to vary in shape. Practically, the image will stretch along different direction at under-focus and over-focus condition. This imperfection on the electromagnetic lens is called astigmatism. For this reason, a series of coils surrounding the electron beam can be used to correct this error and achieve an image with higher resolution: the so-called stigmators. Generally, the astigmatism correction is performed while operating at the increased

magnification, which ensures higher quality for images at lower magnification even when there is not a perfect compensation. The portion of the image that results acceptably in focus is called the depth of field. This is influenced also by the working distance (WD): at short WD the sample will be scanned with a wide cone of electrons, so the depth of field is little; by contrast, at a longer WD, the depth of field results enhanced due to a narrow cone of electron beam. A long WD, however, does not mean a better resolution: if the topography of the specimen is relatively flat, a short WD is preferred as depth of field is less important and higher resolution can be achieved in this way.

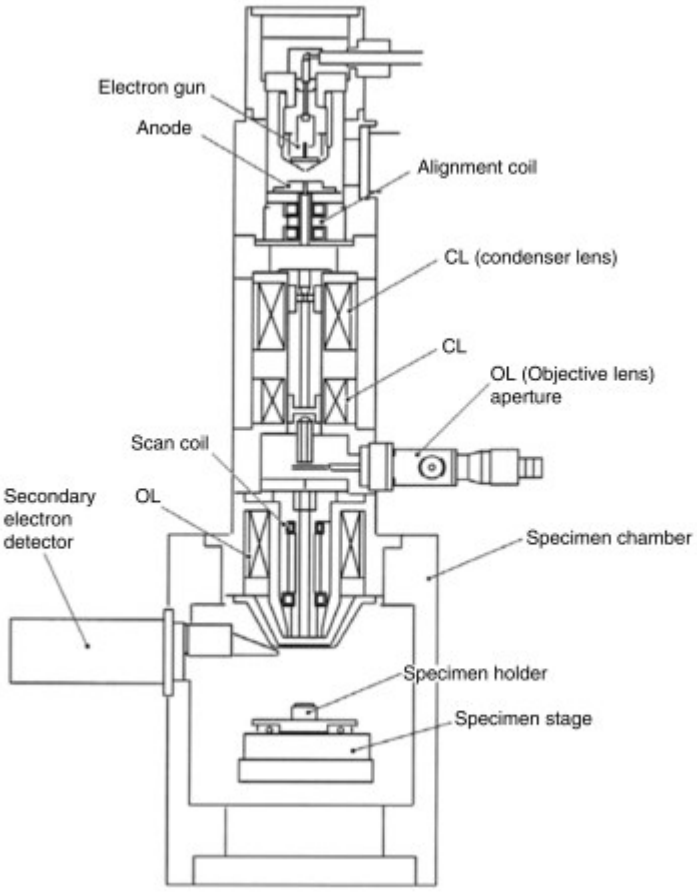

Figure 2: Scanning electron microscope diagram, extracted from "Fundamentals of scanning electron microscopy" of Zhou and co-workers.

X-rays diffraction (XRD)

X-rays diffraction patterns of the samples were obtained by a PW3040/60 X'Pert PRO MPD diffractometer from PANalytical, working at 45 kV and 40 mA, used in Bragg–Brentano geometry. The source is a high power ceramic tube PW3373/10 LFF with Cu anode. WAXS profiles were acquired using a Ni-filtered Cu Kα radiation (λ = 0.15418 nm) with a continuous scan of 0.04°/s. The X'celerator detector, that implements the latest RTMS (Real Time Multiple Strip) X-ray detection technology, allows data collection at rates about 100 times faster than conventional single-point counters.

The index of crystallinity (x_c) was evaluated by the ratio between the intensity of diffraction peaks belonging to the polymer crystalline phase and the intensity of the total sample diffraction pattern. The intensity of the HDPE crystalline phase was determined by subtracting the amorphous phase and the fillers contribution from the total intensity of the diffraction spectra. The profile of amorphous phase was approximated using the profile recorded for an ethylene–propylene copolymer with 17.5 mol% of propylene synthesized by using a metallocene complex biphenyl cyclopentadienyl fluorenyl zirconium activated with methylalumoxane (MAO) at 10 °C.

The equation used to quantify the crystallinity degree is reported in (1):

$$x_c = \frac{I_{c(PE)}}{I_{TOT} - I_{cATZ}} * 100 \qquad (1)$$

Where $I_{c(PE)} = I_{TOT} - I_{AM(PE)}$ and $I_{TOT} = I_{AM(PE)} + I_{c(PE)} + I_{cATZ}$.

In Figure 3, a schematic diagram of diffractometer is shown. The incident beam is generated by the Coolidge tube. This X-Rays source is a high vacuum tube containing a tungsten filament cathode and a massive anode, generally constituted by a heavy block of copper, as in the diffractometer used. The electrons, produced by heating the cathode, are accelerated versus the metallic anode by a potential of 100kV. Electrons

from the filament strike the target anode, producing characteristic radiation via the photoelectric effect. The use of high sensitivity detectors in modern diffractometers allows to overcome the problem related to the low efficiency of this process, since less than 1% of the electrical energy is converted into radiation.

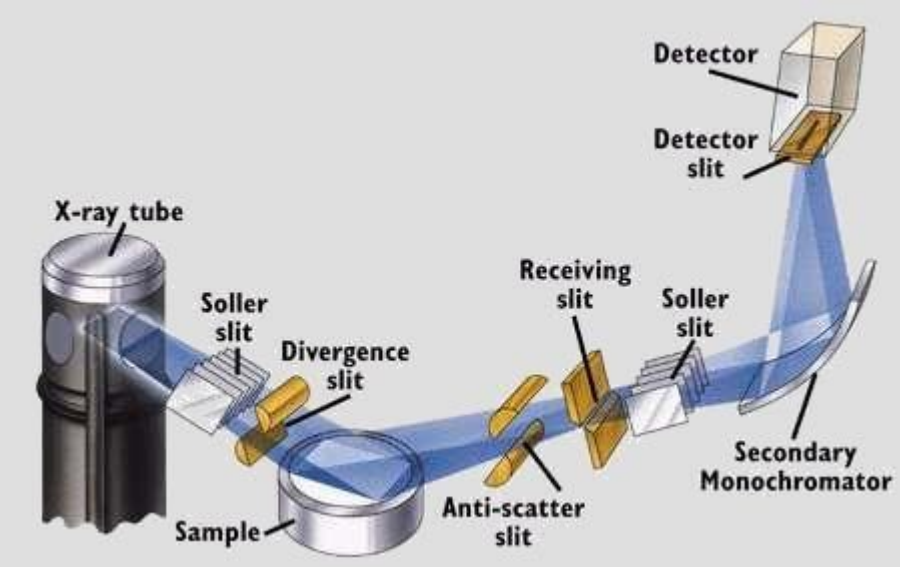

Figure 3: Schematic diagram of a X-rays diffractometer used in Bragg-Brentano geometry.

The characteristic X-ray emission of copper (Figure 4) appears as a continuous spectrum to which a striped spectrum is superimposed. Two emissions at a wavelength of 0.139 nm and 0.154 nm respectively called K_β and K_α are visible. In order to irradiate the sample just with K_α radiation, a Nichel filter has been used.

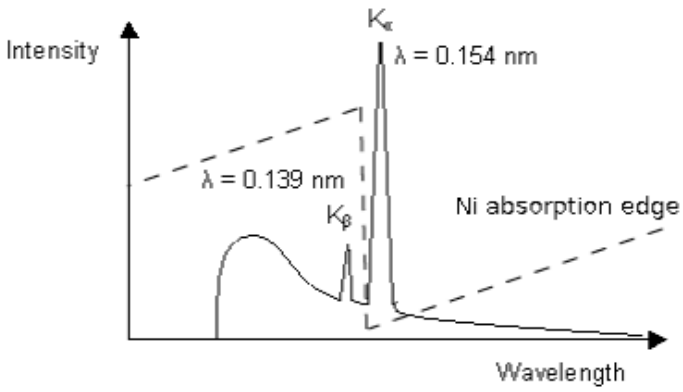

Figure 4*:* X-ray emission spectrum of copper with Nichel absorption edge.

However, a doublet of K_α will almost always be present, identified as $K_{\alpha 1}$ and $K_{\alpha 2}$. The intensity of the $K_{\alpha 1}$ line is twice that of the $K_{\alpha 2}$ line. Usually an average value of K_α is given by a weighted average calculated by the following equation:

$$K_{medio} = \frac{2(K_{\alpha 1}) + 1(K_{\alpha 2})}{3} \qquad (2)$$

In the case of powder diffraction, the Bragg-Brentano parafocusing geometry is used. In this configuration, a point detector and sample are moved so that the detector is always at 2θ and the sample surface is always at θ with respect to the incident X-ray beam: the incident and diffracted beam slits move on a circle centered on the sample. Divergent X-rays from the source hit the sample at different surface points. This arrangement provides the best combination of intensity, peak shape and angular resolution for the widest number of samples.

The detector could be of two types: point detector or position sensitive detector. The first kind observes one point of space at a time, making the analysis slow, but compatible with most optics. The position sensitive detectors are of different kind: in this work a solid state real-time multiple semiconductor strips was used, that provides high speed with high resolution.

The detector and the sample can be moved continuously or by step: it is possible to choose either the type of movement, the scan speed (for a continuous scan) or the width of the step and the counting time between two successive steps (for a scan per steps).

The data collected, intensity and diffraction angles, are plotted by a computer that manages the instrument. The resulting diffraction spectrum comprising both the positions and the intensity of the effects of diffraction is a fundamental physical property of the substance, useful not only for its rapid identification but also for a complete interpretation of its structure.

Mechanical properties

The tensile properties of materials were evaluated using an Instron 5966 tensile tester (Figure 5). The experiments were conducted on the compression-molded plats, according to the standard test method ASTM D882 at room temperature. The dimensions of the specimens were 0.5 mm of thickness and 5 mm of width. The parameters at break (elongation (ε_b) and strain (σ_b)) were determined with constant stretching speed, in order to maintain the ratio v/L_0 equal to 10 mm/(mm/min); (υ = stretching speed and L_0 = initial length of the specimen). The Young's modulus E was measured at a constant speed, given from the ratio υ/L_0=0.1 mm/(mm/min). The mean values of the mechanical properties were averaged over at least five independent experiments.

Figure 5*:* Instron 5966 tensile tester.

The impact behavior of the composites has been investigated by a Zwick/Roell Charpy impact testers. The V-notched specimens with dimensions of 80 mm x 10 mm x 4 mm were prepared in accordance with ISO 179/1 standard. Four specimens were tested for each composition. All experiments were carried out at room temperature.

Tensile tests allow to evaluate the resistance and mechanical behavior of a material subjected to a tensile load.

The stress (stress) corresponding to each elongation is obtained as a ratio of the measured force F on the area A of the specimen section perpendicular to the stretching direction. If A_0 is the initial area of the section and if it is assumed that the volume remains constant during the elongation, the area A during the elongation is $(A_0\ L)\ /\ L_0$, where L is the corresponding elongation and L_0 the initial length of the specimen, the strain will be described by the following equation:

$$\sigma = (F\ L_0)\ /\ (A_0\ L) \qquad (3)$$

A typical stress-strain curve for a polymer material has reported in figure 5. For most materials, stress-strain curves have an initial region characterized by a linear variation of stress-strain. In this region, the material deformation is still reversible; by removing the applied load, the material returns to its original size. In this case, the elasticity is of the Hookian type (i.e. the Hooke's law is valid).

The coefficient of proportionality between stress and strain in the linear region is the Young's modulus (E). The higher the modulus, the more stress is needed to create the same amount of strain.

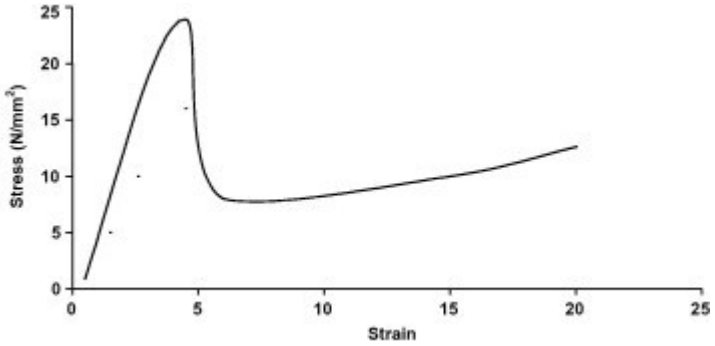

Figure 5*:* Typical stress-strain curve for a polymer material.

E is a specific characteristic of the sample depending not only by the type of material, but also by the preparation process and the possible presence of defects, of branches and by the method of cooling the material.

The elastic region ends with a maximum point, called the Yield point, beyond which there can be a sharp decrease in the slope of the stress-deformation curve: in this region the force to be applied to obtain the same deformation is lower. In this case the applied stress is no longer proportional to the deformation (Hooke's law is no longer valid) and the material undergoes a permanent deformation, defined as plastic deformation. Subsequently and before the breakage, the stress necessary to deform the material could increase: in this region the macromolecular chains reach a more extended conformation and show a greater resistance to deformation. This phenomenon is called strain hardening.

Dynamic-mechanical characterization

Dynamic-mechanical (DMTA) analyses on the composites HDPE/ATZ were performed using a DMA Q800 (TA Instruments) in tensile configuration. The following experimental conditions were adopted: temperature range from 25 to 100 °C, heating rate of 3 °C/min, 1 Hz frequency and 0.05% of oscillation amplitude in strain-controlled mode. The storage modulus (E'), loss modulus (E") and tanδ curve were recorded.

Dynamic-mechanical (DMTA) analyses on the composites HDPE/chitosan were performed using a Triton TTDMA (TA Instruments) in dual cantilever bending configuration. The following experimental conditions were adopted: temperature range from -150 to 80 °C, heating rate of 3 °C/min, 1 Hz. The storage modulus (E'), loss modulus (E") and tanδ curve were recorded.

For both sets of materials, the tests were repeated two times at least and the experimental error was calculated as standard deviation for all the measured parameters.

Dynamic Mechanical Analysis (DMTA) is a technique that is widely used to characterize a material's properties as a function of temperature, time and frequency. It allows to apply cycling stress or strain to a sample and analyze the response in order to obtain phase angle and deformation data. These data allow the calculation of the damping or tan delta (δ) as well as modulus and viscosity data. Two approaches can be used: forced frequency, where the signal is applied at a set frequency and free resonance, where the material is perturbed and allowed to exhibit free resonance decay. It is estimated to be 100 times more sensitive to the glass transition than differential scanning calorimetry (DSC), and it resolves other more localized transitions that are not detected in the DSC. In addition, the technique allows the scanning of a material's modulus and viscosity as a function of temperature, strain, or frequency.

If a constant oscillatory load is applied to a sample, the sample will deform sinusoidally as well. This two sinusoids, the load and the resulting deformation, will be reproducible if the material is deformed within its linear viscoelastic region, thus is fundamental to remain in the elastic deformation region. The resulting strain wave shape will depend on the ratio between the viscous and the pure elastic behavior that the polymer has. The two extremes of the material's behavior, elastic and viscous, provide the limiting extremes that will sum to give the strain wave.

The difference between the applied stress and the resultant strain is an angle, δ, described by the following equation:

$$\varepsilon(t) = \varepsilon_o[\sin(\omega t)\cos\delta + \cos(\omega t)\sin\delta]$$

This equation can be separated into the in-phase (elastic, sinusoidal curve) and out-of-phase strains (viscous, co-sinusoidal curve) that corresponds respectively to the storage modulus and the loss modulus.

Tribological characterization

Tribological tests were performed on the HDPE/ATZ composites with the aim to evaluate the influence of ATZ on the wear behavior of the polymer matrix. A CSEM High Temperature Tribometer was used for these tests (Figure 6), in ball-on-disk configuration. A polished disk sample of the composites (neat HDPE, 93/7 and 88/12 HDPE/ATZ) were coupled against an upper stationary alumina ball (Ø = 6 mm). The tests were conducted at 37°C under 10N of load using 20ml of fetal bovine serum (FBS) as lubricant (sliding distance: 25000 lap, r = 5 mm). The friction coefficient (COF) obtained by tribological test is the average value of the COF collected after reaching the steady state.

Figure 6: CSEM High Temperature Tribometer.

A contact profilometer (Form Talysurf 120) equipped with a 2µm diamond conical stylus was used to estimate the volume loss of the composites after the tribological test. For each sample, the measure was repeated at least five times at room temperature.

The value of wear volume was calculated as the average area of sections multiplied for trace circumference. Knowing the wear volume, the wear rate k (mm^3/Nm) was calculated using the modified Archard's formula, generally applied in literature:

$$k = \frac{V}{SF} \tag{2}$$

where V (mm^3) is the volume loss, S is the sliding distance (m) and F is the applied load (N).

Thermal characterization

Thermogravimetric analysis (TGA)

Thermogravimetric analyses (TGA) were performed in nitrogen and in air, from 50 to 800 °C, with a heating rate of 10 °C/min, using a TA Discovery thermo balance (TA Instruments) (experimental error:± 0.5% wt.,±1 °C), shown in Figure 7. The samples (ca. 10 mg) were placed in open platinum pans and fluxed with nitrogen or with air (gas flow: 25 ml/min). T_{10}, and T_{max} were extracted from the curves: T_{10} is the temperature corresponding to a sample weight loss of 10%, and T_{max} is the temperature at the inflection point of the curve (detected at the maximum of the peak of the first derivative of the curve), which corresponds to the maximum rate of the sample degradation. The final residue at 800°C was used to evaluate the effective composition of the composites.

Figure 7: TA Discovery thermo balance (USA).

Differential scanning calorimetry (DSC)

Differential scanning calorimetry (DSC) was carried out in a TA DSC Q20 (USA) (Figure 8) with a heating rate of 10 °C/min. The experiments consisted of a first heating cycle, performed to delete the thermal history of the materials followed by a cooling step, to study the crystallization of the composites and the starting component, and a last heating step to evaluate the melting temperature of materials. The experiments were carried out using 6.0 ± 0.5 mg of material, according to the following cycle: (1) heating from 25 °C to 250 °C at a rate of 10 °C/min; (2) cooling down to -10 °C at 10 °C/min; and (3) heating from -10 °C to 250 °C at a rate of 10 °C/min.

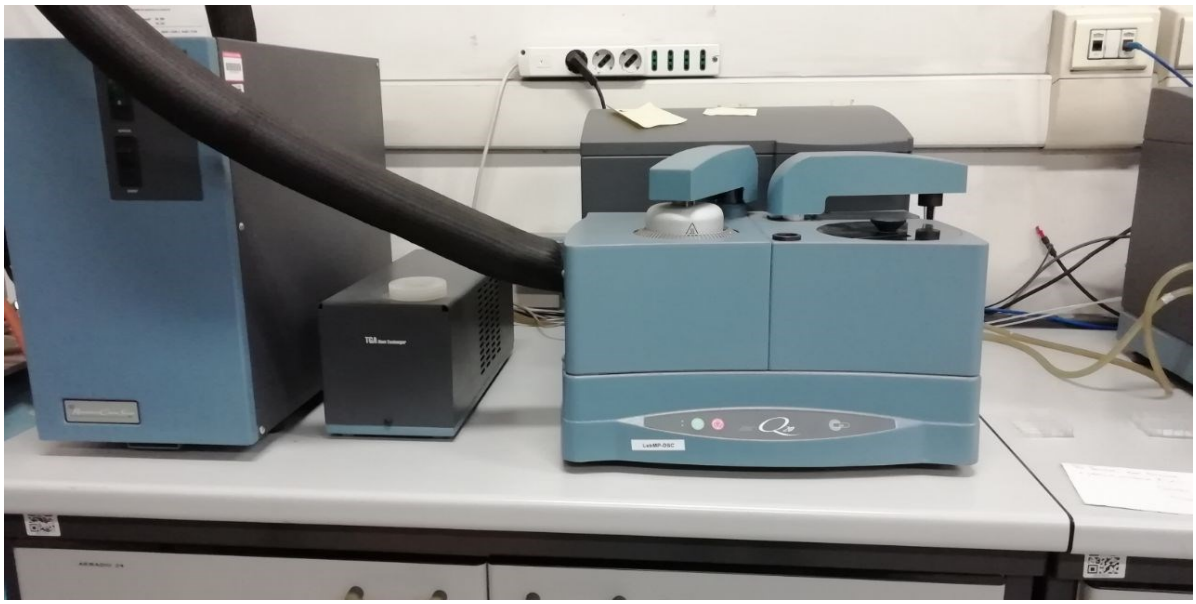

Figure 8: TA DSC Q20 (USA).

Differential scanning calorimetry is a thermoanalytical technique in which the difference on the amount of heat required to increase the temperature of a sample and reference is measured as a function of temperature. Both the sample and reference are maintained at the same temperature, which increases at a constant rate, during the experiment. This technique is widely used for the characterization of polymer samples to identify their physical and chemical transformation such as: degradation, melting, glass transition and some others phase transitions, using a small amount of materials. It is widely used in industries as a quality control instrument due to its applicability in evaluating sample purity and for studying polymer curing. Also chemical reactions such as oxidation and degradation of the sample can be observed.

The basic principle underlying this technique is that when the sample undergoes a physical transformation such as phase transitions, more or less heat will need to flow to it than the reference to maintain both at the same temperature. Whether less or more heat must flow to the sample depends on whether the process is exothermic or endothermic, for example crystallization is exothermic and melting is endothermic, it requires more heat to complete the transformation from solid to liquid state. By observing the difference in heat flow between the sample and reference, differential

scanning calorimeters are able to measure the amount of heat absorbed or released during such transitions.

The result of a DSC experiment is a curve of heat flux versus temperature. Depending on the type of instrument, the exothermic transition can be measured as a positive or negative peak. Integrating the peak area is also useful to calculate the transition hentalpy.

Glass transitions appears as a step in the baseline of the recorded DSC signal. This is due to the sample undergoing a change in heat capacity; no formal phase change occurs.

A.2.2 Grafted materials characterization

Wettability measurements

Changes of the surface wettability of the grafted materials was evaluated by contact angle measurements. The sessile drop method was used, and the measurements were taken at room temperature. The optical contact angle was evaluated by a Kruss DSA 100 apparatus with 25x optical zoom available. The analysis was performed with double distilled water. Contact angles were measured on at least five independent locations of the samples surface.

Infrared spectroscopy

Infrared spectroscopy (IR) is a vibrational spectroscopy, due to the conversion of radiation energy in vibrational energy. The molecules strike by infrared radiation could vibrate in two fundamentals way: stretching and bending. A stretching vibration is the rhythmic movement of bond axis with

increase and decrease of interatomic distance. A bending vibration could be the variation of an angle between two bonds with a common atom or the movement of a group of atoms respect the entire molecule. In this last case, there is another subdivision of vibrational mode into vibration in plane and out of plane. The in plane vibrations are called scissoring and rocking, while the out of plane vibrations wagging and twisting.

A vibration is IR active only when there is a change in the molecule's dipolar moment as a consequence of radiation interaction. In fact, when this condition is satisfied, the molecule produces an oscillating electric field which makes possible the exchange of energy with electromagnetic waves.

The intensity of a band depends from the value of bond dipolar moment, and then depends from the relative electronegativity of bond atoms. The dipolar moment can be calculated according to the formula: = $q * \bar{d}$, where μ is the dipolar moment, q the electric charge and d the vector distance.

To know the frequency at which a functional group would absorb the electromagnetic radiation, one can use the Hooke's law. In this case, two linked atoms are considered as a simple harmonic oscillator, in which the frequency depends on atom's mass and bond strength. In fact, the Hooke's law is:

$$\nu_{vibr} = \frac{1}{2\pi c} * \sqrt{\frac{k}{\mu}}$$

in which ν_{vibr} is the vibration frequency, c is the light speed, k is the strength constant and μ the reduced mass. Then, higher the constant of strength k, higher is the absorbance frequency, while higher the reduced mass, lower is the frequency.

Attenuated Total Reflectance (ATR) experiments were performed on the grafted materials by using a Perkin Elmer Frontier FT-IR instrument (Figure 9) equipped with a diamond crystal cell. Spectra were recorded as an average of 16 scans in the 4000–400 cm^{-1} range. ATR corrections were performed using the Nicolet Omnic 5.2 software.

ATR enables to examine samples directly in the solid or liquid state. It is based on the property of total internal reflection resulting in an evanescent wave. A beam of infrared light is passed through the ATR crystal, where it reflects at least once off the internal surface in contact with the sample. This reflection forms the evanescent wave, which extends into the sample with a penetration depth typically between 0.5 and 2 μm. The exact value is determined by the wavelength of light, the angle of incidence and the indices of refraction for the ATR crystal and the medium being probed.

The evanescent effect only works if the crystal is made of an optical material with a higher refractive index than the sample being studied. Otherwise light is lost to the sample.

Figure 9: Perkin Elmer Frontier FT-IR instrument.